UNIVERSITÉ DE STRASBOURG

Ecole et Observatoire des Sciences de la Terre

INSTITUT DE PHYSIQUE DU GLOBE DE STRASBOURG (UMR 7516)

ESKİŞEHİR OSMANGAZİ ÜNİVERSİTESİ

THÈSE

Présentée à

L'UNIVERSITE ESKİŞEHİR OSMANGAZİ

Pour obtenir

Le grade de Docteur de l'Université de Strasbourg et de l'Université Eskişehir Osmangazi
Discipline : Sciences de la Terre et de l'Univers
Spécialité : géophysique

par

Cahit Çağlar Yalçıner

Investigation of buried objects with Ground Penetrating Radar: Application to archaeoseismology and palaeoseismology in the Buyuk Menderes Graben (Turkey)

Soutenue le **13 avril 2009** devant la commission d'examen :

Directeur de thèse	MEGHRAOUI Mustapha, *Université Louis Pasteur, Strasbourg, France*
Co-Directeur de thèse	ALTUNEL Erhan, *Université Eskişehir Osmangazi, Turquie*
Co-Directeur de thèse	BANO Maksim, *Université Louis Pasteur, Strasbourg, France*
Rapporteur interne	SAILHAC Pascal, *Université Louis Pasteur, Strasbourg, France*
Rapporteur externe	ERGINTAV Semih, *TÜBİTAK, Gebze, Turquie*
Rapporteur externe	CAKIR Ziyadin, *Université Technique, Istanbul, Turquie*
Examinateur	AKYUZ Serdar, *Université Technique, Istanbul, Turquie*

Investigation de la proche surface par le Georadar: Application à l'archéosismologie et paléosismologie du graben du Buyuk Menderes (Turquie)

Cahit Çağlar Yalçıner

THESE DE DOCTORAT
Sciences de la Terre Géophysique, Proche Surface

Avril 2009

Investigation of buried objects with Ground Penetrating Radar: Application to archaeoseismology and palaeoseismology in the Buyuk Menderes Graben (Turkey).

Cahit Çağlar Yalçıner

PHD THESIS
General Geology

April 2009

Gömülü Yapıların Yeraltı Radarı (GPR) Yöntemi ile Araştırılması: Büyük Menderes grabeni'nde Paleosismolojik ve Arkeosismolojik Uygulamalar

Cahit Çağlar Yalçıner

DOKTORA TEZİ
Genel Jeoloji

Nisan 2009

SUMMARY

Western Anatolia is one of the most active regions in the world and is represented by horsts and grabens faulted on the margins. The subject of this work, the Büyük Menderes graben, is one of the most active structures in the region and extends between the Aegean Sea in the west and the Denizli Basin in the east. Detailed mapping shows that the active faults bounding the northern boundary of the graben were ruptured with surface breaks in historical periods. These ruptures identified in detail during the field studies. Where direct observations were not possible, however, the characteristic features of the faults were identified by using the Ground Penetrating Radar (GPR), one of the shallow geophysical methods.

The GPR method works on the basis of recording of the reflections of the electromagnetic waves from the interfaces by a horizontal receiver which were transmitted to the ground with high velocity by using a horizontal antenna. Data collected is filtered to eliminate the environmental and instrumental noise by using computers and then interpreted to determine the buried structures in high resolution and sensitivity.

In scope of the investigation, GPR studies were conducted in six different locations (two trenches, three faulted archaeological site and a buried archaeological site). The trace of the fault, width of the fault zone and the amount of the offset of the young units along the fault were determined by the GPR method before the excavation of the trenches. In the archaeological site where the offset remnants of the archaeological objects were observed, the trace of the faults and the width of the deformational zones were determined by the GPR and the amount of offset obtained from GPR profiles were compared with the offset amounts measured on the surface. In order to locate the exact location of the ancient road entering the ancient Nysa town GPR, studies were conducted and a previously unknown temple was discovered.

In the trenches which were excavated based on the GPR findings, it was found that the amount of the offset obtained by the GPR method and the actual offset measured on the trench wall were agreeable with each other. Where the offset archaeological structures exist, it was observed that the faults on the GPR profiles correspond to the ruptures on these structures. In Nysa ancient town, the image obtained from GPR was interpreted to belong to a structure rather than the road expected; in fact, the excavations conducted later on revealed a temple which was not known to exist before.

Key Words: Ground Penetrating Radar (GPR), Büyük Menderes graben, buried structure, active fault.

ÖZET

Batı Anadolu, tektonik açıdan dünyanın en aktif bölgelerinden biridir ve bölgede kenarları aktif normal faylar ile sınırlı horst ve grabenler ile temsil edilir. Bu çalışmanın konusu olan Büyük Menderes grabeni batıda Ege Denizi ile doğuda Denizli Havzası arasında uzanan en önemli aktif yapılardan biridir. Yapılan ayrıntılı haritalama çalışmaları, grabenin kuzey kenarını sınırlayan aktif fayların tarihsel dönemlerde meydana gelen depremlerde yüzey kırıkları oluşturduklarını ortaya koymuştur. Tarihsel depremlere ait yüzey kırıklarının özellikleri ayrıntılı arazi gözlemleri ile belirlenmiştir. Ancak arazide doğrudan gözlem yapmanın mümkün olmadığı yerlerde sığ jeofizik yöntemlerden biri olan Ground Penetrating Radar – Yeraltı Radarı (GPR) kullanılarak aktif fayların özellikleri belirlenmeye çalışılmıştır.

GPR yöntemi, yatay doğrultuda konumlanan bir anten aracılığıyla yüksek hızda yeraltına gönderilen elektromanyetik dalgaların ara yüzeylerden yansımasının yine yatay doğrultudaki alıcı tarafından kayıt edilmesi prensibi ile çalışmaktadır. Toplanan veriler bilgisayar programları yardımı ile çeşitli filitreler kullanılarak çevresel ve aletsel gürültülerden temizlendikten sonra yorumlanarak gömülü yapılar yüksek çözünürlükte ve hassasiyette belirlenebilmektedir.

Çalışma kapsamında toplam altı lokasyonda (iki adet hendek, üç adet faylanmış arkeolojik kalıntı ve bir adet gömülü arkeolojik kalıntı alanında) GPR çalışmaları yapılmıştır. Hendek lokasyonlarında yapılan GPR çalışmalarında aktif fayın yeri, fay zonunun genişliği ve genç birimlerdeki yerdeğiştirme miktarları önceden belirlenmiş ve daha sonra hendekler açılmıştır. Ötelenmiş arkeolojik kalıntılarda fayların kesin yerleri ve deformasyon zonlarının genişliği GPR ile belirlenmiş ve GPR profillerinden elde edilen ötelenme miktarları yüzeydeki ölçümler ile karşılaştırılmıştır. Nysa antik kentine batıdan giren antik yolun yerinin belirlenebilmesi amacıyla yapılan GPR çalışmalarında varlığı bilinmeyen bir tapınak ortaya çıkarılmıştır.

Hendek lokasyonlarında GPR sonuçları doğrultusunda yapılan kazılarda, GPR profillerinden elde edilen ötelenme miktarları ile hendek duvarlarında ölçülen ötelenme miktarlarının birbirleri ile uyumlu olduğu görülmektedir. Ötelenmiş arkeolojik yapıların bulunduğu alanlarda, GPR profillerinde görülen fayların kalıntılarda kırılmanın olduğu yerlere karşılık geldiği ortaya konmuştur. Nysa antik kentinde yolun yerinin belirlenmesi amacıyla yapılan GPR çalışmalarında, alınan görüntünün yol değil bir yapıya ait olduğu ileri sürülmüş ve daha sonra yapılan kazılarda önceden varlığı bilinmeyen bir tapınak ortaya çıkarılmıştır.

Anahtar Kelimeler: Ground Penetrating Radar (GPR), Büyük Menderes grabeni, gömülü yapı, aktif fay

RESUME

L'Anatolie occidentale est une des régions les plus sismiquement actives du monde, comme en attestent les structures actives en horst et graben qui la délimitent. La présente étude est focalisée sur le Fossé de Büyük Menderes, une structure majeure qui s'étend de la Mer Egée à l'ouest jusqu'au Bassin de Denizli à l'est. Une cartographie de détail montre que les failles actives qui forment la limite nord du graben ont produit des séismes durant la période historique. Ces ruptures ont été décrites en détail lors de campagnes de terrain. Lorsque l'observation directe s'est révélée impossible, nous avons eu recours à la prospection géophysique par géoradar.

La méthode géoradar s'appuie sur l'émission active puis l'enregistrement d'ondes électromagnétiques réfléchies par les différentes interfaces du sous-sol. Les données sont enregistrées puis filtrées afin d'éliminer le bruit environnemental et instrumental puis interprétées pour identifier les structures enfouies avec une haute résolution et une grande sensibilité.

Dans le cadre de ces travaux, des campagnes d'acquisition GPR ont été réalisées sur six sites différents : deux tranchées, trois sites archéologiques affectés par des failles et un site archéologique enterré. En amont de toute campagne d'excavation, nous avons ainsi pu déterminer la géométrie de la trace de la faille, la largeur de la zone de faille ainsi que la quantité de déplacement affectant les unités récentes. A l'un des sites, des structures archéologiques portent la trace de mouvements récents le long d'une faille. La géométrie de la faille tout comme la largeur de la zone de déformation ont été définies, ainsi que le déplacement total qui correspond aux mesures de surface.

Les travaux de tranchée, réalisés sur la base des résultats du géoradar, ont révélé des quantités de déplacement co-sismique cumulé très comparables aux quantités déterminées par le géoradar. D'autre part, la trace de faille identifiée dans les profiles géoradar correspond bien, en profondeur, à des décalages de structures archéologiques. Ainsi, sur le site de la ville antique de Nysa, les mesures destinées à détecter le passage de l'ancienne route d'accès à la ville, le géoradar a révélé des déplacements affectant un temple jusqu'ici inconnu.

Mots-clés: Géoradar, Fossé de Büyük Menderes, structure enfouie, faille active.

This thesis is dedicated to the memory of my dear mother

Necla Yıldırım, who passed away during this study

Acknowledgements

My sincere thanks go to my supervisors, Prof. Dr. Erhan Altunel, Prof. Dr. Maksim Bano and Prof. Dr. Mustapha Meghraoui, for their continued enthusiasm, encouragement and most importantly advice about how to structure a scientific report. I have three great supervisors but in separately I earn several things from them, Prof. Dr. Altunel was a perfect example to be a good guy and to be a hard worker, Prof. Dr Meghraoui always showed me how to be a scientist with his never ending patience and Prof. Dr Bano is the guy who teach me the deep of geophysics with his eternity knowledge.

I am very happy to know a person like Assistant Prof. Dr. Ziyadin Çakır. He is my friend, my teacher and my brother with all his patience and help on this thesis. I am also indebted to the two great scientists, Prof. Dr. Serdar Akyüz and Associated Prof. Dr. Semih Ergintav, they always supported me with their knowledge since I was a undergraduate student in ITU.

I could not ignore the support of my colleagues, Bayram Demir, Emre Evren, Dr. İsmail Kuşçu, Dr. Volkan Karabacak, Gülsen Uçarkuş, M. Ersen Aksoy, Cengiz Zabcı, Önder Yönlü, Taylan Sançar, Dr. Ahmet Akoğlu, Dr. Mathieu Ferry, Dr. Samir Belabbes and Dr. Florence Beck.

Without moral and financial support of my dear sisters Pınar, Duygucan and especially my deceased mother this work would never have been completed.

I never forget my old supervisor Prof. Dr Aykut Barka

Finally, my thanks go to my dear wife Dr. Ezcan Yalçıner for her moral support, love and my son Kaan Yalçıner.

This thesis financially supported by TÜBİTAK (105 Y 348), Research Foundation of Eskisehir Osmangazi University (200415001, 200615026), CNRS-UMR 7516 Strasbourg and Embassy of France in Turkey

TABLE OF CONTENTS

Sayfa

LIST OF FIGURES

LIST OF TABLES

1 INTRODUCTION

1.1 Scope of the study:

This study is the application of the Ground Penetrating Radar (GPR) to buried tectonic and archaeological structures in the Büyük Menderes Graben (Figure 1.1). GPR is one of the shallow geophysical survey methods in which underground bodies and structures are identified by digital identification of changes in electromagnetic signals. GPR method has been used for several applications such as archaeological investigations, geophysical and geological investigations, contaminated land investigations, forensic investigations, snow and ice investigations etc. This method is also used extensively and successfully on active tectonic and archaeological researches (Bano, et al., 2000; Meghraoui, et al., 2001; Audru, et al., 2001; Gross et al. 2002; Green et al. 2003; Ferry et al. 2004; Conyers, 2006; Negri and Leucci, 2006; Leucci and Negri, 2006 and Limp, 2006). Bano, et al. (2000), conducted GPR method on a Quaternary sedimentary site to image the structures and tectonic features. Audru, et al. (2001) measured three GPR profiles on an active strike-slip fault within the urban area and exposed the noise effects and solutions on GPR profiles. Gross et al. (2002) and Green et al. 2003 applied 3D GPR surveys to showing shallow geometry and displacements on the San Andreas Fault. Meghraoui et al. (2001) applied GPR measurements with other shallow geophysical methods to determine precise location for trenching. Green et al. (2003) applied 3D GPR surveys to investigate the location and direction of the buried fault zones. For archaeological researches, Conyers (2006) conducted a grid measurement to have a 3D map of subsurface. Leucci and Negri (2006) applied GPR near an urban area for archaeological evidence.

Although Turkey is an ideal application field for GPR studies in terms of active faulting and archaeological sites, application of GPR studies are few. The first application of GPR in Turkey is made by Ferry et al. (2004) who identified offset buried Ottoman aqueduct and channels on the North Anatolian Fault (NAF). There are examples of successful GPR applications on archaeological sites in Turkey (e.g. GPR investigations in Hierapolis for man-made structures located under the Temple of Appollo (Negri and Leucci, 2006)).

Active fault studies require detail investigations and identification of precise location of the fault, amount of the offset on the fault and width of the deformation zone is one of the most essential stages in active fault studies. Such parameters can easily be obtained where evidence for faulting is preserved in geological and geomorphological records (Figure 1.2). However, as Figure 1.3 shows, regional conditions play important role on the preservation of surface evidence of faulting. In addition, man – made activity (e.g. agriculture, construction etc.) erases geological and geomorphological records. In these cases, identification of fault parameters (e.g. precise location, amount of offset and width of the deformation zone) become impossible with surface evidence. In this circumstance, subsurface investigations can help to obtain necessary data. In this study, GPR is applied to determine the precise location of surface rupture, width of the deformation zone and amount of offset related with historical earthquakes in the Büyük Menderes Graben. Buried archaeological structures are also surveyed in this study.

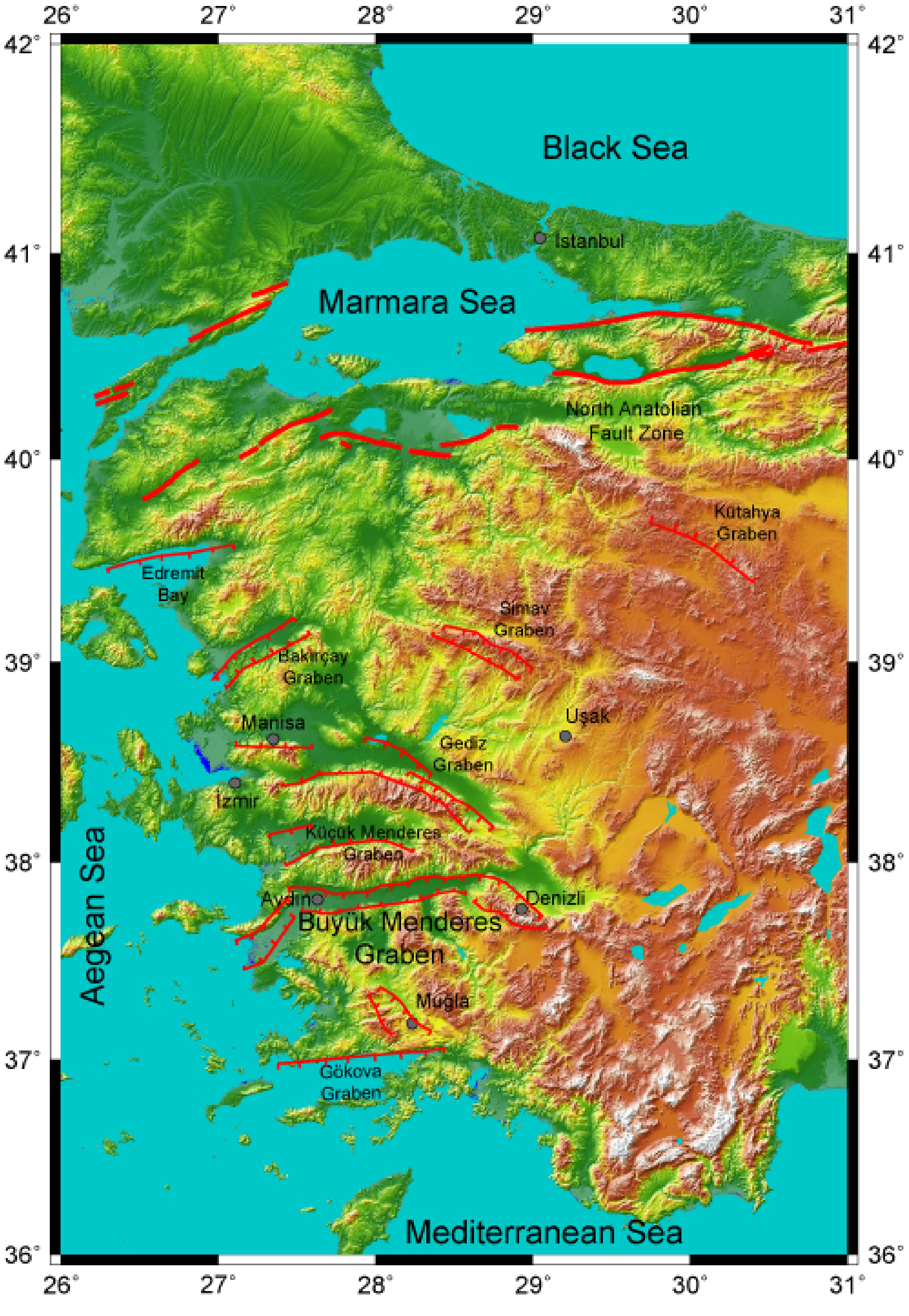

Figure 1.1: Tectonic setting of Western Turkey. Major active faults are from Bozkurt (2000). Topography is from SRTM data.

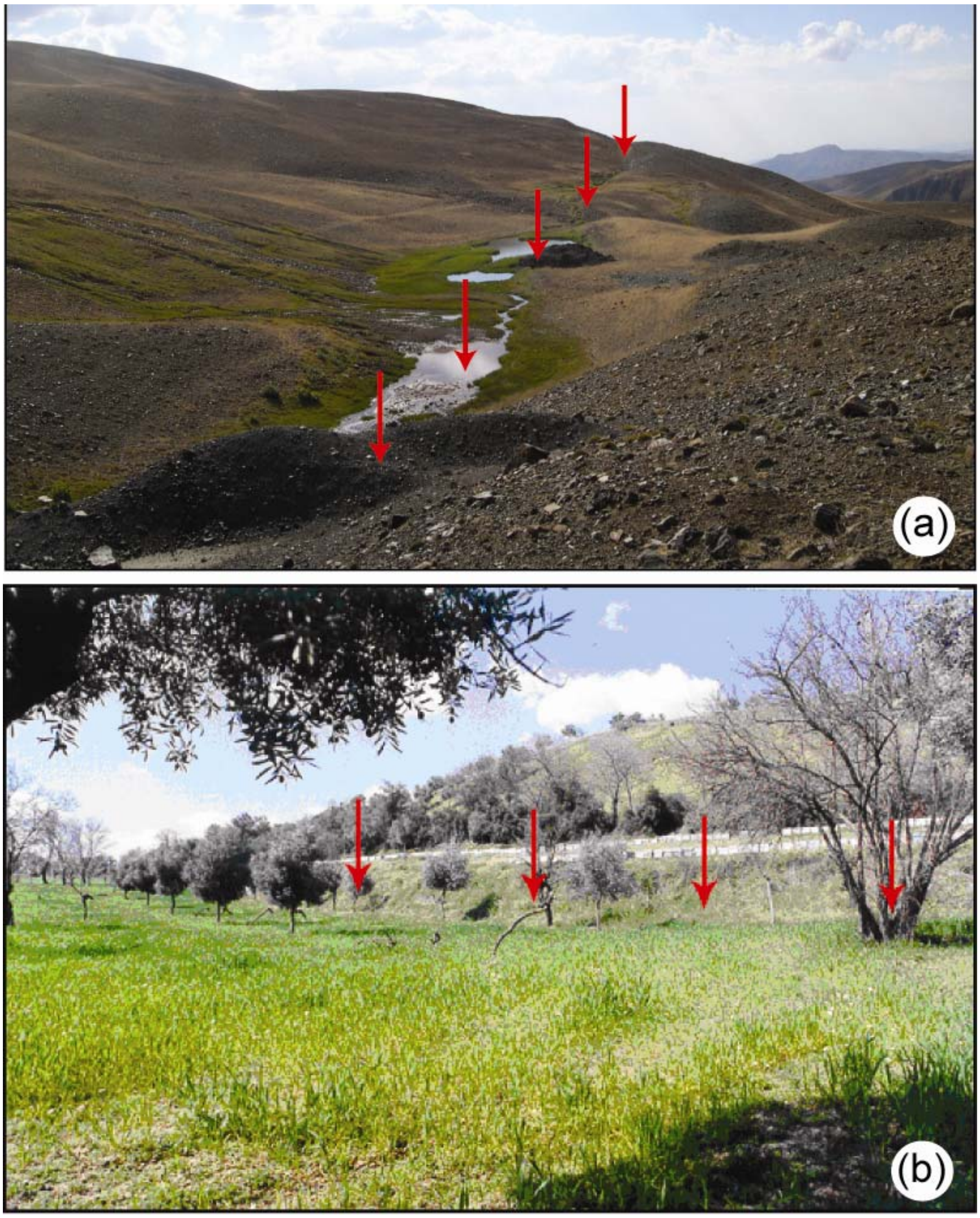

Figure 1.2: (a) Surface trace (red arrows) of the North Anatolian fault near Erzincan. No vertical displacement along the fault but the morphological evidences expose the fault trace. (b) An approximately 3.5 m high E – W-trending fault scarp cutting Quaternary deposits in the foot of Neogene hills (red arrows). Bee hives are on the up-thrown side. View towards west (Altunel 1999).

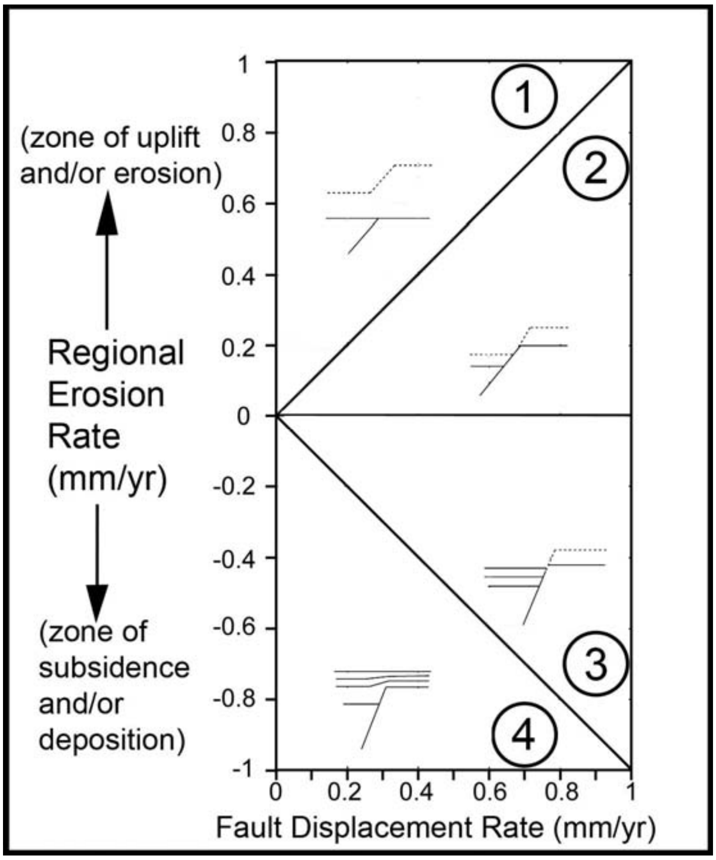

Figure 1.3: Schematic diagram showing the effects of relative rates of deformation versus geomorphic process on the preservation of a fault scarp (an example of primary, on-fault evidence). Many other types of paleoseismic features are subject to the same effects. In quadrant 1 (circled number) the regional erosion rate exceeds the fault displacement rate and the scarp is rapidly destroyed. In quadrant 2, the fault displacement rate is greater than the regional erosion rate, so the scarp is partially eroded yet some relief. In quadrant 3, the fault outcrops on a landscape undergoing slow subsidence and deposition, but the scarp is still partially preserved because the fault displacement rate is greater than the regional deposition rate. In quadrant 4, both sides of the fault are buried by sediments deposited at a more rapid rate than the rate of fault displacement. No surface scarp is formed under these conditions, but the evidence of paleoseismicity is preserved as onlapping strata in the subsurface (redrawn from McCalpin & Nelson 1996).

The Büyük Menderes Graben is suitable for GPR application for the following reasons.

1. The Büyük Menderes Graben is bounded by active faults (McKenzie, 1972, Dewey and Şengör 1979, Seyitoğlu and Scott 1991, Bozkurt 2000). Large historical earthquakes occurred on these faults and involved surface ruptures (Allen, 1975, Sipahioğlu 1979, Ambraseys and Finkel 1995, Altunel, 1999). Thus, the possibility of obtaining geological and geomorphological evidence for faulting is high.

2. The Büyük Menderes graben is rich in archaeological sites and there are ancient man – made structures, such as road, wall and bridge along the graben. It is likely that these man – made structures are offset by the fault or collapsed as a result of strong ground shaking.
3. There is active sedimentation in the graben either from tributaries of Menderes river or high topography along the northern side of the graben. Thus, surface ruptures or collapsed man – made structures are being covering.
4. There has been agricultural activity in the graben from the historical times (Akurgal, 1995). Such activity and natural erosion remove evidence of faulting in time.

1.2 Methodology of the study:

In this thesis, GPR studies are applied in selected locations along the northern part of the Büyük Menderes graben between Aegean Sea in the west and Kuyucak in the east (Figure 1.4). At the beginning, surface ruptures of historical earthquakes were mapped on the basis of geological and geomorphological evidence along the northern side of the graben. Then, man – made linear structures (e.g. roads and walls) were put on the fault map. Intersections of the fault and man – made structures were investigated in detail using GPR. In addition, GPR is applied to two trench locations to locate the fault precisely where there is no enough surface evidence and to determine the trench length. Furthermore, GPR is used to identify subsurface archaeological relics in the ancient city of Nysa. For a successful and reliable GPR result, the following criteria play important role.

(a) Thickness of the cover layer: this is important in selection at the GPR antenna type.
(b) Topography: flat surface or very gentle slope is required because for real reflections, signal must be vertical.
(c) Side effects: there should not be any other source for electromagnetic (EM) waves or secondary flat reflectors.
(d) Smoot survey surface: antenna coupling is necessary to reduce the attenuation of EM signals. Thus rough surface is not preferred.

The right selection of acquisition and processing software for GPR surveys are playing important role on the interpretation of raw GPR data. In this study, we used Ramac GroundVision™ software for acquisition, ReflexW™, RadLab (Girard, 2000) and Ramac Easy3D™ software for processing.

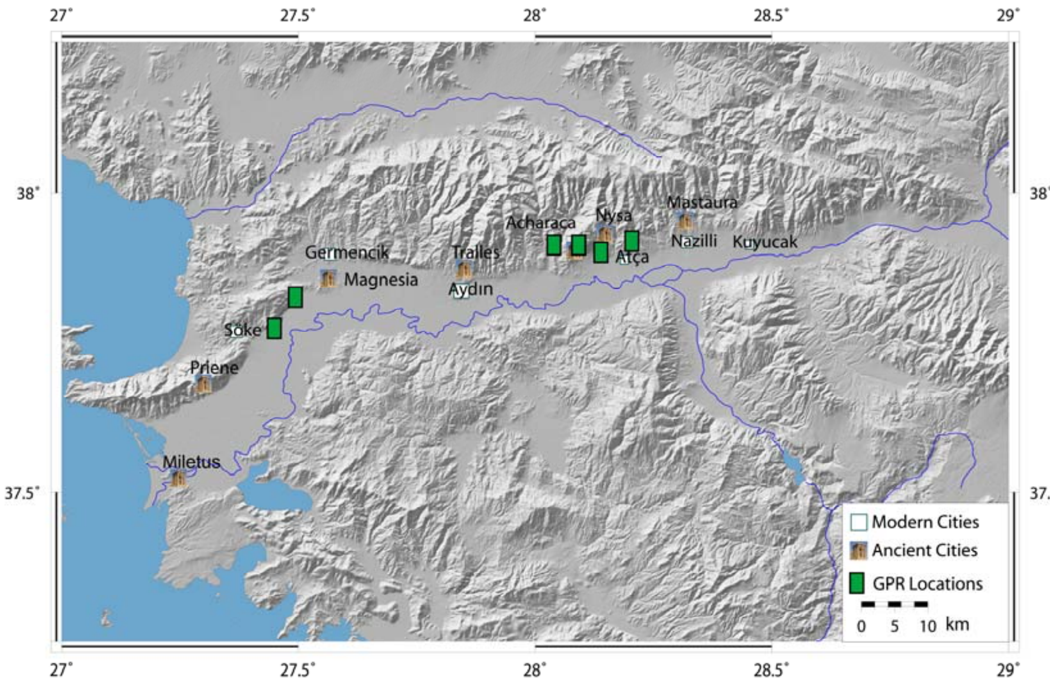

Figure 1.4: GPR study sites, ancient cities and modern cities locations in Büyük Menderes graben.

The study area is characterized by normal faults. Since slip is vertical on normal faults a scarp forms at the surface after faulting (Figure 1.5a). In the areas of active sedimentation, colluvial wedges devellope in front of the scarp (Figure 1.5b) that may cover the fault zone partially or totally (Figure 1.5c). Trenching provides fresh outcrops to document faulting episodes as shown in Figure 1.6. Thus, it would be possible to identify offset levels and colluvial wedges with GPR because the contact between two different units would reflect a continuous line. In this study, GPR is applied two paleoseismological locations and GPR results correlated with paleoseismological results.

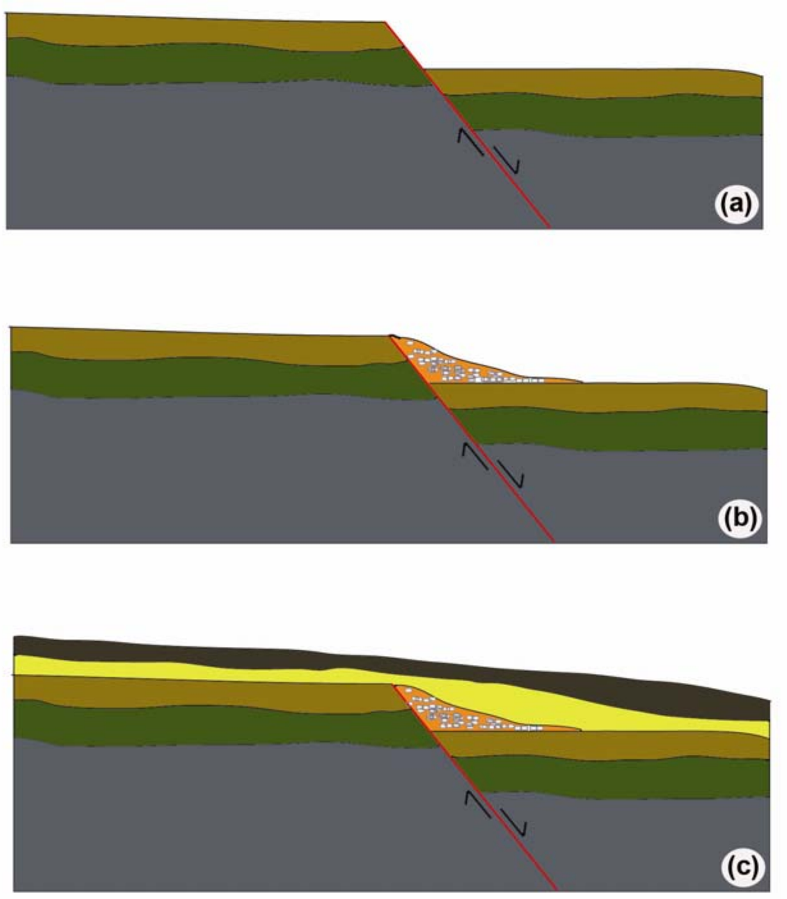

Figure 1.5: Schematic view of a normal fault (a) Surface scarp after faulting. (b) Colluvial wedges form in front of the scarp. (c) Sedimentation covers the fault zone.

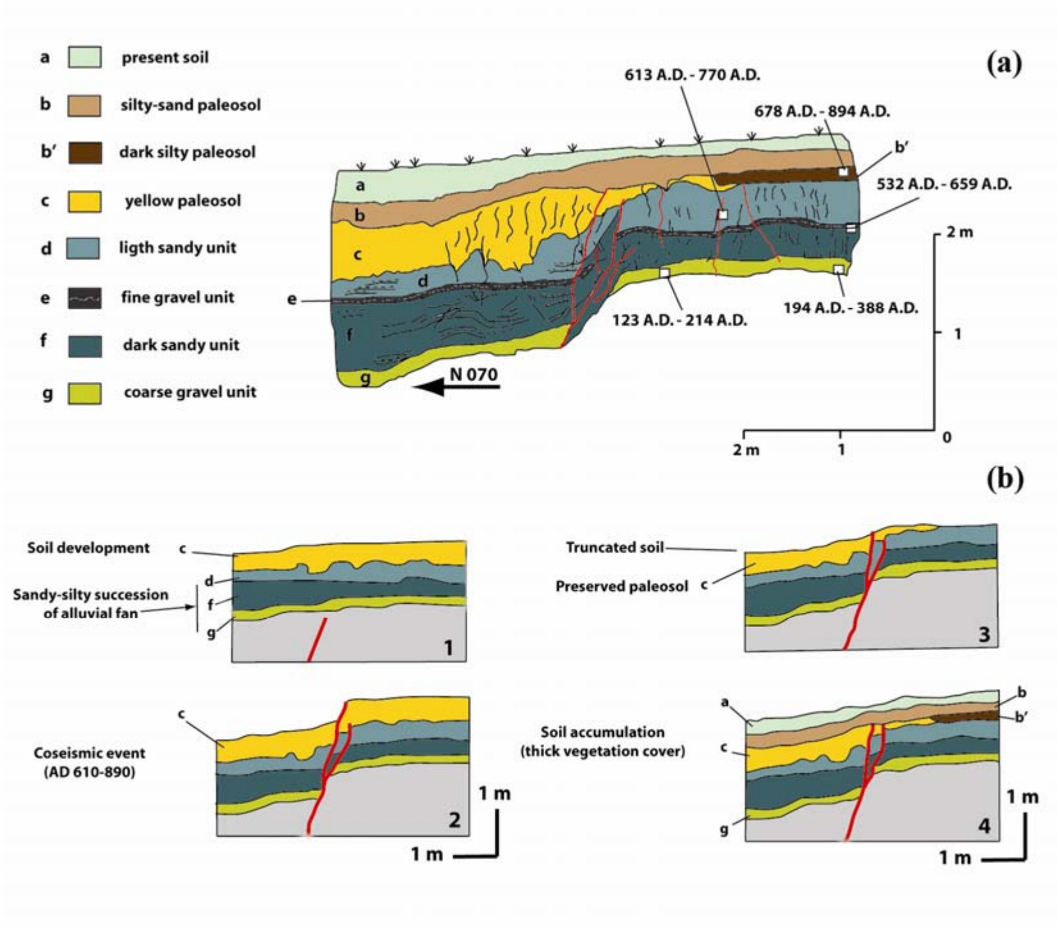

Figure 1.6: (a) Detail of faulted section of a trench. Paleosol unit c is preserved and indicates a downthrown movement along the fault after unit c and before unit b' (between A.D. 610 and 890). Vertical offset measured from layers e and g near the fault yield 0.5 m. With warped units in the hanging wall and footwall, the vertical offset reach 1.0 m. (b) Reconstruction of the most recent faulting in the same trench. Preserved paleosol unit c near fault indicates the occurrence of a single faulting event before units b and b' (Meghraoui et al., 2001).

GPR is also applied to locate ancient structures in the ancient city of Nysa. After GPR applications, the area is excavated by archaeologists and GPR results correlated with excavation results.

1.3 Geographic Location of the Study Area

The Büyük Menderes graben is a main corridor between the Aegean coast and central Anotolia. Thus, different scales of settlements have been established within time. The main historical settlements are Miletus, Priene, Magnesia, Tralles, Acharaca, Nysa and Mastaura. Main modern settlements are Söke, Germencik, Aydın, Nazilli and Kuyucak (Figure 1.7).

Büyük Menderes is the longest river of western Anatolia and the main water source for Büyük Menderes basin. The normal fault system around the river formed the Büyük Menderes graben. Büyük Menderes River born at Afyonkarahisar province, Dinar district, Suçıkan location then poured to Aegean Sea at Aydın province, Söke district, Dipburun location with a length of 560 km.

Figure 1.7: A general view of Büyük Menderes graben on Turkey geographic map.

Büyük Menderes basin is one of the main agricultural potential areas which are including huge plains from Denizli to Aegean Sea. General products are cotton, vegetables and fruits and it's also important for national economy with high productive intensive agriculture.

Büyük Menderes graben is located mostly in Aydın province with 90 % and it's under control of Aegean climate system with a 17.5 °C average per year. The hottest month is July with 28.4 °C average and the coldest month is January with 8.2 °C average. For elevation of graben average is 59 meter (city center of Aydın), but some parts of the graben are nearly sea-level (western part). Because of the geo-strategical situation and high productive agricultural farms, Büyük Menderes graben is really attractive for humans for settling. In archaeological records first settling starts 7000 B.C.

2 GPR (Ground Penetrating Radar) METHOD

The expressions 'ground-probing radar', 'ground penetrating radar (GPR)', 'sub-surface radar' or 'surface-penetrating radar (SPR)' refer to a variety of electromagnetic techniques designed mainly to locate the buried objects or interfaces. On the other hand, the description of 'ground penetrating radar' (GPR) is mostly used to describe the technique as it has become almost universally accepted. The system design of GPR is largely applications-oriented and the hardware choice is usually dependent on the target type and the material of the target and its surroundings. The range of applications for GPR methods is wide and the sophistication of signal recovery techniques, hardware designs and operating practices is increasing as the technology develops.

GPR data are usually collected along closely spaced transects within a grid. It is an active method that transmits electromagnetic pulses from surface antennas into the ground, and then measures the time elapsed between when the pulses are sent and when they are received back at the surface (called two-way travel time) (Conyers, 2004). As the radar pulses are transmitted through various materials on their way to the buried target feature, their velocity will change, depending on the physical and chemical properties of the material through which they are traveling. When the travel times of the energy pulses are measured, and their velocity through the ground is known, the depth in the ground can be accurately estimated. Radar travel times are measured in nanoseconds (10^{-9} sec). As the antennas are moved along the ground surface individual reflections are recorded about every 2-10 centimeters along transects, using a variety of collection techniques. The depth to which radar energy can penetrate depends largely upon two factors: 1) the frequency of antenna being used, and. 2) the characteristics of the soil being surveyed, most specifically its water content. This second factor has been shown to be much more critical in the depth to which an EM pulse can travel and how much energy attenuation occurs. The two major components to affecting energy propagation include the electrical and magnetic permeability. The form of the individual reflected waves (called a waveform) that are received from within the ground are digitized into a reflection trace, and when many traces are stacked next to each other a two-dimensional vertical profile is produced along the transect. Thousands of reflection traces in many profiles within a grid can then be analyzed to produce both two and three-dimensional images of what lies below the surface.

GPR uses transmitting and receiving antennas. The transmitting antenna radiates short pulses of the high-frequency (usually polarized) radio waves into the ground (Figure 2.1). When the wave hits a buried object or a boundary with different dielectric constants, the receiving antenna records variations in the reflected return signal.

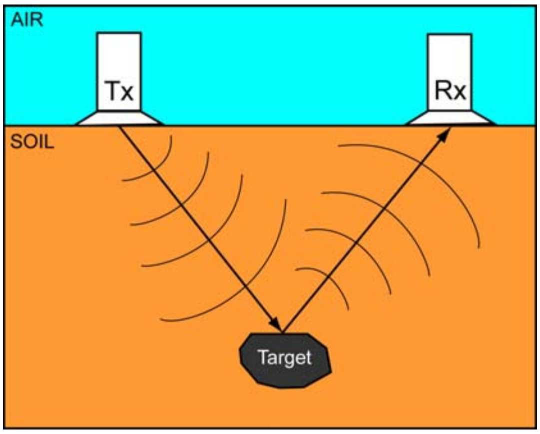

Figure 2.1: Schematic view of GPR antennas working system.

GPR is often compared with seismic reflection surveys. Just as seismic reflections are generated when a seismic wave hits a layer in the subsurface with different material properties, GPR reflections are generated when a pulse hits an object or layer with different electromagnetic characteristics. Objects with different electromagnetic characteristics may be buried tanks, sedimentary layers, the water table, or the archaeological remnants. Essentially, a reflection occurs when there is an abrupt change in the dielectric constant of materials in the subsurface. The dielectric constant is defined as the capacity of a material to store a charge when an electric field is applied relative to the same capacity in a vacuum, and can be computed using $\boldsymbol{\varepsilon_r = (c / v)^2}$, where ε_r is the relative dielectric constant, *c* is the speed of light (30 cm/nanosecond) and υ is the velocity of electromagnetic (EM) energy passing through the material. Therefore, the relative dielectric constant is inversely related to the velocity of EM waves, and this is shown in Figure 2.2.

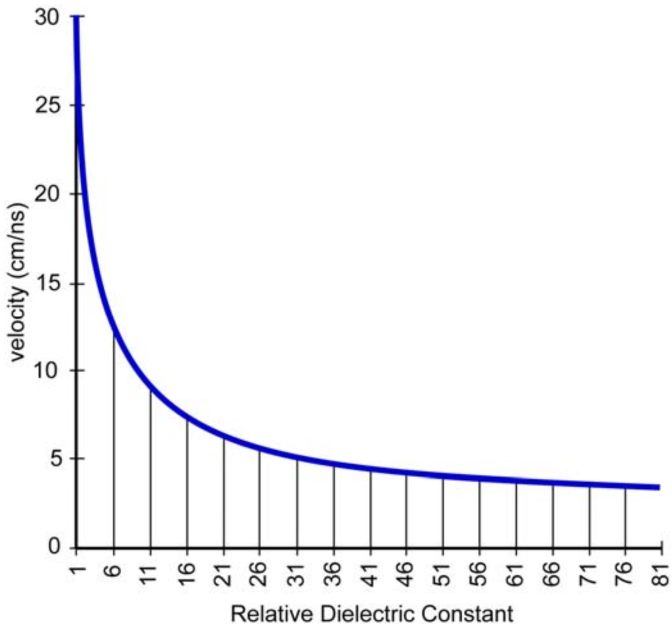

Figure 2.2: Relation between velocity and relative dielectric constant (Daniels, 2004).

At the radar frequencies, the water has a relative permittivity of ~81, while the dry rock constituents of most soil have ε_r typically in the range of 3 – 5. Then the values of ε_r for soils will strongly depend on the water content and lies in the range 6 – 30. Table 2.1 (modified from Davis and Annan (1989)) lists approximate values of the relative dielectric permittivities at 100 MHz for a range of geophysical materials.

Table 2.1: Relative dielectric constant (RDC) and velocities of common geological materials. Modified from Davis and Annan (1989).

Material	RDC	Velocity (cm/ns)
Air	1	30
Dry sand	3 – 5	15
Dry silt	3 – 30	5.5–17
Ice	3 – 4	15
Asphalt	3 – 5	15
Volcanic ash/pumice	4 – 7	11–15
Limestone	4 – 8	10–15
Granite	4 – 6	13
Permafrost	4 – 5	13–15
Coal	4 – 5	13–15
Shale	5 – 15	8–13
Clay	5 – 40	5–13
Concrete	6	12
Saturated silt	10 – 40	5–10
Dry sandy coastal land	10	10
Average organic-rich surface soil	12	8.5
Marsh or forested land	12	8.5
Organic rich agricultural land	15	8
Saturated sand	20 – 30	5.5 – 6.7
Fresh water	80	3.3
Sea water	81 – 88	3.3

2.1 History and Application Areas of GPR

James Clerk Maxwell in 1864 and Heinrich Hertz in 1886 developed the basic theory behind electromagnetic waves and their reflections. But it was not until 1924 that the British physicist Sir Edward Victor Appleton estimated the height of the ionosphere (a layer in the upper atmosphere that reflects long radio waves) using basic electromagnetic reflection principles. Then, in 1935, the British physicist Sir Robert Watson-Watt developed the first practical radar system (Calligeros *et al*., 1997).

According to Olhoeft, (2000), a GPR survey was first performed by the German geophysicist W. Stern in 1929. But GPR was largely forgotten until the late 1950's when the radar systems in US Air Force planes saw through ice in Greenland, causing them to misread their altitude and crash into the ice. In 1960, John C. Cook made the first proposal for using radar to detect subsurface reflections in his article "Proposed monocycle-pulse, VHF radar for airborne ice and snow measurements" (Cook, 1960). Cook and others continued to develop radar systems to detect reflections beneath the ground surface.

One of the original and most promising ground penetrating radars was presented by Moffatt and Puskar (1976). Their system used an improved antenna that gave a better target-to-noise ratio and was able to more accurately detect important subsurface reflections. Moffatt and Puskar used their system for several applications. With their GPR unit, they estimated the location of an underground tunnel, a fault, and mines. They also attempted to detect the variation of moisture content in subsurface soils. Their conclusion was that GPR is a useful tool for detecting anomalies and variations in subsurface rocks and soils. Ulriksen (1982) and other scientists described better methods of processing and analyzing subsurface GPR data. Then, Wyatt *et al.* (1996) published a brief list of articles describing methods of obtaining, processing, and analyzing GPR data. The key future development area will be signal processing and image recognition methods, and this requires development of core strategies generally based on deconvolution techniques.

The new generation of GPR systems is considered to be based on shallow geophysical exploration and nondestructive investigation. For shallow geophysical exploration ground penetrating radar has already achieved some significant results. It is, however, in the area of nondestructive investigation of structures such as tunnels, roads, buildings, and other examples of physical infrastructure of modern civilization that GPR has an increasingly important role to play. The GPR is also used in geology, neotectonics, hydrology, archaeology and contaminated sites... For example it has been used for surveying many different types of geological strata ranging from exploration of the Arctic and Antarctic icecaps and the permafrost regions of North America, to mapping of granite, limestone, marble and other hard rocks as well as geophysical strada (Daniels, 2004). On the other hand nowadays GPR applications on active tectonic investigations become very popular and lots of successful work have been done and published (e.g. Bano *et al.*, 2000, Audru *et al.*, 2001, Meghraoui *et al.*, 2001, Gross *et al*. 2002 and Green *et al*. 2003).

Finally the application of GPR technique can be summarized by the list shown below.

- Archaeological investigations
- Active tectonic investigations
- Geophysical & Geological investigations
- Building assessment
- Borehole inspection
- Planetary exploration
- Pipes and cables
- Road survey
- Snow and ice
- Wall condition
- Rail track
- Bridge deck analysis
- Contaminated land investigations
- Forensic investigations
- Mines (anti-personnel and anti-tank)
- Reinforced concrete
- Tunnel linings

2.2 Investigation Depth and Resolution of GPR Method

Ground penetrating radar presents the system designer with significant limitations on the types of antennas that can be used. The upper frequency of operation of the system, and hence the antenna, is therefore limited by the properties of the material. Investigation depth depends on the frequency used and the physical parameters (attenuation, conductivity) of the soil. Thus, lower the frequency used, higher the investigation depth and on the other hand, higher the attenuation of the soil, lower the investigation depth. The need to obtain a value of range resolution requires the antenna to exhibit ultra-wide bandwidth, and in the case of impulsive radar systems, linear phase response. The requirement for wide bandwidth and the limitations in upper frequency are mutually conflicting and hence a design compromise is adopted whereby antennas designed to operate over some portion of the frequency range 10 MHz to 5GHz depending on the resolution and range specified (Daniels, 2004). The requirement for portability for the operator means that it is normal to use electrically small antennas, which consequently results generally in a low gain and associated broad polar radiation patterns.

The vertical resolution is the power of one method to separate the base from the top of a layer. As it is inconvenient to physically rotate the antenna it is also possible to electronically switch (commutate) the transmit/receive signals to a set of multiple co-located antenna pairs. As revealed at Figure 2.3, depending on the frequency of energy transmitted into the ground and the distance between two planar interfaces (Δd) reflections from the top and bottom of a layer may or may not be visible in a reflection profile. High frequency energy will generate a small enough wavelength so that the top (A) and bottom (B) will produce a reflection, and the composite reflection trace of the two (C) can define both interfaces. Medium frequency antennas with a longer wavelength will just barely have enough definition from the top and bottom (D and E) to produce a composite reflection trace (F) that exhibits both interfaces. Low frequency antennas may produce a wave that will reflect off both interfaces (G and H), but the composite reflection trace is affected by constructive and destructive interference of the two waves, and only the top of the interface is visible in the composite reflection trace (I).

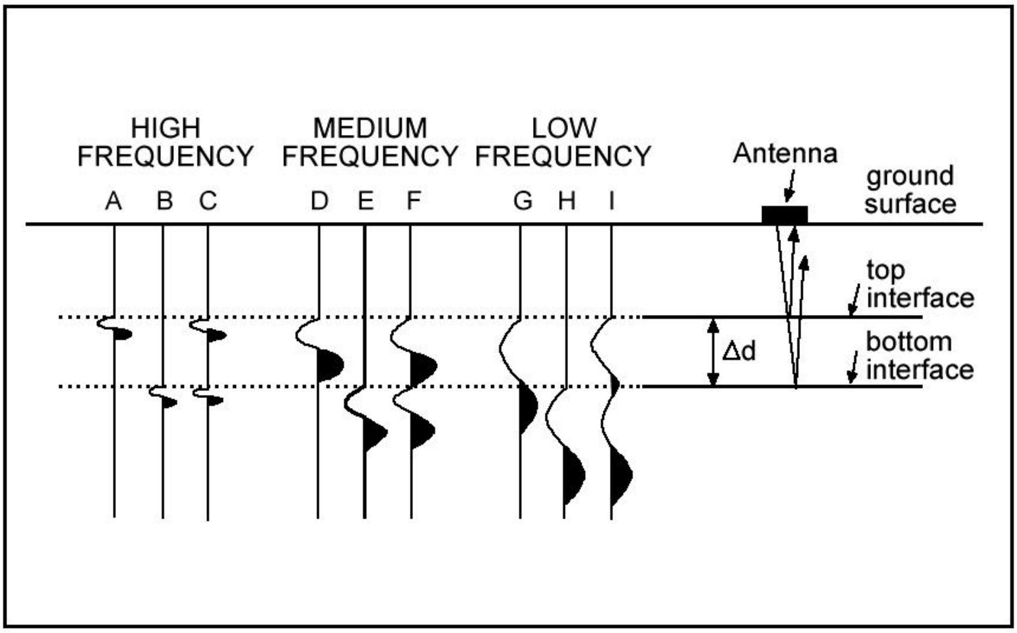

Figure 2.3: Schematic view of GPR trace between two planar interfaces (Redrawn from Conyers, 2004).

The selection of the acquisition frequency and the type of antenna (shielded or unshielded) and its polarization depends on a several factors, including the size and shape of the target object, the transmission properties of the intervening medium, and the optimum economics of the survey operation, as well as the characteristics of the surface (e.g. smooth, vegetated, rough and sloppy). The specification of a particular type of system can be prepared by examining the various factors which influence detectivity and resolution. A further step along this overall strategy is to employ circular polarization, which is essentially a means of automatically rotating the polarization vector in space. However, circular polarization inherently requires an extended time response of the radiated field, and in consequence either hardware or software deconvolution of the received signal is needed (Daniels, 2004).

The ability to resolve buried features is mostly a function of the wavelength of energy reaching them at the depth they are buried. A guiding principle is that the minimum object size that can be resolved is about 75% of the downloaded wavelength reaching them. Downloading of radar energy always occurs as energy passes in the ground and decreases in frequency. For instance, a 250 MHz center frequency antenna will generate downloaded energy of about 180 MHz in the ground (Weymouth, 1986).

The choice of the frequency of the antenna depends on the depth of the target to be studied, larger the depth of the target, lower the frequency of the antenna. This is the case of GPR on geological studies. On the other hand, shallower the depth of the target, higher the frequency of the antenna to be chosen. This is the case of GPR on archaeological studies.

Usually GPR antennas are placed on the surface of the ground or slightly elevated above it. The antenna's sensitivity to the ground parameters variation should be minimal. The antenna ringing and coupling should be minimal as well in order to avoid overlapping of target returns with ground reflection or with the coupling. The basic rule for the use of different antennas is; antennas with low frequency detect large objects at large depths. High frequency antennas detect small objects at small depths (Table 2.2).

Table 2.2: The target size and depth range relation between antenna frequencies (Schukin, 2000).

Antenna Frequency (MHz)	**Suitable Target Size (m)**	**Approx Depth Range (m)**
25	1.0	5 – 50
50	0.5	5 – 40
100	0.1 – 1.0	2 – 20
200-250	0.05 – 0.5	1 – 10
500	0.04	0.5 – 5
800	0.02	0.4 – 2
1000	0.01	0.3 – 2
1600	0.01	0.2 – 1
2300	0.01	0.1 – 0.5

Spatial resolution is determined by the area of the region illuminated by a GPR antenna, often referred to as the Fresnel zone or antenna footprint (area illuminated on a buried surface). Most commercial antennas are dipole antennas that radiate linearly polarized energy and the majority of the radiated electric field is orientated along the long axis of the dipole (Annan et al., 1975; Annan and Cosway, 1992; Roberts and Daniels, 1996). For dipole antennas, the area of the antenna footprint is shown in Figure 2.4 and can be approximated using the relationships:

$$A = \frac{\lambda}{4} + \frac{d}{(\varepsilon_r - 1)^{1/2}} \quad \text{and} \quad B = \frac{A}{2} \qquad (1)$$

With λ the center frequency wavelength, d the depth of reflection surface and ε_r the average relative dielectric permittivity to depth d. Equation (1) and Figure 2.4 point out that the GPR pattern becomes more focused with increasing dielectric constant, resulting in higher spatial resolution. Equation (1) can be used to determine antenna frequencies suitable for imaging subsurface targets with known spatial dimensions. The theoretical target areas (Fresnel zone), presented in Table 2.3, are computed using an average dielectric permittivity of 9.

Table 2.3: Footprint diameters A and B at several depths.

Depth(m)	0.5	1	2	3	4	5
A(m)	0.58	0.75	1.11	1.46	1.81	2.17
B(m)	0.29	0.37	0.55	0.73	0.90	1.08

Most antennas have a relatively small footprint, which means that rapid and wide area surveying can only be achieved with multi-channel radar systems or with parallel and several profiles. For road surveys such methods are cost effective and practical. An alternative to planar antenna is the TEM horn, which can be used with a surface to antenna spacing of up to 1 m.

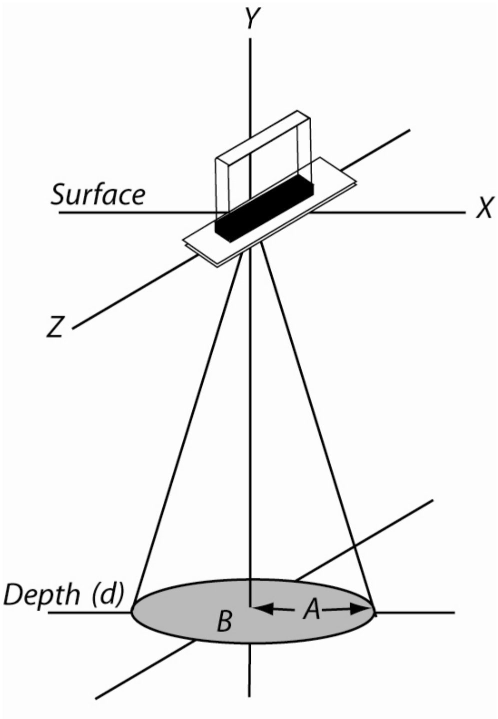

Figure 2.4: Approximate GPR-antenna footprint (Fresnel zone) for bistatic, dipole antennas (adapted from Martinez and Byrnes, 2001). This footprint is calculated using Equation (1). A = long radius; B = short radius; Y = elevation, where X is the surface elevation and d is the depth of the Fresnel zone.

2.3 Data Acquisition

There are several antenna configurations for data acquisition in GPR method. The most used are: *i)* constant offset and *ii)* common midpoint (CMP) antenna configuration. The common offset antenna configuration involves keeping the separation between transmitting (Tx) and receiving (Rx) antennas fixed at all sample locations (Figure 2.5). And this kind of antenna configuration provides single man operation benefit. On the other hand the fixed antenna separation implies that subsurface reflection points will be imaged once only (Figure 2.5b). In the common midpoint antenna configuration the separation between antennas is incrementally increased about some fixed surface location (midpoint) (Figure 2.6). The common midpoint method is mostly used to estimate the velocity of the medium (Figure 2.6b). Nowadays, shielded antennas are used for constant offset acquisitions and unshielded antennas are used for common midpoint acquisition.

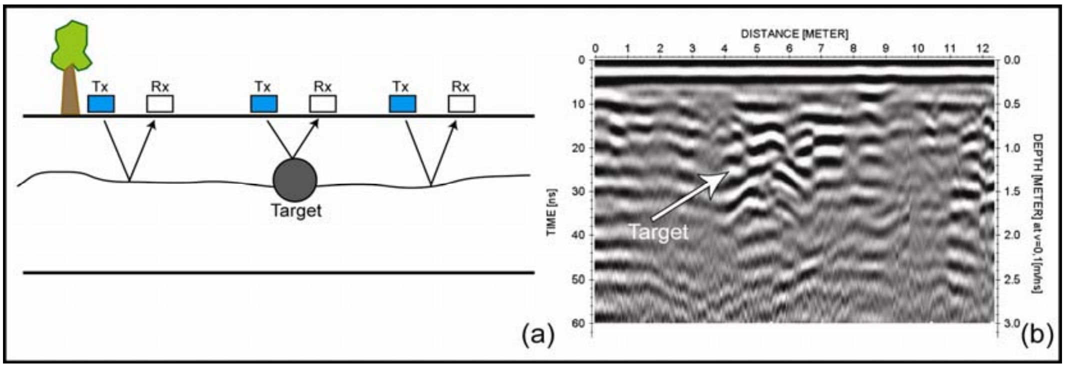

Figure 2.5: GPR acquisition using the constant offset antenna configurations. (a) Schematic diagram view of constant offset acquisition. (b) An example GPR section acquired using constant offset.

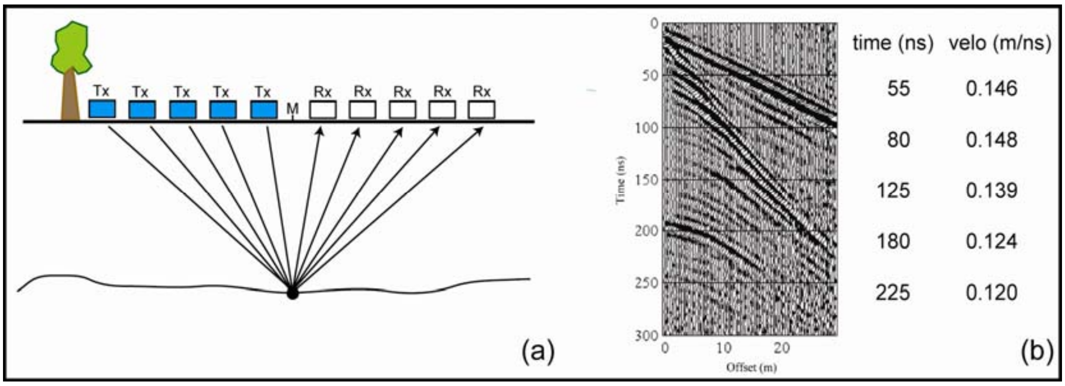

Figure 2.6: GPR acquisition using the common midpoint antenna configurations. (a) Schematic diagram view of common midpoint acquisition. (b) An example GPR section acquired using common midpoint (example GPR section redrawn from Travassos and Menezes 2004).

In our surveys we used shielded antennas to collect GPR reflections. It is located within a box and moved along the ground in transects with a constant offset (Figure 2.7). The transmitting antenna (Tx) generates the propagating radar waves and the receiving antenna (Rx) records the reflection traces generated from subsurface. When many hundreds or even thousands of reflection traces are stacked together, as they are collected along an antenna transect, a reflection profile is produced.

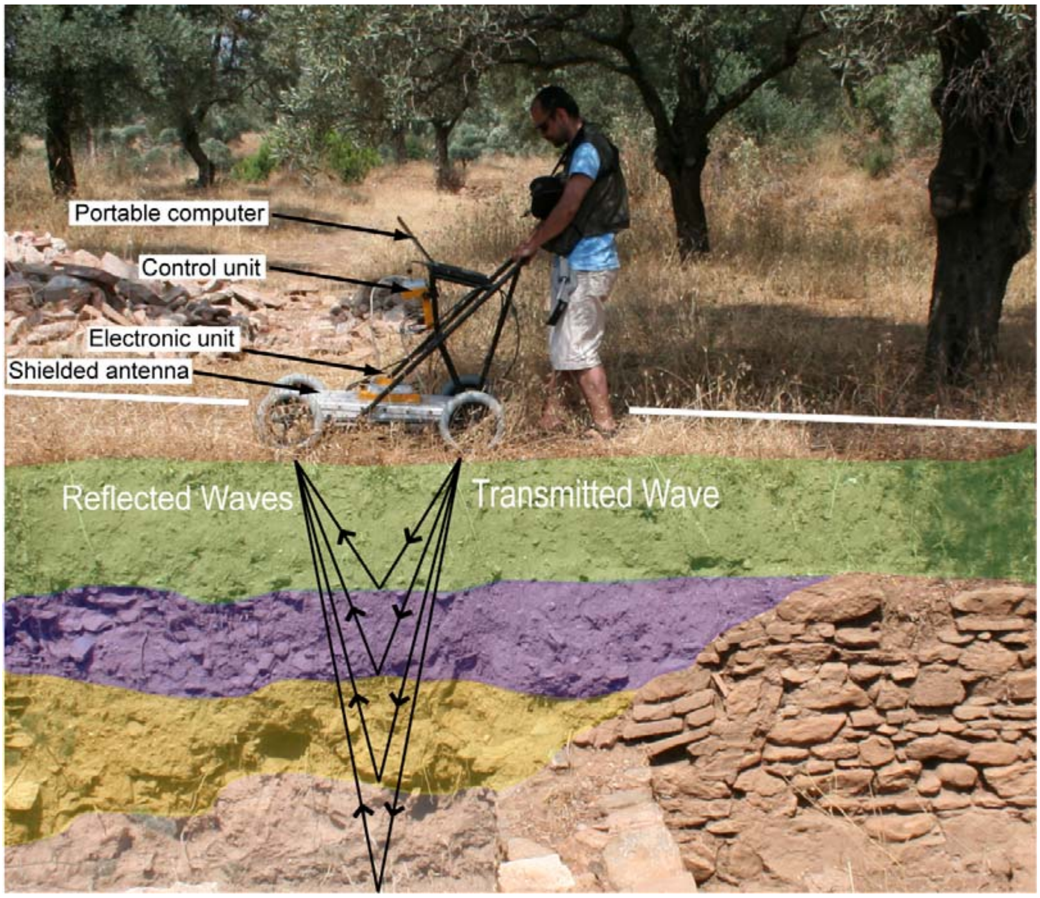

Figure 2.7: Collecting GPR data with 250 MHz shielded antenna with constant offset (Commercial Mala Geoscience Ramac GPR sytem).

Reflection profiles are collected by moving antennas in transects. Within this fiberglass housing, there is a pair of transmitting and receiving antennas, with several center frequencies. Energy is transferred to and from the control system by means of a fiber cable. Most systems can also be programmed to collect data with a survey wheel, or some similar device that can measure where the antennas are in distance along each transect, which can expedite data processing as all recorded reflection traces can be assigned a specific location within a grid.

Usually antennas are placed directly on the ground surface or close to the ground within a fiberglass or hard plastic sled. If antennas are located too far above the ground, energy will not as effectively penetrate the ground as most will be reflected back to the receiving antenna from the ground surface. And also, the operator has to be careful about field conditions. So many times at urban areas GPR system design has to have covered against the medium noise (like using shielded antennas). Or for deeper investigations like mining, geological and structural the operator could choose new kind of low frequency antennas. The new generation of GPR antennas, such as rough terrain antenna provides flexible and rapid surveying.

Generally, GPR surveys are carried out by setting a grid over the preferred area. Rectangular or rectilinear grids are preferable to other grid designs for a number of important reasons. Digital reflection data from a rectangular grid can easily be exported to computer display and imaging processing programs that are pre-set for this gridding method. In this way the data can be quickly processed and interpreted without time consuming transect surveying and drafting. In addition, with a rectangular grid, important reflections in each profile can be immediately correlated to others and reflections can be "tied" to parallel or perpendicular transects throughout the grid. In all cases a sketch of the grid, with notes on the transect length, orientation and beginning and end locations should be noted. The antenna is pulled along profile within the grid. Profiles are typically spaced about 50 to 200 cm apart, depending largely on the antenna frequency being used and the amount of coverage preferred. Time and financial restraints are also common factors affecting collection procedures, since smaller profile spacing will require more surveying time.

The most unexciting, but also important, part of a survey is performed by the person pulling the antennas. This job is the most difficult during continuous data acquisition because the person pulling the sled must not only walk backward but must also make sure that the antennas are moving parallel to the designated transect line. Some people use a cart or other devices to move equipment across the ground.

If data are being acquired in continuous acquisition mode, where radar pulses are being generated at a programmed number per second, the antenna puller must also pay attention to when the antennas move past designated surface markers. At each presurveyed location a marker button must be pushed to place marks in the reflection records. When a survey wheel is used, or antennas are moved in steps, manual marks of this sort are not necessary and antenna pulling is an easier task. Another important aspect of moving the antennas along the ground is making sure that the antennas are in the same orientation and the same distance above the ground, or directly touching it at all times. Changes in antenna orientation with respect to the ground will potentially cause variations in the recorded reflections that can be confused with "real" changes in the ground (Conyers, 2004). This event is called antenna coupling loss. GPR energy coupling variations are also important because these changes can be confused with variations in reflectivity of materials in the ground when viewed in profiles (Figure 2.8).

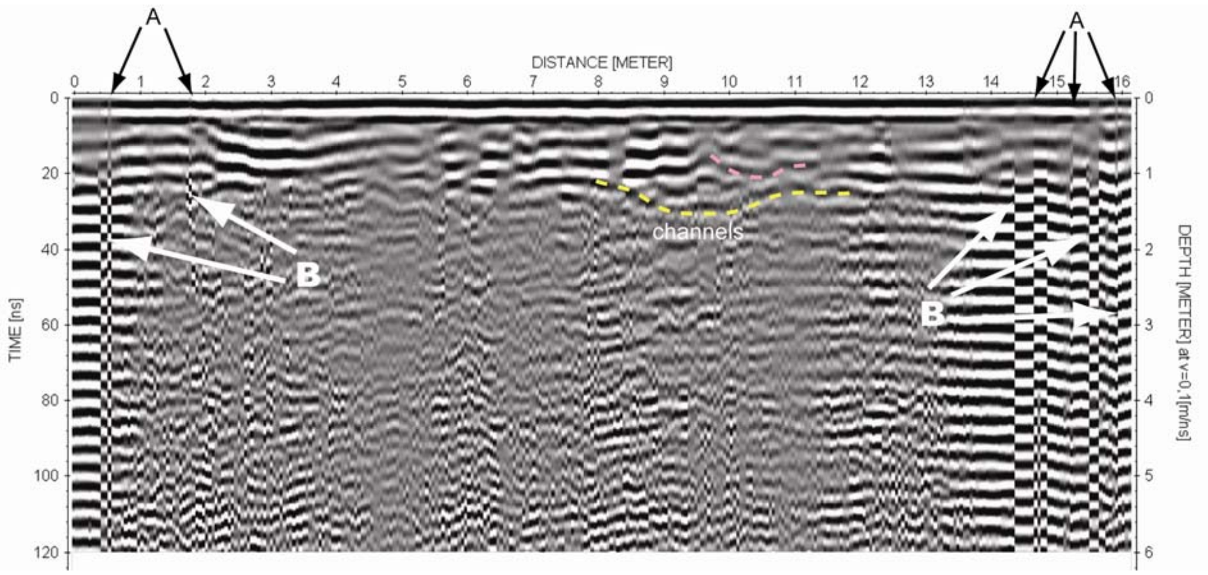

Figure 2.8: A sample GPR profile for showing antenna coupling loss (arrows represent with "A"indicate un-even ground and clumps of vegetation and arrows represent with "B" indicate anomalous amplitude changes).

When antennas move over un-even ground and clumps of vegetation (A), antenna coupling changes the nature of waves traveling through the ground, producing anomalous amplitude changes (B), which can be misinterpreted as geological or archaeological changes.

2.4 Data Processing

The general objective of data processing as applied to GPR is either to present an image that can readily be interpreted by the operator or to classify the target return with respect to a known test procedure or template.

For Daniels 2004, data processing is primarily a means of reducing the noise (called as "clutter" in his book). Fundamentally, the signal to noise ratio of the radar data is the key target detection. Most system noise in GPR systems can be reduced by averaging. GPR is heavily contaminated by noise and reduction of this is a key objective. The cost-benefit of implementation should be clearly demonstrated before superficially attractive but practically unsound methods are incorporated. Clearly, the wide range of targets, applications and situations encountered is likely to task even the strongest algorithm, and the user should assess the most agreeable algorithm with some care.

The image of buried target generated by GPR will not, correspond to its geometrical representation (Figure 2.9). The fundamental reasons for this area related to the ratio of the wavelength of the radiation and the physical dimensions of the target. In most cases for GPR the ratio is close to unity. This compares very differently with an optical image, which is obtained with wavelengths such that the ratio is considerably greater than unity.

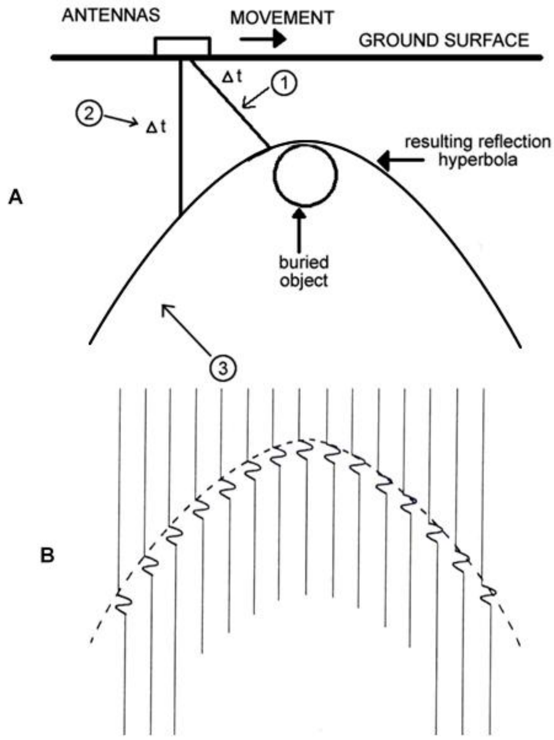

Figure 2.9: Hyperbolic spreading of GPR data. (a) The conical projection of radar energy into the ground will allow radar energy to travel in an oblique direction to a buried point source. The two-way time (Δ t) is recorded and plotted in depth directly below the antenna where it was recorded (1 and 2). (b) When many such reflections are recorded as the surface antennas move toward and then away from a buried object, the result is a reflection hyperbola (3), when all traces are viewed in profile (Redrawn from Conyers 2004).

As the surface antenna moves closer to a buried point source, the receiving antenna will continue to record reflections from the point source prior to arriving directly on top of it, and continue to "see" it after it has passed. A reflection hyperbola is then generated because the time it takes for the energy to move from the antenna to the object along many oblique paths is greater the farther the antenna is away from the source of the reflection. As the antenna moves closer to the buried object the reflection from it is recorded closer in time until the antenna is directly on top of it. The same extraordinariness is repeated in reverse as the antenna passes away from the source, resulting in a hyperbola where only its apex specify the actual location of the buried source, with the arms of the hyperbola creating a record of reflections that traveled the oblique wave paths.

There can also be point-source reflections that are generated from one distinct point feature in the subsurface. The buried materials that generate these types of point-source reflections could be individual rocks, metal objects, pipes that are crossed at right angles, and a great variety of other smaller objects of this sort. They are visible in two-dimensional profiles as reflection hyperbolas (Figure 2.10).

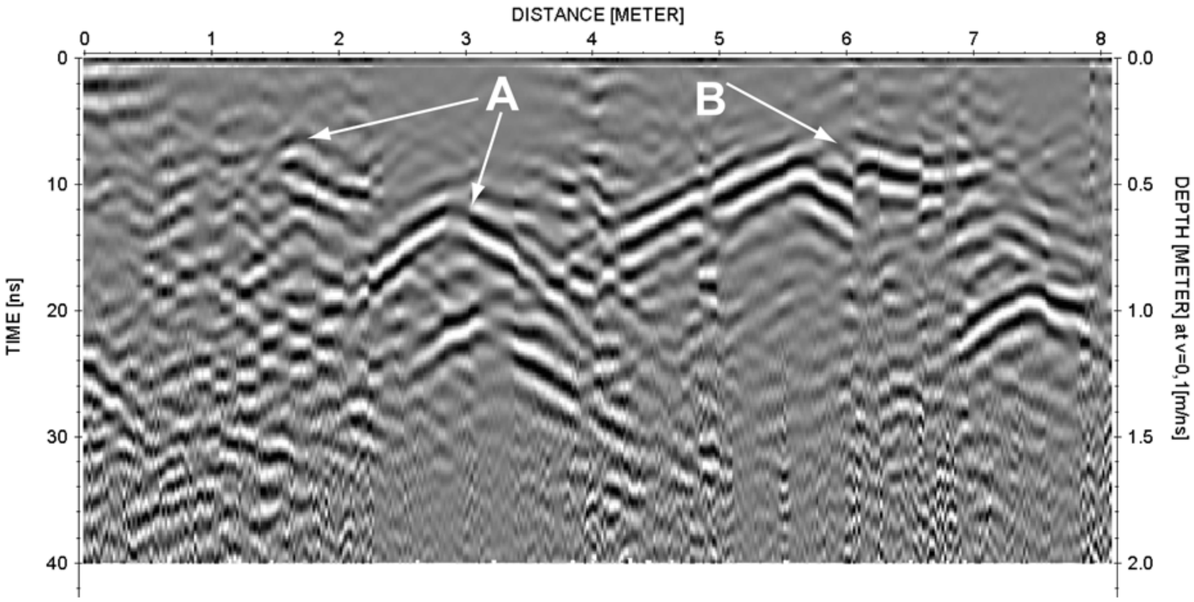

Figure 2.10: A sample GPR profile for showing point source hyperbolas. Point source hyperbolas (A) are generated from buried objects of a limited size. In this case the hyperbola on the right was generated from a metal pipe and the lower amplitude hyperbola on the left from a plastic pipe. The series of high amplitude reflections that are stacked vertically at location B were generated by a large piece of metal near the ground surface.

Point source reflection hyperbolas, also termed diffractions, are generated because most GPR antennas produce a transmitted radar beam that propagates downward from the surface in a conical pattern, radiating outward as energy travels to depth (Conyers, 2004). The pattern of energy dispersal will therefore spread out and be reflected from buried features that are often not located directly below the transmitting antenna (Figure 2.9).

The quality of the original data required an appropriate processing for easier interpretation. For this processing work we used commercially available Reflex W (Sandmeier, 2003) software. The main processing steps can be summarised as follows;

- **a.** Raw data (Figure 2.11a)
- **b.** Move starttime (manual input): The filter acts on each trace independently. The processing step move starttime facilitates a static correction in time direction by a given value (Figure 2.11b).
- **c.** Subtract-mean (dewow): The filter acts on each trace independently. With this option activated a running mean value is calculated for each value of each trace. This running mean is subtracted from the central point (Figure 2.11c).
- **d.** Energy decay: The filter acts on each trace independently. By activating this option a gain curve in y-(time-) direction is applied on the complete profile based on a mean amplitude decay curve which is automatically determined. The information of the true amplitude is lost, of course. First a mean decay curve is determined from all existing traces. After the application of a median filter on this curve every data point of each trace is divided by the values of the decay curve. After the multiplication of the energy decay curve all data points are automatically multiplied by a scaling factor (Figure 2.11d).
- **e.** Subtracting average: This filter acts on the chosen number of traces. The filter performs a subtracting average over an eligible number of traces for each time step. The filter performs a so called sliding background removal. For a bandwidth of 4 the current sample, the next two in horizontal direction to the left and the next two in horizontal direction to the right, i.e. five samples for each time value, are taken into account. If between the current sample and the first or the last trace are fewer samples than half the window width, the window width is decreased on one side. From these five samples the mean value is calculated. This mean value is subtracted from the value of the current sample and the result is assigned to the current sample as new value (Figure 2.11e).
- **f.** Velocity analysis with the diffraction hyperbolas method (Figure 2.11f).
- **g.** Topographic correction (where needed).

A way to obtain visually useful maps for understanding the plan distribution of reflection amplitudes within specific time intervals is the creation of horizontal time slices. This data representation plays an important role in GPR investigations as it allows an easier correlation of the most important anomalies found in the area at the same depth, thus facilitating the interpretation (Leucci and Negri, 2006).

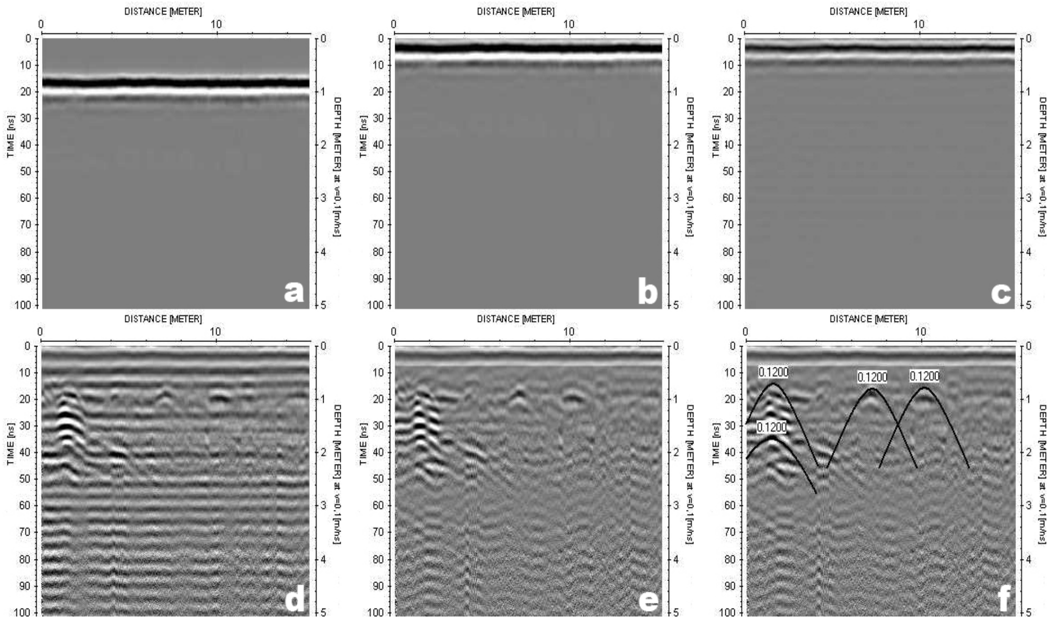

Figure 2.11: An example GPR profile and its processing steps. (a) Raw data. (b) After filtered with move starttime. (c) After filtered with subtract-mean (dewow). (d) After filtered with energy decay. (e) After filtered with subtracting average. (f) After velocity analysis with the diffraction hyperbolas method.

Nevertheless GPR applications in an urban area also have other problems like artificial frequency noise from military radio, mobile phone antennas and the other transmitting factors (Figure 2.12). With this kind of frequency (different from our central frequency) the GPR data has emulated hyperbolas and reflectors. For solving the frequency noise a bandpass frequency filter could be applied. This filter band is specified by the setting of four frequency values (Figure 2.13). The first point determines the low-cut frequency (f_1 in Figure 2.13), the second one the beginning of the plateau (lower plateau) (f_2 in Figure 2.13). Between the low-cut frequency and the beginning of the plateau the filter is represented by a cosine-window. The third point determines the end of the plateau (upper plateau) (f_3 in Figure 2.13) and the fourth the high cut frequency (f_4 in Figure 2.13). Between these points the filter is represented by a cosine-window, too. The frequency spectrum below the low cut (f_1 in Figure 2.13) and above the high cut frequency (f_4 in Figure 2.13) is set to zero. By the corresponding choice of the points of the bandpass either a lowpass or a highpass can be approximately realized.

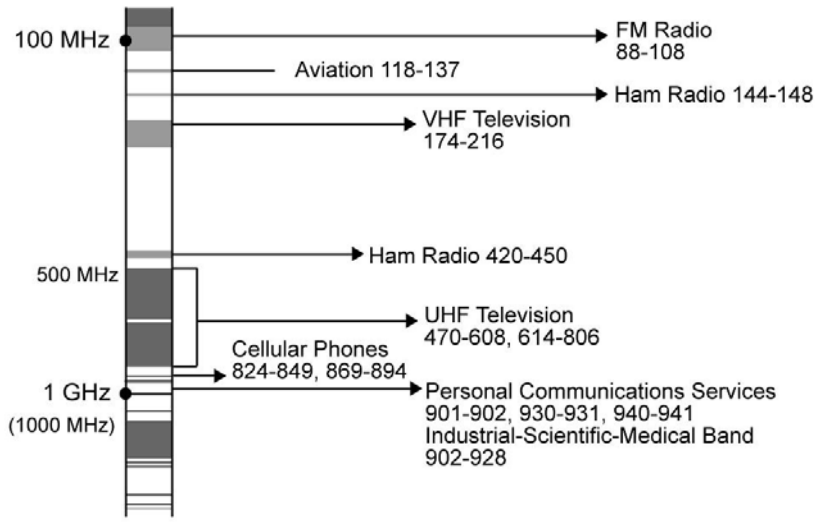

Figure 2.12: Radio spectrum in an urban area.

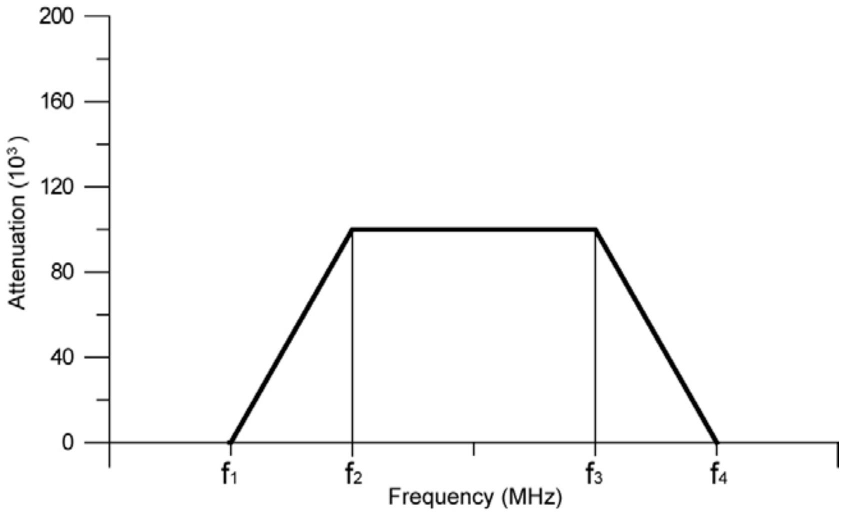

Figure 2.13: Schematic description of bandpass frequency filter.

A common complication that affects resolution of reflections in the ground is background noise, which is almost always recorded during GPR surveys. Ground-penetrating radar antennas employs electromagnetic energy of frequencies that are similar to those used in television, FM radio and other radio communication bands, so there is almost always nearby noise generators of some kind (Figure 2.12).

In summary the following steps must be considered prior to selecting an antenna that will allow for the best subsurface resolution at any study site (Conyers, 2004):

1. Obtain as much information as possible about the electrical and magnetic properties of the soils and sediments at a site. If this cannot be determined by direct field measurements (which is often very difficult to do), the type of soil and geologic materials and their moisture, should be known in advance and estimates of RDC can be made (Table 2.1).
2. Define the depth of the prospective target features and their approximate dimensions and composition. Using estimates of RDC, the cone of transmission can be predicted and potential resolution of features of interest can be estimated from the footprint size using different frequency antennas (Figure 2.4). From this calculate whether energy can be transmitted to the depth necessary to resolve the features of interest with the antennas available.
3. Decide whether or not it is physically possible to use the selected antenna frequency at the site to be surveyed. Transportability to and from the site and deployment over and around obstacles and obstructions once surveying is begun must be accounted for.
4. If it is known that there is a substantial amount of radio interference present at a site, and if the source can be identified, then it may be appropriate to choose an alternate antenna frequency so as to minimize that influence. In general this is not a simple task because it is difficult to identify sources and the risk of compromising survey objectives exists if the wrong antenna is chosen for only this reason.

The GPR data are sometimes contaminated by diffractions from above-ground objects, such as poles, power lines, metallic fences, trees and building (Figure 2.14). Thus, it is very important to recognize the diffractions and determine whether they are from subsurface heterogeneities or from surface scattering (Bano et al., 2000).

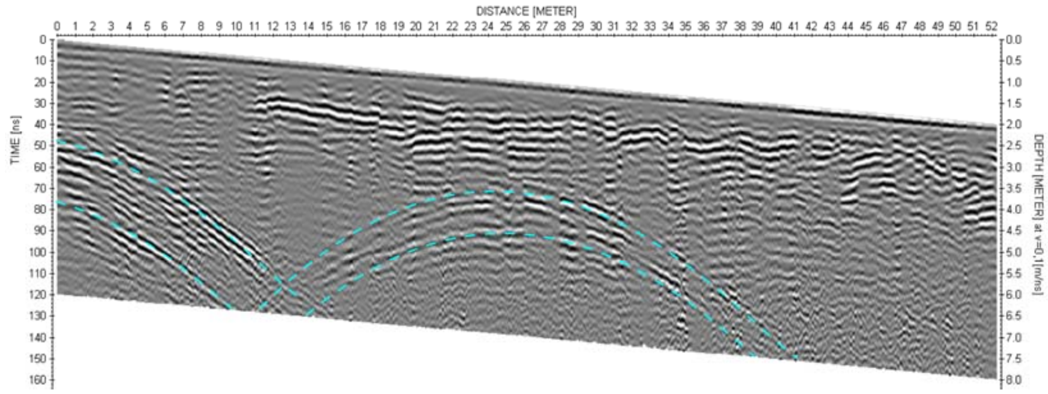

Figure 2.14: GPR data with modeled diffractions from the surface scatterers (light blue hyperbolas) superimposed. With a velocity of 0.3 m/ns was used.

After acquiring of GPR data some other processing programs could be helpful for presenting the data. For example Radlab (Girard, 2000) is a processing program written in MATLAB® programming language.

3 GEOLOGICAL SETTINGS OF STUDY AREA

Although this study does not address some of the plate tectonic problems in western Turkey, this section contains a tectonic overview of the region because the Büyük Menderes graben is one of the main products of the geodynamic processes. Western Turkey is a neotectonic domain of Anatolia (McKenzie, 1972 & 1978; Şengör, 1979; Dewey & Şengör, 1979; Şengör et al. 1985) within the larger extensional province that occupies western Turkey, the Aegean Sea and most of Greece. Present-day deformation in western Turkey is the result of westward motion of Anatolia mainly along the North and East Anatolian fault zones. This motion is leading to the province experiencing roughly N – S extension (McKenzie, 1972 & 1978; Le Pichon & Angelier, 1979; Şengör, 1987; Görür *et al*. 1995; Yılmaz et al. 2000) which has given rise to a distributed horst and graben topography that characterizes most of western Turkey. The initiation age of the present tectonic regime of western Turkey is in debate but it is agreed that western Turkey has been dominated by extensional deformation since the subduction of African plate commenced (Dewey & Şengör, 1979; Angelier, 1979; Seyitoğlu *et al.* 2000 and 2004;).

Considering the aim of this study, previous geological studies are not given in detail; stratigraphy, tectonic structures and seismological activity of the region are outlined in this chapter.

3.1 Stratigraphy

The Büyük Menderes graben extends between the Aegean Sea in west and Denizli basin in east (Figure 1.1) but the study area is located between Kuyucak to the east and the Aegean Sea to the west (Figure 1.4). The width of the graben changes between 8 and 12 km. Mapping of geological units by MTA (1964), and recent geological studies (MTA, 1964; Cohen *et al.* 1995; Emre & Sozbilir, 1995; Bozkurt, 2000; Ocakoğlu *et al.* 2007) showed that there are three main rock associations in the Büyük Menderes graben (Figure 3.1). These are Pre-Neogene basement rocks, Neogene units and Quaternary deposits.

Pre-Neogene basement rocks including mainly marbles, schists and limestone crop out along both sides of the graben (Figure 3.1). Neogene units consist of continental clastic sediments and they crop out in west of Bafa Lake, around Söke, between Ortaklar and Kuyucak along the northern side of the graben and around Yenipazar (Figure 3.1). As observed by previous researchers (e.g. Cohen *et al.* 1995; Hakyemez et al. 1999; Paton, 1992; Bozkurt, 2000) the lower part of part of Neogene units include polygenetic conglomerate, siltstone, mudstone, shale alternations and sandstones. The upper part of Neogene units includes conglomerates, sandstone, siltstone, mudstone and claystone (Figure 3.2).

Quaternary units include alluvial fan deposits and graben floor sediments. Alluvial fans are mainly located along the northern margin of the graben and their source is the Pre-Neogene basement rocks and Neogene units.

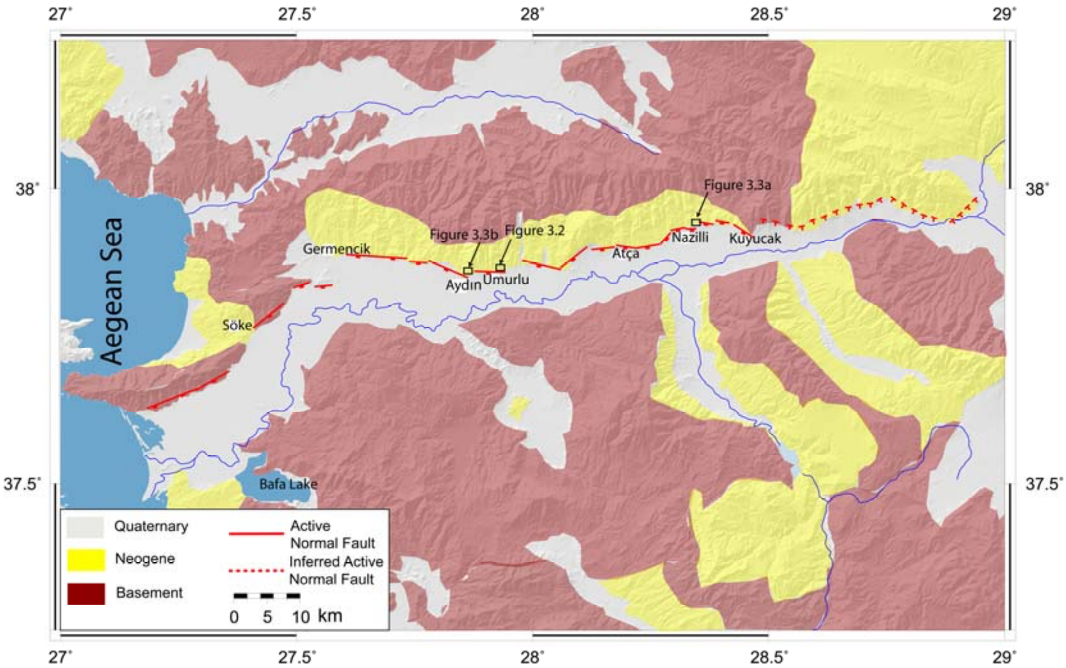

Figure 3.1: Simplified geological map on elevation map of the Büyük Menderes Graben showing general geological units (MTA 1/500.000 geological map of Turkey).

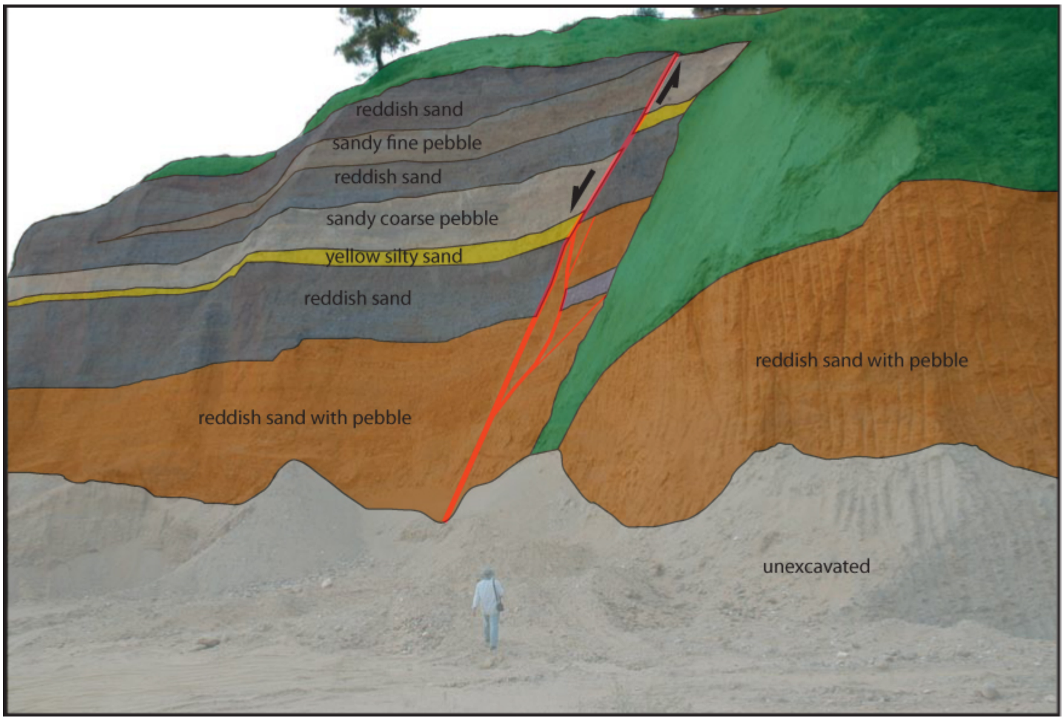

Figure 3.2: Upper Neogene units in northwest of Umurlu (see Figure 3.1 for location).

The units of the study area are bounded by faults. Western side of the graben, Neogene units are not visible near Priene and Sazlıköy (on the north) and the boundary of the Pre-Neogene units and Quaternary units are controlled by fault (Figure 3.1). Low angle normal faults separates Neogen units from Pre-Neogene bed rock in the northern margin of the E-W trending part of the graben. (Figure 3.3a) (Bozkurt, 2000). In this part of the graben the contact between Neogene units and Quaternary basin fills is also a fault which is the active boundary fault of the graben (Figure 3.3b).

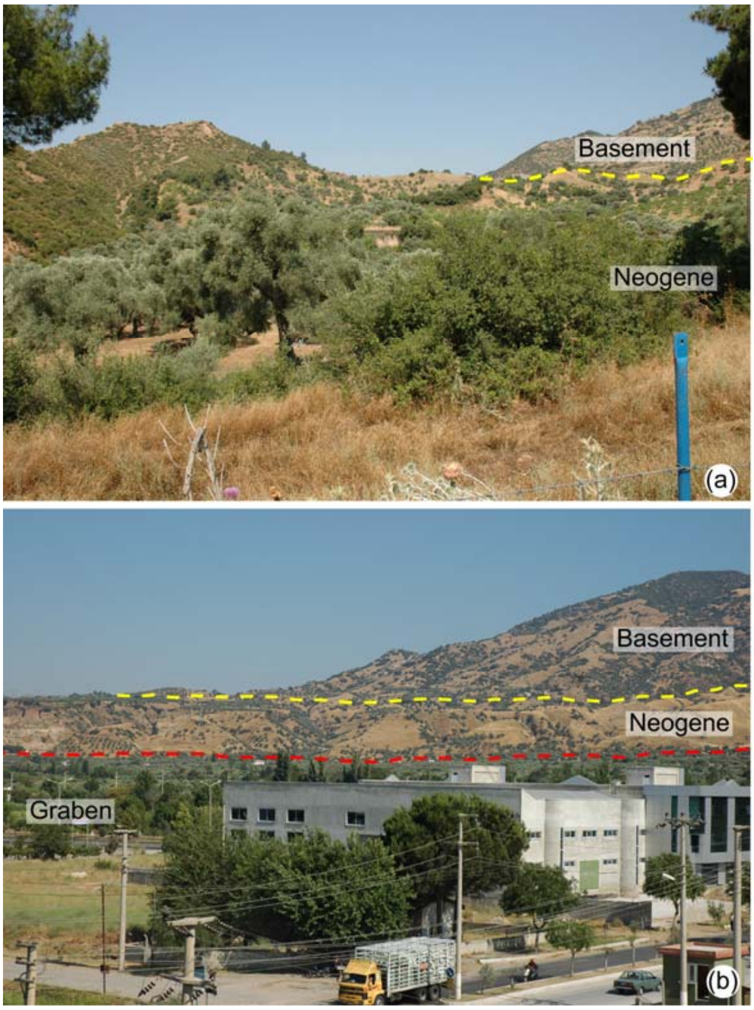

Figure 3.3: Relation between geological units in the study area. (a) Neogene clastics are separated from Pre-Neogene basement (Menderes massive) by a low angle normal fault (yellow dashed line) (b) Neogene clastics are separated from Pre-Neogene basement (Menderes massive) by a low angle normal fault (yellow dashed line)and the active fault (red dashed line) separates graben deposits from Neogene clastics (see Figure 3.1 for location).

Pre-Neogene and Quaternary graben fill has contact on the southern margin of the graben the area between Bafa Lake and Yenipazar town. However Neogene rocks and Quaternary units have contact around Yenipazar town and west of Bafa Lake. These contacts are probably faulted on the southern margin of the graben (Cohen *et al.* 1995).

3.2 Tectonic Features of the Study Area

3.2.1 A General Overview of the Menderes Graben

The initiation age of neotectonics and development of grabens in western Turkey are under discussion (Dewey & Şengör, 1979; Şengör et al. 1985; McKenzie, 1978; Le Pichon & Angelier, 1979; Seyitoglu & Scott, 1991, 1992; Bozkurt & Park, 1994, 1997). However, it is agreed that western Turkey has been experiencing roughly N-S extension and major grabens (such as Büyük Menderes and Gediz) are the results of this active stretching (Figure 3.4). Considering the aim of this study, previous discussions about neotectonic of western Turkey are not given in detail and only major active faults of the graben are described here.

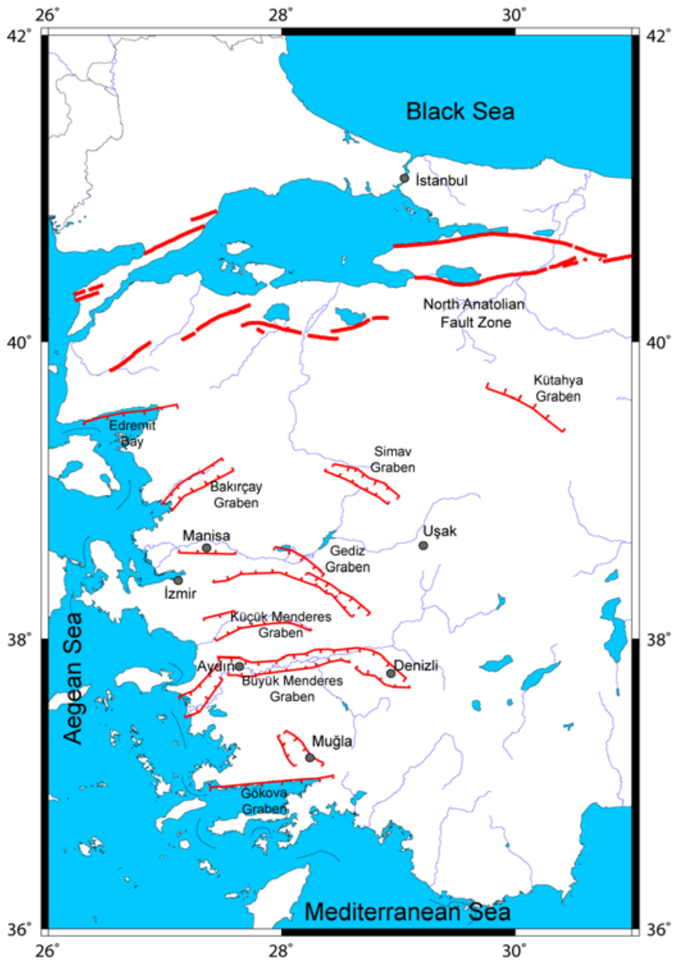

Figure 3.4: Main active tectonic structures in Western Anatolia (simplified from Bozkurt, 2000).

Main active faults are located along the northern side of the Büyük Menderes Fault Zone are located on the northern margin of the graben (Figure 3.5). Active faults of the northern margin cannot be located in east of Kuyucak due to large alluvial fans sourced from high topography in the north (Figure 3.6). The fault extends linear between Güzelköy village and east of Nazilli and the fault is located between Pleistocene units and Holocene sediments. The fault is traced as a single line until west of Nazilli where it makes a stepover to south. After the stepover, the fault is sited in Quaternary units around Atça town. The fault extends as a single line from Atça to Sultanhisar and makes a stepover to south about 2 km west of Sultanhisar. From Köşk, it continues as a single segment towards west until Aydın and it defines the boundary between Neogene and Quaternary units in this part of the graben. The fault cannot be traced in the city center of Aydın because of intense construction. Fault morphology is clear between Aydın and

Germencik but it is difficult to map it due to man – made activity and wide alluvial fans. North of Germencik, fault can be traced by fault scarps and it makes a big stepover to south around Morallı village. Morphological evidences of the western part of the graben can be traced from Reisköy Village. Fault continues to Sazlıköy village on NE-SW direction and its trend changes to NE-SW near Söke town. Because of the dense urbanization, it cannot be traced in the city center of Söke and it makes a stepover to south. It is very complicated to determine the active fault on this stepover area because of wide alluvial fans that produced by well developed streams. From this area active fault continue through west on NE-SW direction. On the western end of the graben fault extends approximately NE-SW direction from Güllübahçe town to the Aegean Sea. This area is bounded by limestones on 1000m elevation and Neogene units cannot be determined. In western end of the graben, it is hard to distinguish the morphological features of the faults because of the recent activity of the Meander River and well developed alluvial fans.

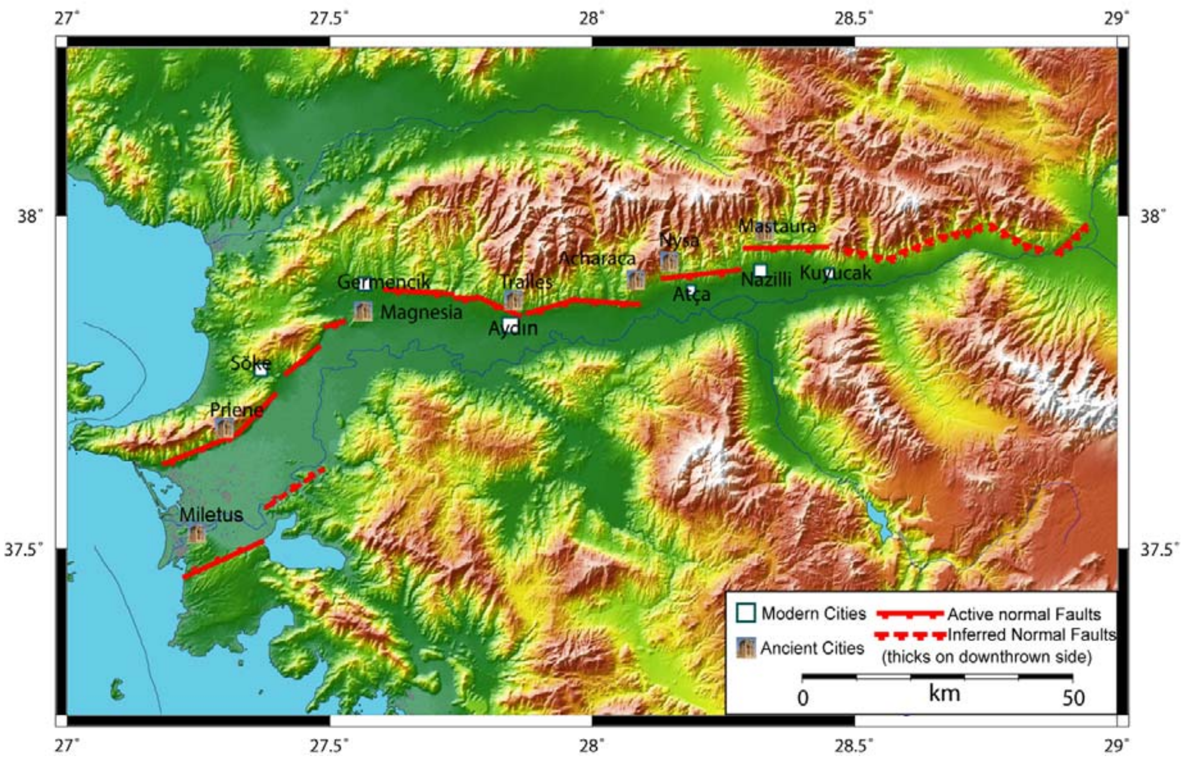

Figure 3.5: The morphotectonic map of the Büyük Menderes graben and its cities (Altunel et al., 2009).

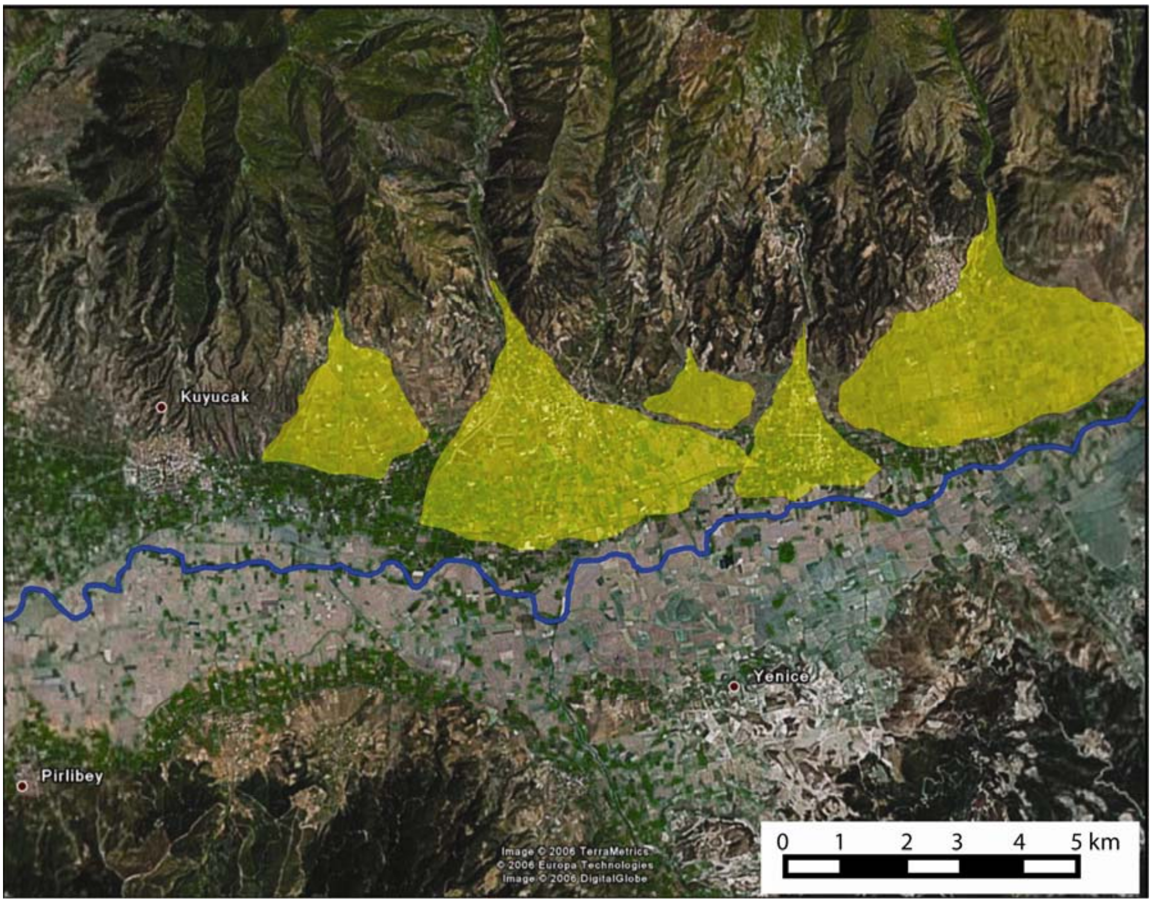

Figure 3.6: The satellite view of Kuyucak and its neighborhood. The large alluvial fans cover the fault traces (the satellite view taken from Google earth).

3.2.2 Characteristics of Faults in the Studied Locations

Argavlı Trench site and Ottoman Bridge;

The general trend of the fault between Reisköy and Argavlı is E – W (Figure 3.7). Fault morphology is clear between Argavlı and Morallı villages (Figures 3.8a and 3.8b) but further east of Morallı , the morphology is less clear (Figure 3.8c). The fault makes a right stepover between Argavlı and Morallı villages. It separates Quaternary deposits from Neogene hills around Morallı and Reisköy villages but it is in Quaternary deposits in east of Argavlı village. The study site is located 1.5 km east of Argavlı village. The trend of the fault is NE – SW in south of Argavlı. It separates Quaternary deposits from the basement Limestone (Figure 3.7). The fault plane is well exposed in Limestone and slickenside on fault plane indicate normal throw to south combined with dextral component around Sazlıköy. The trend of the fault is ENE – WSW (Figure 3.9) and the fault separates Quaternary deposits from the Limestone basement (Figure 3.10).

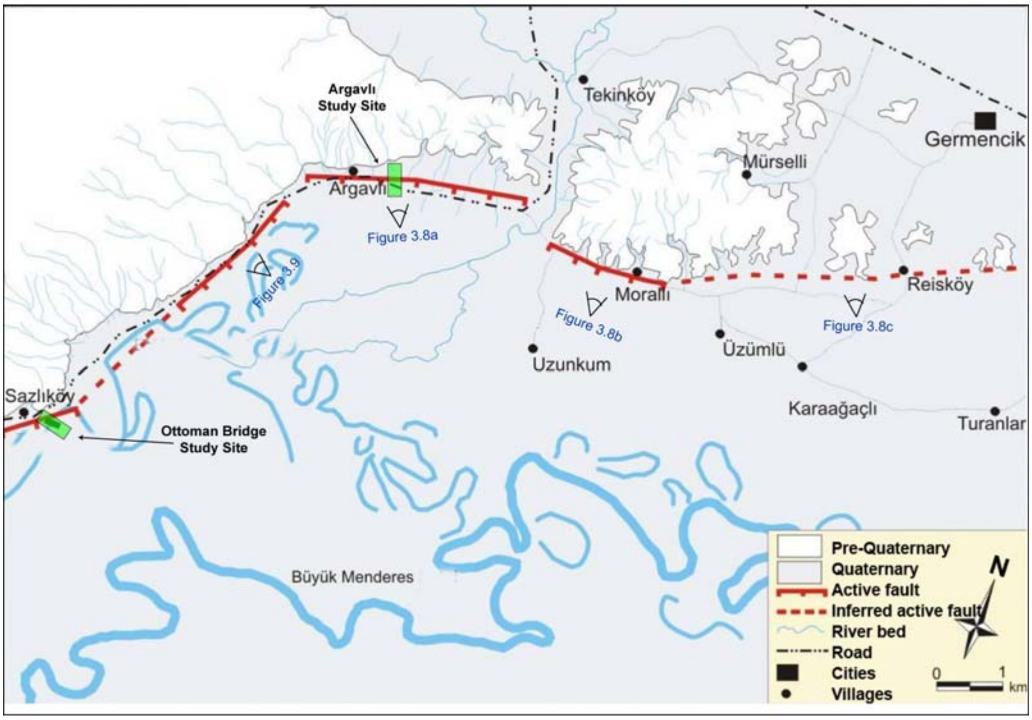

Figure 3.7: Geological and active faults map between Germencik and Sazlıköy.

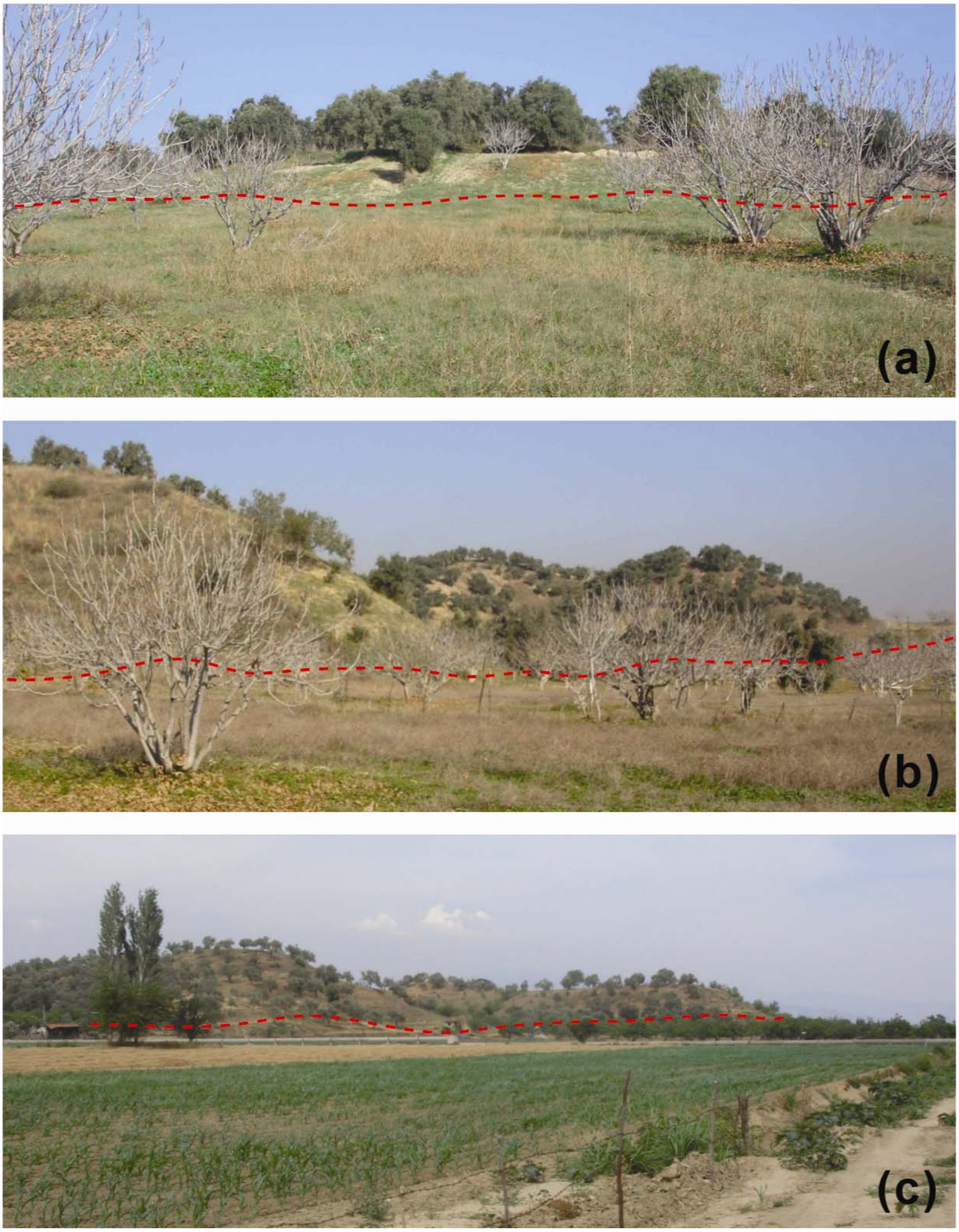

Figure 3.8: (a) The fault scarp near Argavlı village (view towards N). (b) The fault scarp near Moralı village (view towards NE). (c)The fault scarp near Reisköy village (view towards NE) (red dashed lines represent fault zones).

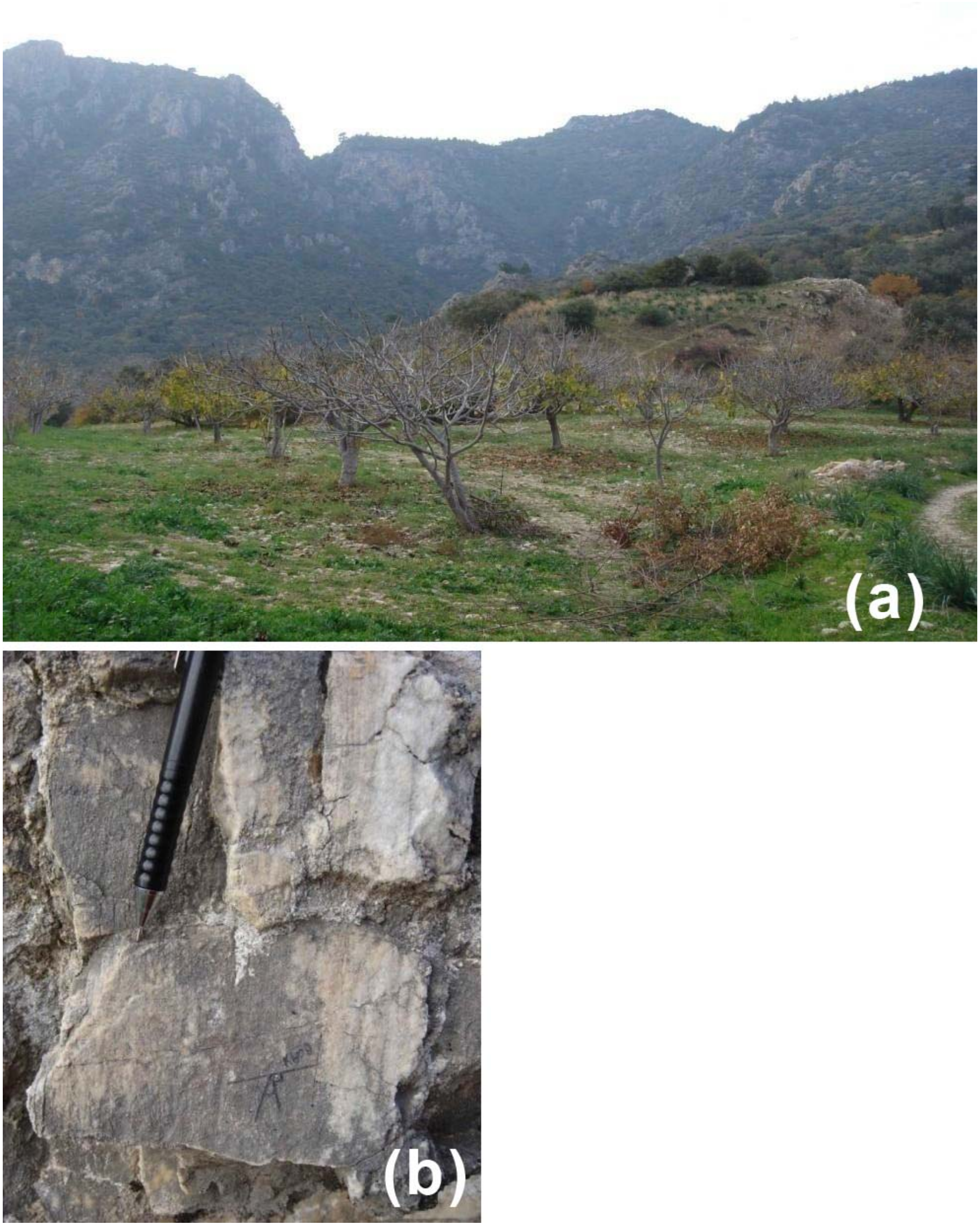

Figure 3.9: (a) The fault trace between Sazlıköy and Argavlı village (view towards NW). (b) The fault plane and fault scratches between Sazlıköy and Argavlı village.

Figure 3.10: The Ottoman Bridge located near Sazlıköy and the fault scarp at the background.

Atça trench site;

The general trend of the fault is N80^{o}E and southern block downthrown along the fault (Figure 3.11). The fault separates Quaternary deposits from Neogene units and the morphological scarp is well exposed (Figure 3.12).

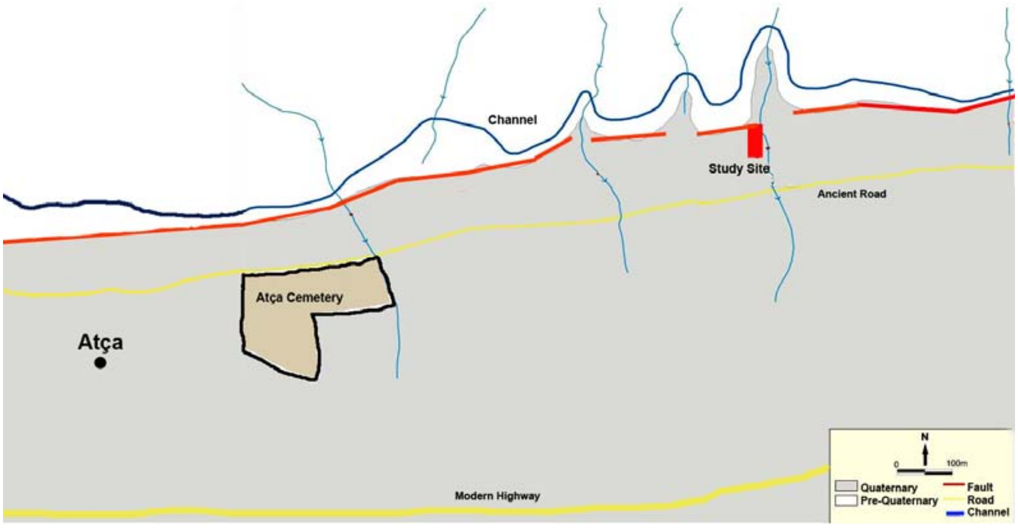

Figure 3.11: Basic geological and active faulting map of Atça trench site and its neighbourhood (red square indicates the surveyed area).

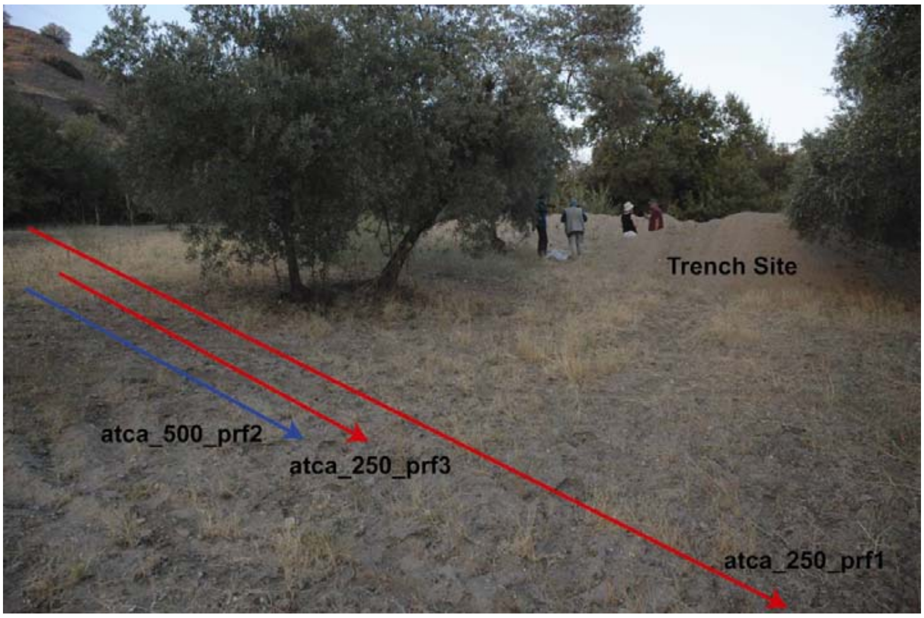

Figure 3.12: GPR profiles and trench location illustration on the site photo (looking towards north).

Roman Wall and Roman Road;

The fault extends in E – W direction in east of Sultanhisar but its trend slightly changes to N80°E in west of Sultanhisar (Figure 3.13). The southern side downthrown along the fault. The fault mainly follows the Quaternary – Neogene border but it is in Quaternary deposits in same places. The morphological scarp is well exposed around Sultanhisar (Figure 3.14).

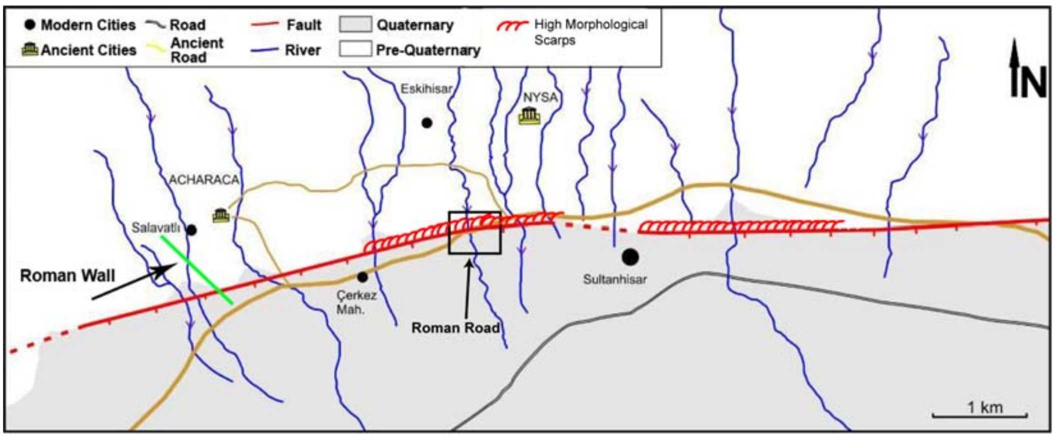

Figure 3.13: The location of the ancient road and active faults around Sultanhisar. The green line indicates Roman Wall and black box indicates intersection point of the Roman Road and the fault.

Figure 3.14: The Roman road (looking towards east) (the dashed red line corresponds with the fault zone between Pre-Quaternary and Quaternary units and the yellow arrows show the vertical displacement (~5 m.) of the road).

3.3 Seismic Setting of the Study Area

Western Turkey is one of the most seismically active regions within the Alpine-Himalayan belt (Jackson & McKenzie, 1988b), the principal active structures being the E-W –trending Büyük Menderes and NW-SE-trending Gediz half grabens. In order to understand the long term seismicity of the region, a historical perspective is necessary, instrumental data being available only for events of the 20th century (Table 3.1). Although such historical and archaeological data can broaden the information base for the study events, it still remains difficult dating and locating specific earthquakes. Despite there are several earthquake catalogues for the region, most are based on secondary sources and thus it is necessary, as argued by Ambraseys (1998), for all the historical and instrumental data to be identified. The detailed list of all earthquakes between 14th century BC and 1900 AD given in Table 3.2 and in Figure 3.15 the earthquakes are shown on elevation map between 14th century BC and 2007 AD.

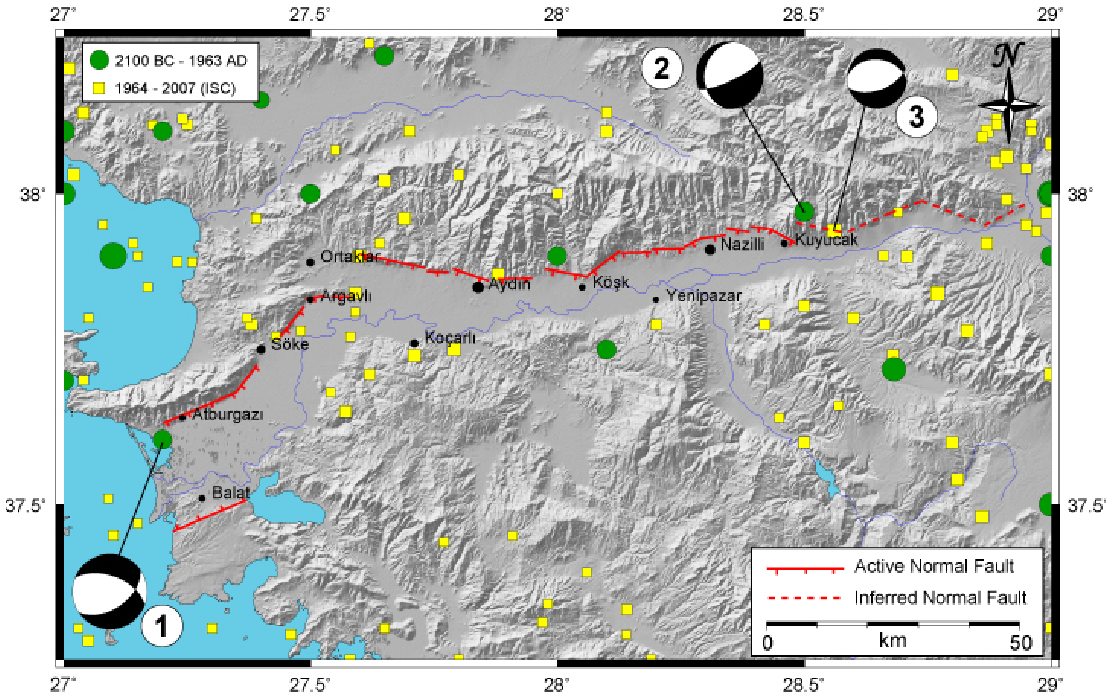

Figure 3.15: Seismicity map of Büyük Menderes graben between 2100 BC – 2007 AD (Tan et al., 2008). And 3 recent earthquakes with focal mechanism (1. Location: 37,600-27,200– Ms: 6,8 – Date: 16-07-1955 (McKenzie, 1972), 2. Location: 37,970-28,500 – Ms: 6,1 – Date: 25-04-1959 (McKenzie, 1972) and 3. Location: 37,940-28,560 – Ms: 5,4 – Date: 11-10-1986 (Taymaz, 1991)).

Table 3.1: Instrumental data of earthquakes at Büyük Menderes Graben between 1938 – 2004 (Tan et al., 2008).

No	Date	Coordinate	h	m_o	M_s	$S_1/D_1/R_1$	$S_2/D_2/R_2$
1	16/07/1955	37,6-27,2	6	6,8	-	55/51/-133	292/55/-49
2	25/04/1959	37,97-28,5	43	6,1	-	65/76/-70	188/24/-144
3	11/10/1986	37,94-28,56	15	5,4	5,4	275/35/-70	71/57/-103

Büyük Menderes graben contains normal fault segments that have ruptured during major events in the historical period and during the 20th century, for which time-reliable instrumental records are available. There are only a few reports of surface faulting although the historical record is long, spanning the period from 2100 B.C. to 1900 A.D. (e.g. Dikmen, 1952; Ergin *et al*. 1967; İlhan, 1971; Sipahioğlu, 1979; Soysal *et al*., 1981 ; Ateş and Bayülke, 1982; Bean, 1989; Gençoğlu *et al*., 1990; Goidobani *et al*., 1994; Ambraseys and Finkel, 1995).

Table 3.2: Earthquakes at Büyük Menderes Graben.

Date	Coordinate	I_0	References
14th century BC	37.93-28.35	IX	Dikmen, 1952
1st century BC	37.86-28.06	VIII	Dikmen, 1952
65 BC	37.45-29.10	VIII	Soysal *et al.*, 1981
40 BC	37.86-28.06	VIII	Dikmen, 1952
31/30 BC	37.85-27.84	VIII	Dikmen, 1952. Sipahioğlu, 1979
26/25 BC	37.85-27.84	VIII	Bean, 1989., Sipahioğlu, 1979
20 BC		VII	Ambraseys and Finkel, 1995. Bean, 1989
12/11 BC	37.84-27.84	VIII	Ergin *et al.,* 1967, Sipahioğlu, 1979
60 AD	37.55-29.10	IX	Ergin *et al.,* 1967, Goidobani *et al.*, 1994, İlhan, 1971, Soysal *et al.*, 1981
68 AD	37.74-27.40	VII	Ergin *et al.,* 1967
3rd century AD			Goidobani *et al.*, 1994
238	37.86-28.06	VIII	Dikmen, 1952
244	37.86-28.06	VIII	Dikmen, 1952

262	37.86-28.06	VIII	Dikmen, 1952
494			Bean, 1989., Goidobani *et al.*, 1994
7th century			Goidobani *et al.*, 1994
747	37.86-28.06	IX	Dikmen, 1952
1354			Ateş and Bayülke, 1982
1651	37.50-29.20	VIII	Ambraseys and Finkel, 1995, Soysal *et al.*, 1981
22.2.1653	37.93-28.35	IX	Ambraseys and Finkel, 1995, Dikmen, 1952, Gençoğlu *et al.*, 1990, Sipahioğlu, 1979
1702/(1703)	37.50-29,20	VIII	Ambraseys and Finkel, 1995, Ergin *et al.,* 1967, Soysal *et al.*, 1981
19.11.1717			Ambraseys and Finkel, 1995
1744	37.93-28.35	VIII	Dikmen, 1952
1744			Ateş and Bayülke, 1982
21.06.1846		IX	Ergin *et al.,* 1967
1848	37.84-27.80	V	Ergin *et al.,* 1967
27.10.1848	37.85-27.84	VI	Sipahioğlu, 1979
09.07.1850	37.85-27.85	VI	Sipahioğlu, 1979
06.1885	37.85-28.20	V	Ergin *et al.,* 1967
04.1886	37.45-29.05	VI	Ergin *et al.,* 1967, Soysal *et al.*, 1981
01.1887	37.50-29.05	VII	Soysal *et al.*, 1981
18.09.1891	37.74-27.40	VI	Ergin *et al.,* 1967
20.08.1895	37.85-27.84	IX-X	Ergin *et al.,* 1967, Sipahioğlu, 1979
14.11.1895	37.84-27.80	V	Ergin *et al.,* 1967
1896	37.84-27.80	V	Ergin *et al.,* 1967
02.1898	37.90-28.0	VI	Ergin *et al.,* 1967
20.09.1899	37.90-28.10	IX	Ambraseys and Finkel, 1995, Dikmen, 1952, Ergin *et al.,* 1967, Gençoğlu *et al.*, 1990, Sipahioğlu, 1979, Soysal *et al.*, 1981
12.1899	37.45-29.05	VI	Ergin *et al.,* 1967, Soysal *et al.*, 1981

The first reported catastrophe in the Büyük Menderes graben was the 60 A.D. earthquake (I_o=IX) at Hierapolis (Pamukkale), located at the eastern end of the graben (Ergin *et al.,* 1967; İlhan, 1971; Soysal *et al.*, 1981). According to Altunel & Hancock (1993b), the approximately 500-m-long fault scarp at the toe of the Pamukkale range-front was possibly created during this earthquake. İlhan, (1971) reported that one of the biggest seismic catastrophes in the Aegean region was the 1653 earthquake (I_o=IX) which affected the whole of western Turkey. According to Allen, (1975), a fault break related to this earthquake, can be followed for a distance of about 70 km from Kuyucak towards the west, the south side having been downthrown by as much as 3 m along the northern boundary of the Büyük Menderes graben. The 20 September 1899 Menderes earthquake (I_o=IX) broke the same segment for about 50 km westwards from Kuyucak, with again the southern block being downthrown south, but this time by less than 1 m (İlhan, 1971; Ambraseys, 1988). According to Altunel (1999), field evidence suggests that, in addition to south-side down-throw by as much as 2 m during this earthquake, there was also at least 1.5 m opening along the surface break. Although Paton (1992) claimed that the displacement in the 1899 event is probably 1 m, and the surface is likely to have been 10-20 km long. According to Allen (1975) the 20 September 1899 displacement took place exactly along the trace of an older Holocene displacement detectable only from geological/geomorphological evidence.

Since the beginning of the 20th century there have been several significant (M_s>6) normal-faulting earthquakes along the principal fault zones in the Büyük Menderes graben. One of the destructive earthquake of the 20th century was the 16 July 1955 Söke – Balat earthquake (M_s=6.8) that took place near the western end of the graben (Figure 3.15). McKenzie (1972) has provided a fault-plane solution indicating that there was normal downthrown southeast combined with subsidiary right-lateral motion.

4 GPR SURVEYS IN THE BÜYÜK MENDERES GRABEN

As outlined in the Introduction section, the Büyük Menderes graben provides a good opportunity for the application of GPR in shallow geophysical investigations. GPR studies were performed in 6 different locations along the graben (Figure 4.1): two of them are trench locations (red stars in Figure 4.1), three of them are offset archaeological features (green rectangles in Figure 4.1) and one of them is buried archaeological feature (yellow triangle in Figure 4.1). Both the 250 MHz and 500 MHz shielded antennas were used and acquisition parameters of GPR surveys for different antennas are given in Table 4.1.

Table 4.1: Acquisition parameters of GPR survey

Antenna Freq.	500 MHz	250 MHz
Trace interval:	0.05 m	0.1 m
Samples:	512	512
Sampling freq.:	6755 MHz	2607 MHz
Time window:	76 ns	196 ns

The quality of the original data requires further processing for easier interpretation (Leucci, 2006). The following processing steps and applied to GPR profiles to obtain better visualization.

1. Time-zero correction (shift the first arrivals by a constant),
2. Running average filter with a length of 4 ns / 2 ns in order to filter the DC component (Dewow filter),
3. AGC with a window length of 61 ns,

4. Subtracting the mean trace (calculated from a sliding window of 5 traces) in order to filter out the continuous flat reflections caused by breakthrough between the shielded antennas and by multiple reflections between the antenna and the ground surface (Daniels, 2004),
5. Band-pass filter: 100/200-300/400 MHz (for 250 MHz) & 200/400-600/800 MHz (for 500 MHz),
6. Time cut 100 ns (for 250 MHz) & 60 ns MHz (for 500 MHz),
7. Topographic correction.

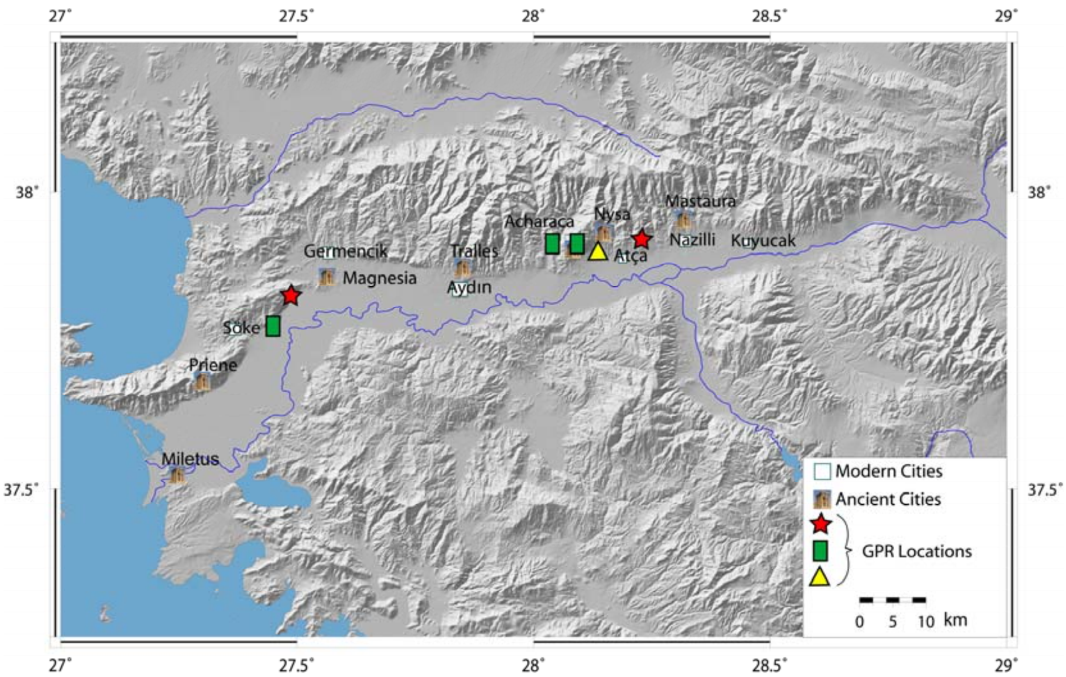

Figure 4.1: Shaded relief image of the Büyük Menderes graben (SRTM) shows GPR locations. Locations of trenches indicated by red fill stars, offset archaeological features indicated by green fill rectangles and buried archaeological features indicated by yellow fill triangle.

4.1 GPR Applications to Paleoseismological Studies

Paleoseismology documents past surface rupturing earthquakes that took place on a fault. This method is limited by the scarcity of geomorphic and sedimentologic environments that contain adequate records of deposition, erosion, and ground motion (McCalpin, 1996). Identifying adequate trenching sites can be difficult where faults are buried or have been eroded since their last motion. GPR is an effective tool to locate suitable sites for trenching. Characteristic reflections are produced by boundaries between elements with contrasting electrical properties, such as grain size distribution (sorting, clay content), porosity, and water content (Davis and Annan, 1989; Anderson *et al.,* 2003). Thus, GPR is capable of resolving faults by imaging offset stratigraphic reflectors or reflections from the fault plane. As outlined in the Introduction chapter GPR has been applied successfully to study near-surface faulting in a wide variety of settings around the world (e.g. Bano, *et al.*, 2000; Meghraoui, *et al.*, 2001; Audru, *et al.*, 2001; Gross *et al*. 2002 and Green *et al*. 2003; Ferry *et al.* 2004).

New types of shielded GPR antennas provide more rapid and reliable results with high resolution but the following parameters should be considered to get reliable GPR data in paleoseismology:

- Thickness of young sediments
- Topographic differences between the beginning and the end points of the profiles
- The artificial effects (e.g. electrical poles, vegetation, trees)
- Crossing the fault perpendicularly

The Büyük Menderes fault zone can easily be traced in the field where it separates Quaternary sediments from Neogene units. However, where the fault cuts loose Quaternary deposits, it is difficult to trace it in the field as a result of rapid erosion. Hence, GPR surveys were performed in two locations to locate the fault zone precisely where there are no clear surface evidence for faulting.

4.1.1 Argavlı Trench Site

The Büyük Menderes graben changes its strike from E-W to NE-SW around Germencik (Figure 4.1). The Argavlı trench site is located near the northeastern end of the NE-SW part of the graben (Figure 4.2). The active fault is mapped using geological and geomorphological indicators (Figure 3.7) but its precise location in the trench site was not clear because the field has been used for agriculture erases surface evidence of faulting (Figure 4.3). GPR surveys were applied to locate the fault precisely and to decide the trench length. The first measurement was taken with the 250 MHz antenna to see general view of subsurface (Figure 4.4). The aim for taking a long profile was to scan a large surface in general, because it provides fast and easy acquisition. Processing of this long profile showed some offset reflectors and hyperbolas between 10 and 25 meters (Figure 4.4). This part of the long profile was measured again with 250 MHz antenna with shorter trace interval (~5cm) to get a higher resolution (argavlı_250_prf2 in Figure 4.3). Then we used the 500 MHz antenna (argavlı_500_prf1 in Figure 4.3) for more detail analysis of offset and for the identification of different sedimentary units.

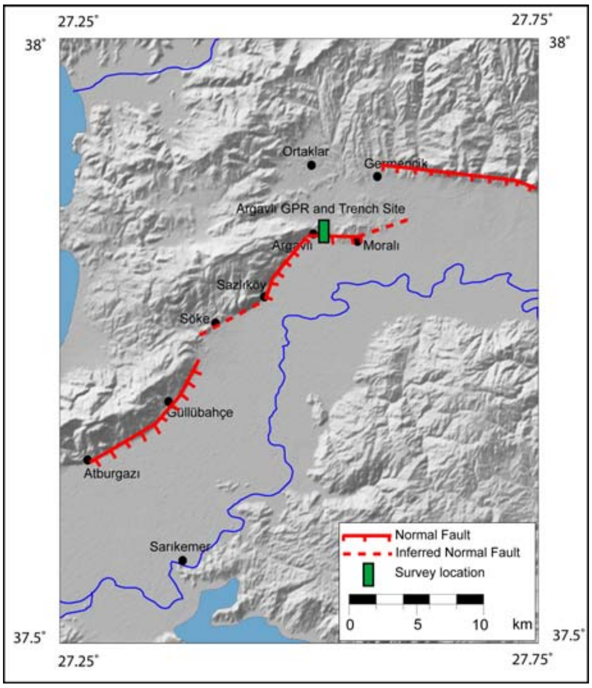

Figure 4.2: Shaded relief image with active faults at Argavlı trench site in western part of the Büyük Menderes graben.

Figure 4.3: General view of the Argavlı trench site (view towards NW) showing locations of GPR profiles and trench.

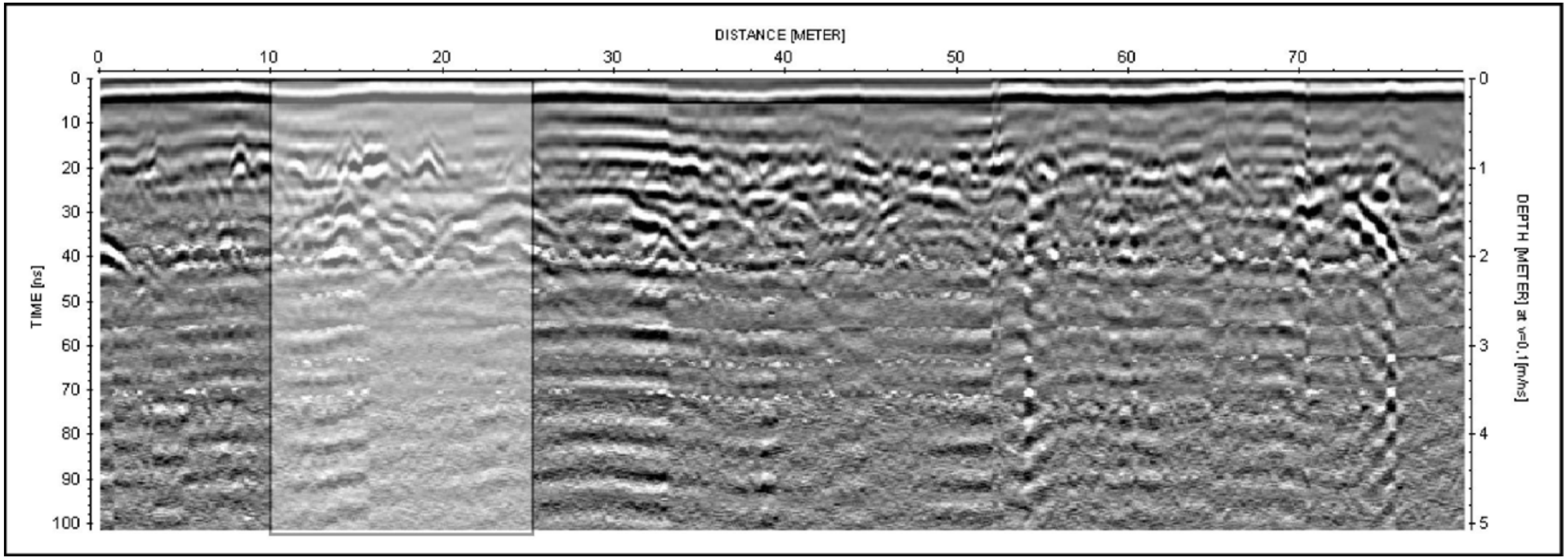

Figure 4. 4: 250 MHz antenna profile (argavlı_250_prf1 in Figure 4.4). Highlighted area indicades the location of anomalous zone.

Results of 250 MHz antenna:

After data acquisition, we applied processing steps listed at the beginning of this chapter. The raw profile of the Argavlı trench site is given in Figure 4.5a, the processed profile in Figure 4.5b and the interpreted profile in Figure 4.5c.

Even though the 250 MHz antenna does not provide good resolution transects, interpreted profile shows 5 different units marked with dashed lines (Figure 4.5c). It is clear that there is a deformation zone between 5 and 11 meter. Although vertical displacements can be recognized in the interpreted profile, the vertical resolution of the 250 MHz antenna is ~20 cm which could be higher than some vertical displacements. Therefore, the 500 MHz antenna was used on the same profile to obtain a better resolution because its vertical resolution is about 10 cm.

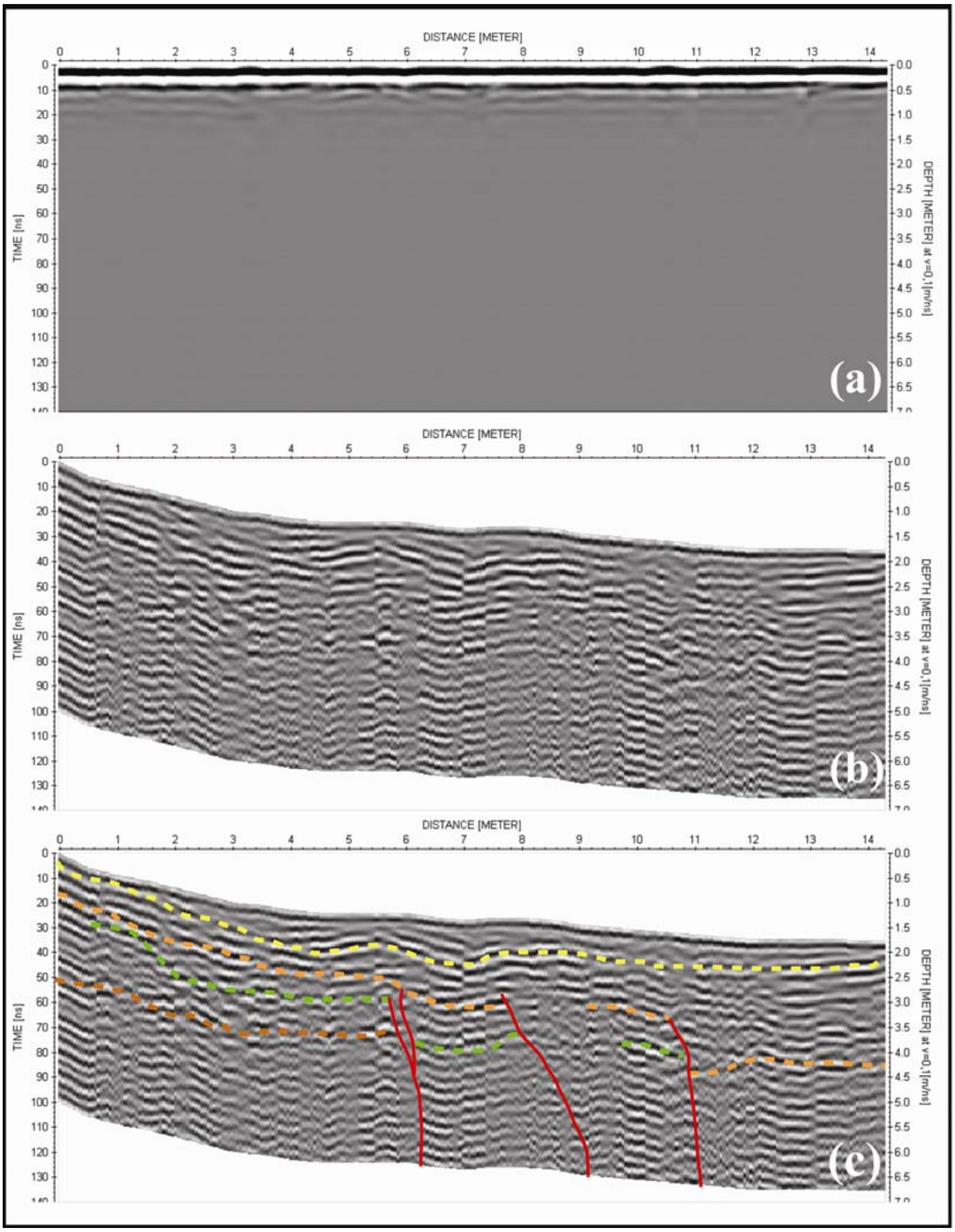

Figure 4.5: 250 MHz GPR profile in the Argavlı trench site. (a) Raw profil, (b) Processed profile, (c) Interpreted profile. Dashed lines represent the layers, thin red line represents possible faults.

Results of 500 MHz antenna:

The 500 MHz shielded antenna gave satisfactory details for the trench site (Figure 4.6). Processing of the profile shows that both reflectors and hyperbolas are much clearer (Figure 4.6a). Different units which were recognized with 250 MHz antenna are clearer in the 500 MHz profile (Figures 4.6a and 4.6b). The dashed lines in Figure 4.6b are representing subsurface layers with a small amount of error-scale (± 5 cm).

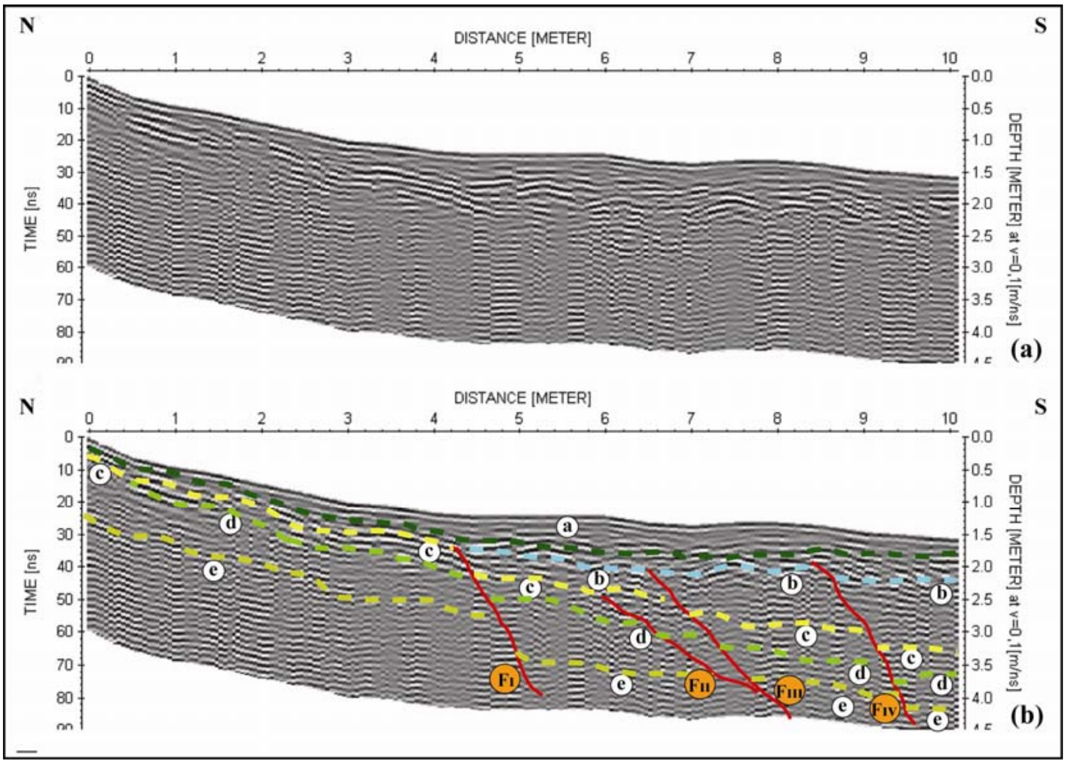

Figure 4.6: 500 MHZ GPR profile in the Argavlı trench site (a) Processed profile. (b) Interpreted profile. Dashed lines and the letters from "a" to "e" represent 5 different layers, thin red line and FI – FIV represents possible fault zones.

Identified units in the interpreted profile are marked as "a" – "e" in Figure 4.6b. The deformation zone is much clear between 4 and 9 meters and four different faults can be recognized (marked as FI – FIV in Figure 4.6b). All units except modern soil (~first 30 cm) offset by these faults. The first fault (marked with "FI" in Figure 4.6b) in the 4th meter causes ~80 cm vertical offset on the units "c", "d" and "e". The second fault (marked with “Fıı” in Figure 4.6b) in the 6th meter offsets units “d” and “e” by about 30cm. The third fault (marked with “Fııı” in Figure 4.6b) in the 7th meter causes ~30 cm vertical offset on units “c”, “d” and “e”. The fourth fault (marked with “Fıv” in Figure 4.6b) in the 9th meter causes ~20 cm vertical offset on units “b”, “c”, “d” and “e”. Interpreted profile also shows that faults ends at different depths; for example “Fı” and “Fııı” end after cutting unit “c”, “Fıı” ends before cutting unit “c” and “Fıv” ends after cutting unit “b”.

Results of Trenching:

The Argavlı trench was excavated on the basis of GPR studies (Figure 4.3). It was ~13 meter long, ~1.5 meter wide and ~2.5 meter deep. Figure 4.7 is the log of eastern wall on which 12 different units were recognized. The width of the deformation zone is ~7 meter and at least 6 main faults (marked as “fı” – “fvı” in Figure 4.7) were recognized in this zone (Altunel *et al*., 2009).

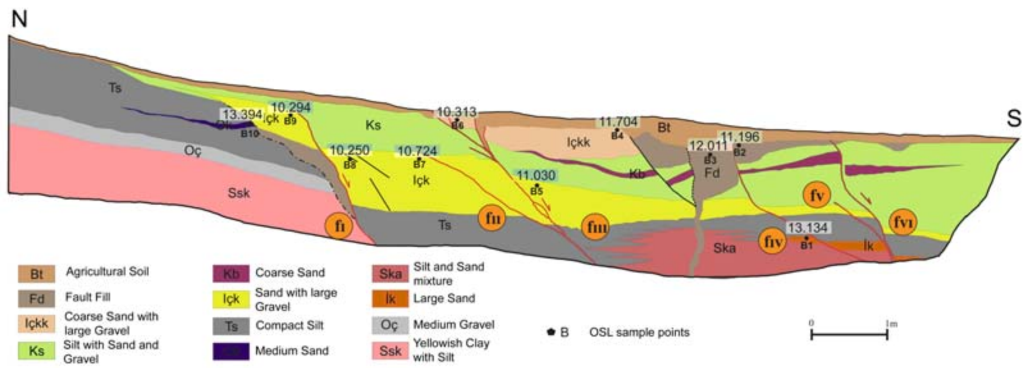

Figure 4.7 Log of Argavlı trench (eastern wall). Main faults are marked as “fı” – “fvı” (Altunel et al.*, 2009).*

Fault “fı” causes ~80 cm vertical offset on the units “Içk” and “Ts”. Fault “fıı” offsets units “Içk” and “Ts” by about 30cm. Fault “fııı” causes ~30 cm vertical offset on units “Içkk”, “Ks”, “Içk” and “Ts”. Fault “fıv”causes ~20 cm vertical offset on units “Ks”, "Içk", "Ts" and "Ska". Fault "fv" causes ~10 cm vertical offset on units "Içk", "Ts" and "Ik". Fault "fvı" causes ~30 cm vertical offset on units "Kb", "Içk", "Ts" and "Ik".

Correlation of GPR results with Trench results:

The location of the Argavlı trench site was selected on the basis of GPR surveys. The GPR studies allowed identifying the deformation zone (Figure 4.8a) which was helpful to decide the trench length. In addition, knowing the precise location of the deformation zone gave the advantage of using time and financial budget in optimum limits.

Figure 4.8a is the interpreted GPR profile (500 MHz antenna) and Figure 4.8b is the trench log. It is clear that while 5 different units were recognized in the GPR profile (Figure 4.8a), 12 units identified in the trench log (Figure 4.8b). Logging in paleoseismological studies requires detail drawing and same lithological unit can be classified in different sub-units on the basis of its content. For example, a silty unit can be classified as silt with gravel, silt with sand or silt with clay. However, in GPR profiles units are identified with their dielectric constants, thus only main lithology can be identified. For that reason, 5 main units are identified in the GPR profile.

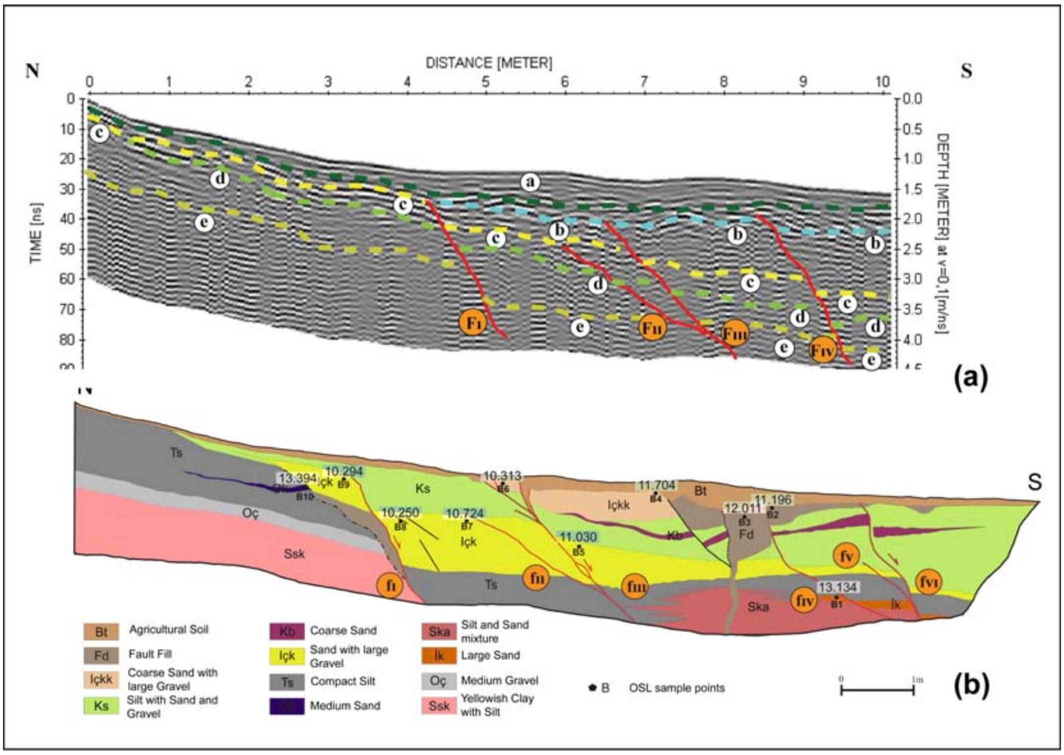

Figure 4.8: Comparison of the 500 MHz GPR profile (a) with the trench log (b). Both figures are in the same scale and no vertical exaggeration.

Table 4.2 compares GPR results with trench results. The offset amounts in interpreted GPR profile fit with the offset amounts in the trench log. GPR surveys show 4 main faults in the Argavlı site (Figure 4.8a), however, in the same area there are more than 4 faults in the trench log (Figure 4.8b). The possible explanation of this difference is that offsets on the units could be smaller than GPR resolution (~10 cm vertical resolution for 500 MHz antenna). For example the “fv” fault in the trench log causes only 10 cm vertical offset. Thus, the fault could not be recognized in the GPR profile. Similarly, “fvı” fault has ~30 cm vertical offset and the resolution of 250 MHz antenna (~20 cm) not enough to recognize this fault. Thus, this fault was not recognized in the 250 MHz profile and this part was not scanned with 500 MHz antenna.

Table 4.2: Amount of offsets recognized in GPR profiles and observed in trench log.

Faults		Offset Amount	
GPR	Trench	Interpreted GPR profile	Trench Log
FI	fI	~80 cm ± 7 cm	~80 cm
FII	fII	~30 cm ± 7 cm	~30 cm
FIII	fIII	~30 cm ± 7 cm	~30 cm
FIV	fIV	~20 cm ± 7 cm	~20 cm
?	fV	?	~10 cm
?	fVI	?	~30 cm

4.1.2 Atça Trench Site

The Atça trench site is located about 2 km east of the town of Atça (Figure 4.9). The active fault scarp defines the border between the Neogene units in north and Quaternary graben deposits in south (Figures 4.9 and 4.10). This fault scarp is also visible in Google earth view (Figure 4.11). Detail field studies in this site showed a gentle slope in Quaternary deposits (Figure 4.10). In order to decide the precise location of the fault and whether the gentle morphological scarp in Quaternary deposits is related with faulting or not, GPR is used in this location.

In the beginning, the site was scanned with 250 MHz antenna from the foot of the high scarp to the end of the field which is also cutting the gentle morphological scarp (Figure 4.10). Processing of this long profile (~50 m long) showed offset reflectors and hyperbolas between 34 and 36 meters (Figure 4.12). After recognizing this change in the profile, which is consistent with the gentle scarp in Quaternary deposits, shorter but detail measurements were taken with 250 MHz and 500 MHz antennas.

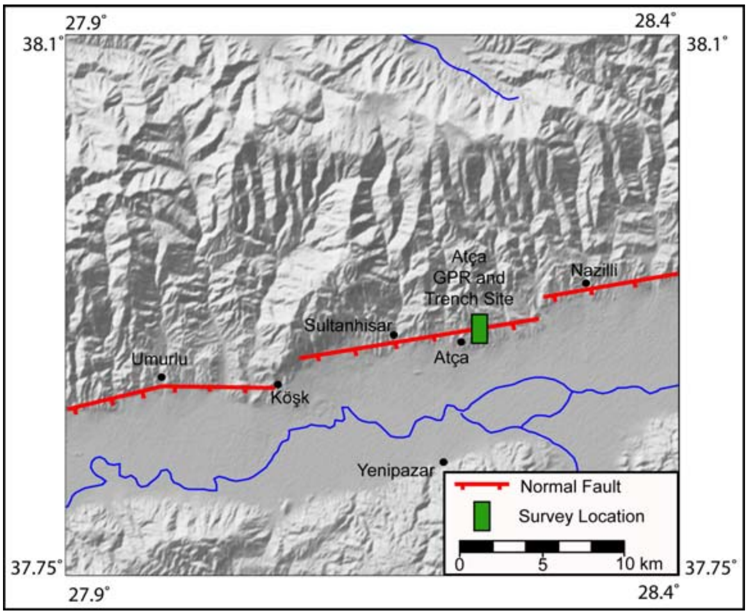

Figure 4.9: Shaded relief image shows active faults and Atça trench site in northern part of the Büyük Menderes graben

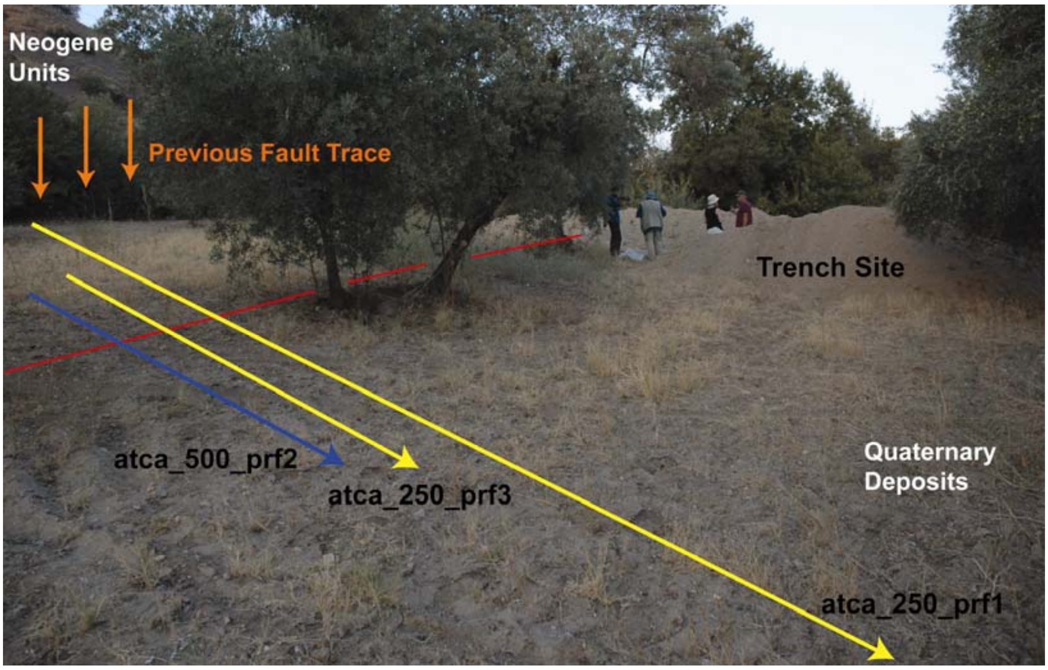

Figure 4.10: GPR profiles and trench location illustration on the site photo. Red thin line indicates active fault and brown arrows indicate previous fault trace between Neogene units and Quaternary deposits (looking towards northwest).

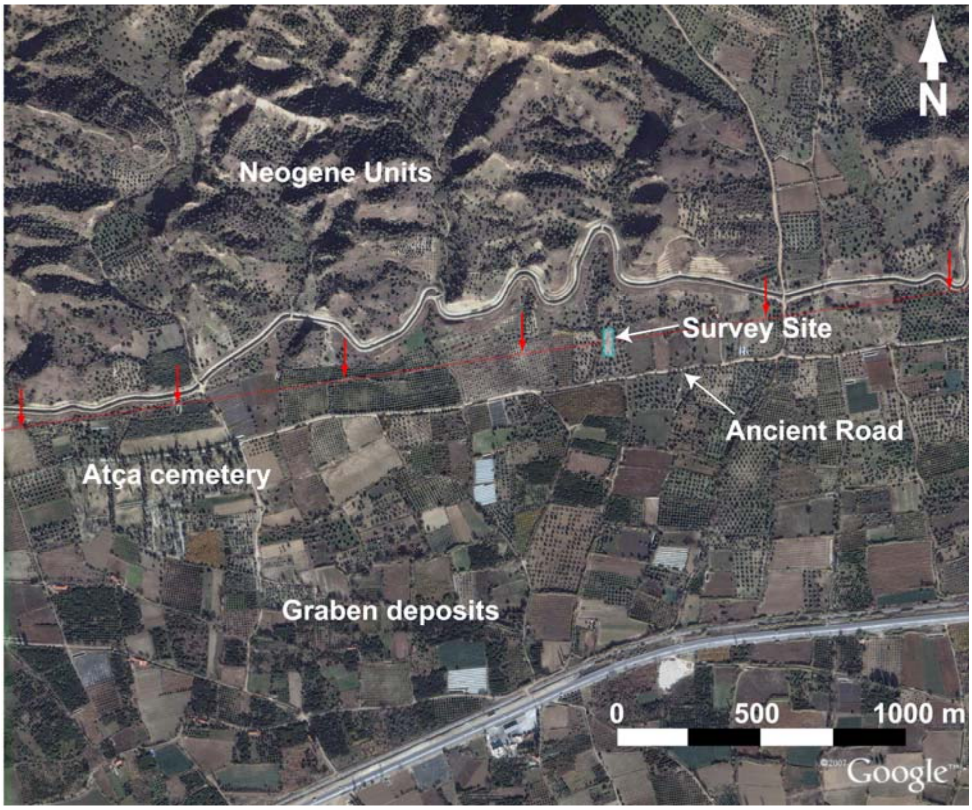

Figure 4.11: Google Earth photo of investigation area between Atça and İsabeyli (red arrows indicate fault zone).

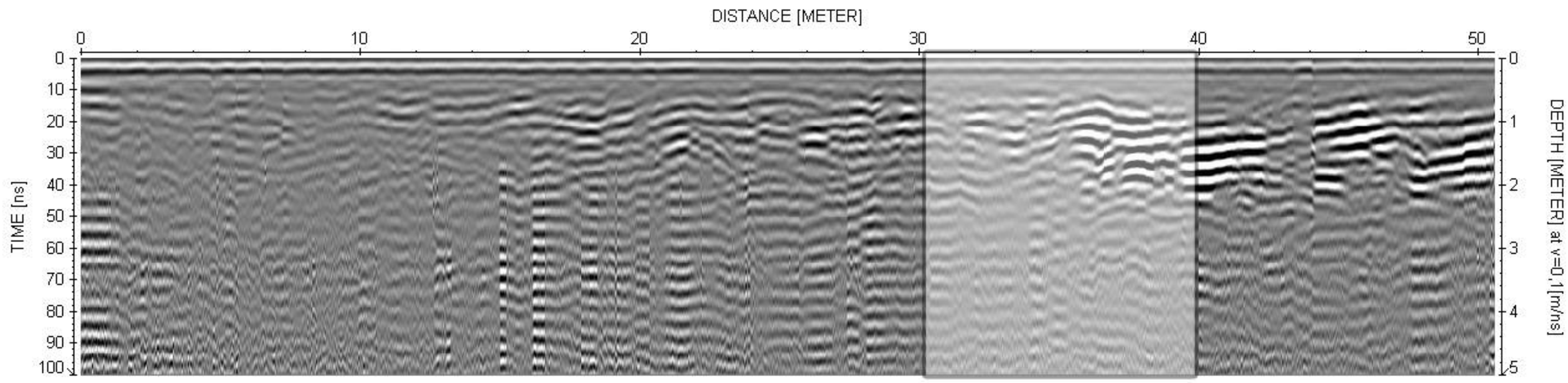

Figure 4. 12: 250 MHz antenna profile (atca_250_prf1 in Figure 4.10). Highlighted area indicades the location of anomalous zone.

Results of 250 MHz antenna:

After data acquisition, we applied processing steps listed at the beginning of this chapter. The raw profile of the Atca trench site (atca_250_prf3 in Figure 4.10) is given in Figure 4.13a, the processed profile is given in Figure 4.13b and the interpreted profile is given in Figure 4.13c. Processed profile shows continuous reflectors and on the basis of this criteria, 5 different units are recognized in the GPR profile (Figure 4.13c). Considering the offset reflectors, two different faults are identified (Figure 4.13c). However, it would not be reliable to estimate vertical offset because it is difficult to mark the same levels in the footwalls and hanging walls (Figure 4.13c).

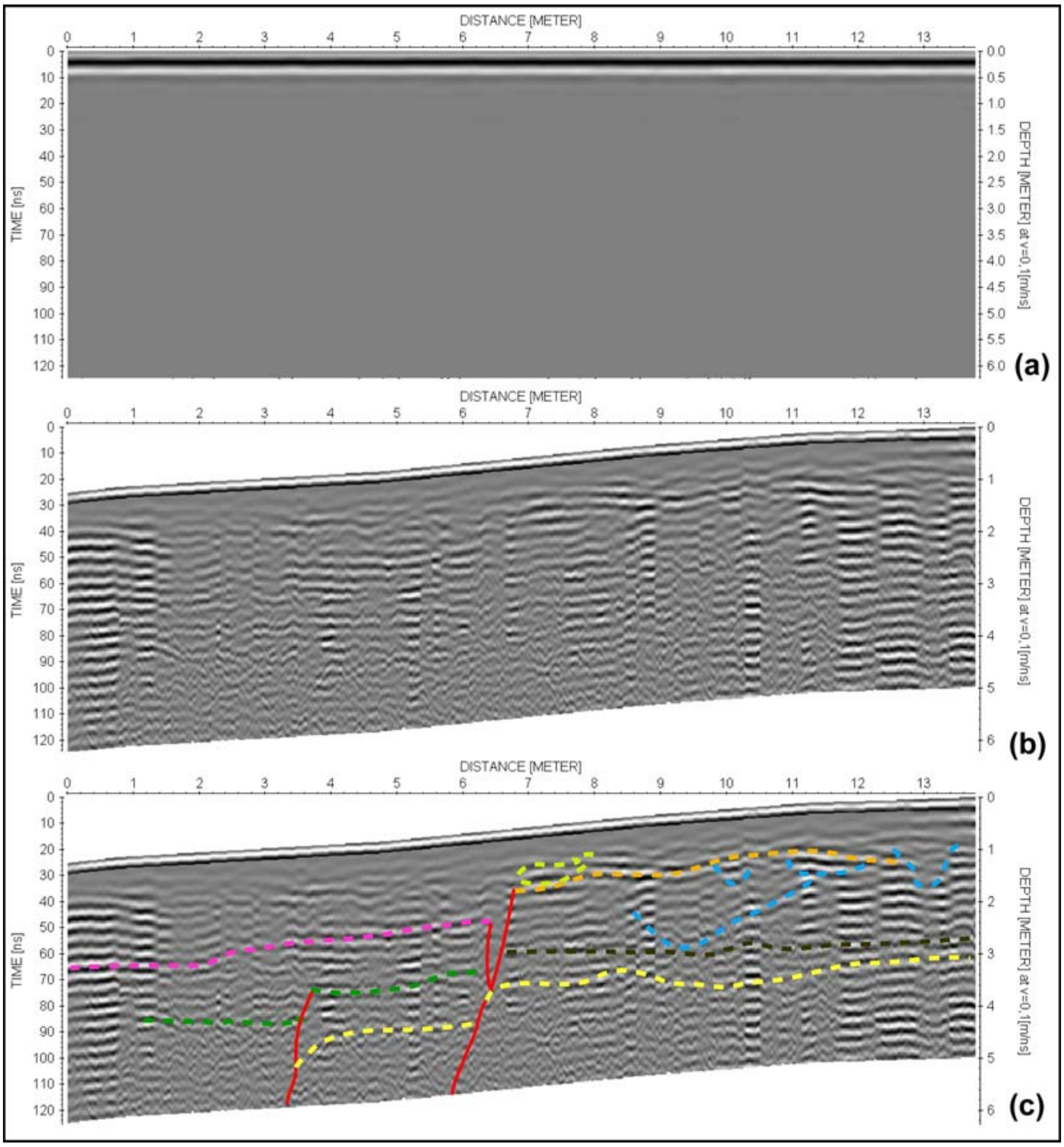

Figure 4.13: (a) Raw data of "atca_250_prf3" GPR profile. (b) Final section of "aca_250_prf3" GPR profile. (c) Interpretation of "atca_250_prf3" GPR profile. Dashed lines represent the layers, thin red line represents possible fault zone.

Results of 500 MHz antenna:

The 500 MHz antenna (~10 cm) provides a much clearer illustration along the same line. The processed GPR profile clearly shows that stratigraphic package on each side of the fault is different than the other (Figure 4.14a). Interpretation of the profile suggests 5 stratigraphic levels and two faults but reflectors are much clear. In addition, some channel shapes (marked with "b" in Figure 4.14b) were recognized in the footwall which were not visible in the 250 MHz profile. Furthermore, the 500 MHz profile provides a good resolution enough to estimate vertical offsets on the fault. The vertical offset is about 80 cm on the "Fı" fault and about 50 cm on the "Fıı" fault (Figure 4.14b).

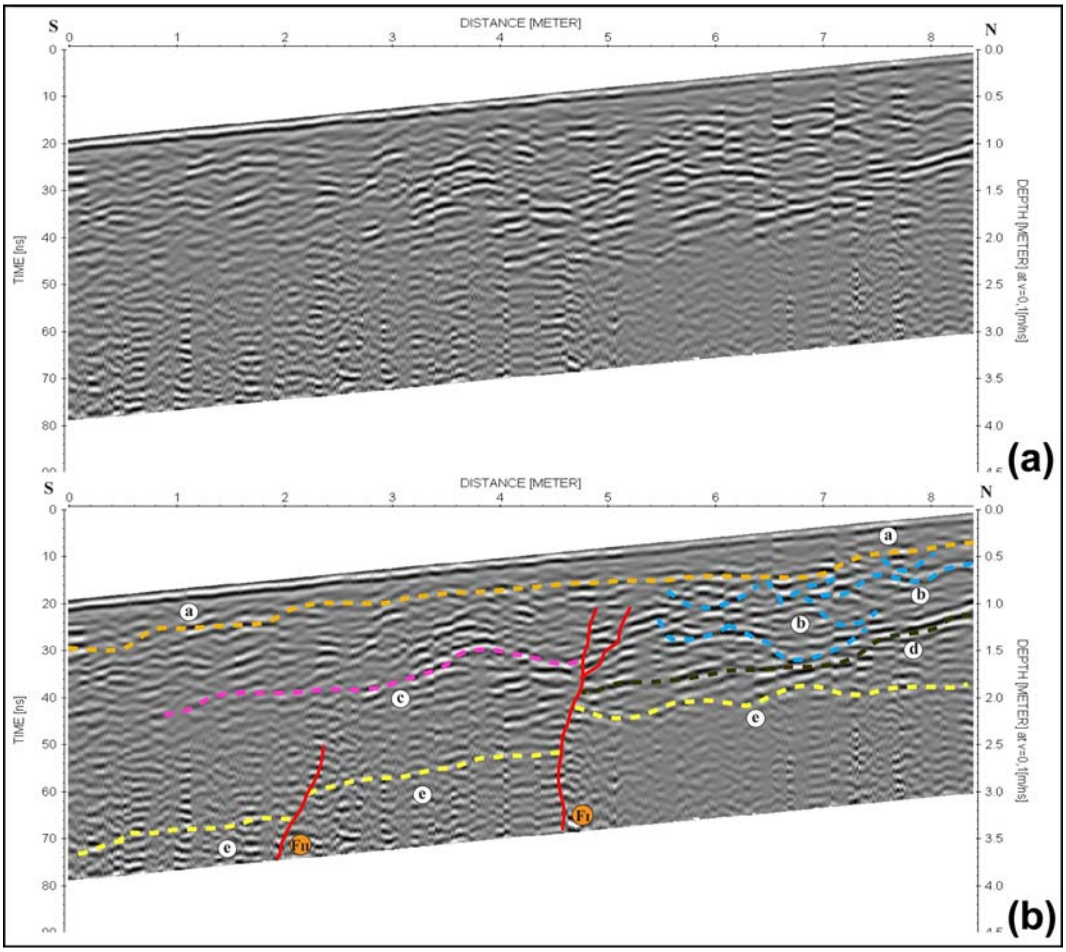

Figure 4.14: (a) Processed data of "atca_500_prf2" GPR profile. (b) Interpretation of "atca_500_prf2" GPR profile. Dashed lines and the letters from "a" to "e" represent 5 different layers, thin red line and Fı & Fıı represents possible fault zones.

Results of Trenching:

The Atça trench was excavated after GPR investigations and interpretations. It was ~13 meter long, ~1.5 meter wide and ~3.5 meter deep (Figure 4.15). 12 different units, 6 channel fills and 2 faults (marked as fı – fıı in Figure 4.15) were recognized on the trench wall (Figure 4.15). Fault "fı" is a shear zone coming up to near the surface. Fault "fıı" is a single branch and it ends about 1.5 m below the surface. The total vertical offset is about 3.5 m on the "fı" fault and ~50 cm on the "fıı" fault (Altunel *et al*., 2009).

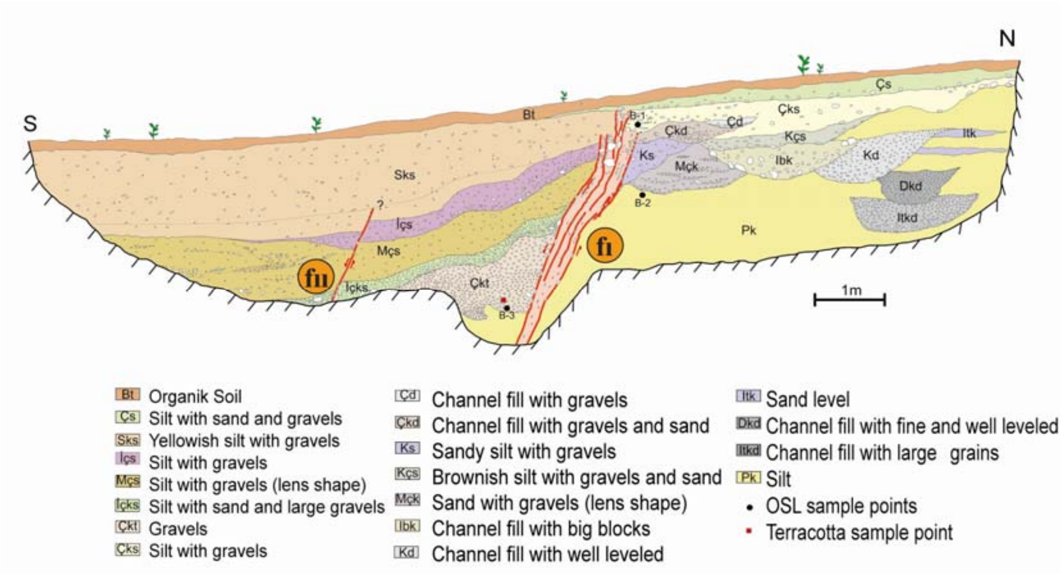

Figure 4.15: Trench exposure for eastern wall of Argavlı. Trench walls are drawn with no vertical exaggeration. (main faults marked as "fı" and "fıı") (Altunel et al.*, 2009).*

Correlation of GPR results with Trench results:

The interpreted 500 MHz GPR profile is compared with the trench log in Figure 4.16. The interpreted faults on GPR profile (Figure 4.16a) fit with the trench log (Figure 4.16b). The “fı” fault was drawn as a single line near the base of the profile but it branches upward. However, trench studies showed that this is about 70 cm wide shear zone. Each slip surface cannot be recognized in the GPR profile but two lines near surface can be considered as the limit of the zone which is about 60 cm in width consistent with the trench log. Location of the “fıı” fault and its extend fit very well in both GPR profile and trench log. Two channel fills were interpreted in GPR profile but the trench studies showed that there are more than two channel fills. Recognition of channel fills in the GPR profile is related with the grain size. Thus, it is difficult to identify different channel fills if the grain size is similar. Since the trench wall allows to make direct observation, it is easy to identify small difference in grain size. This is the probable reason for the difference between the GPR interpretation and trench log about channel fills.

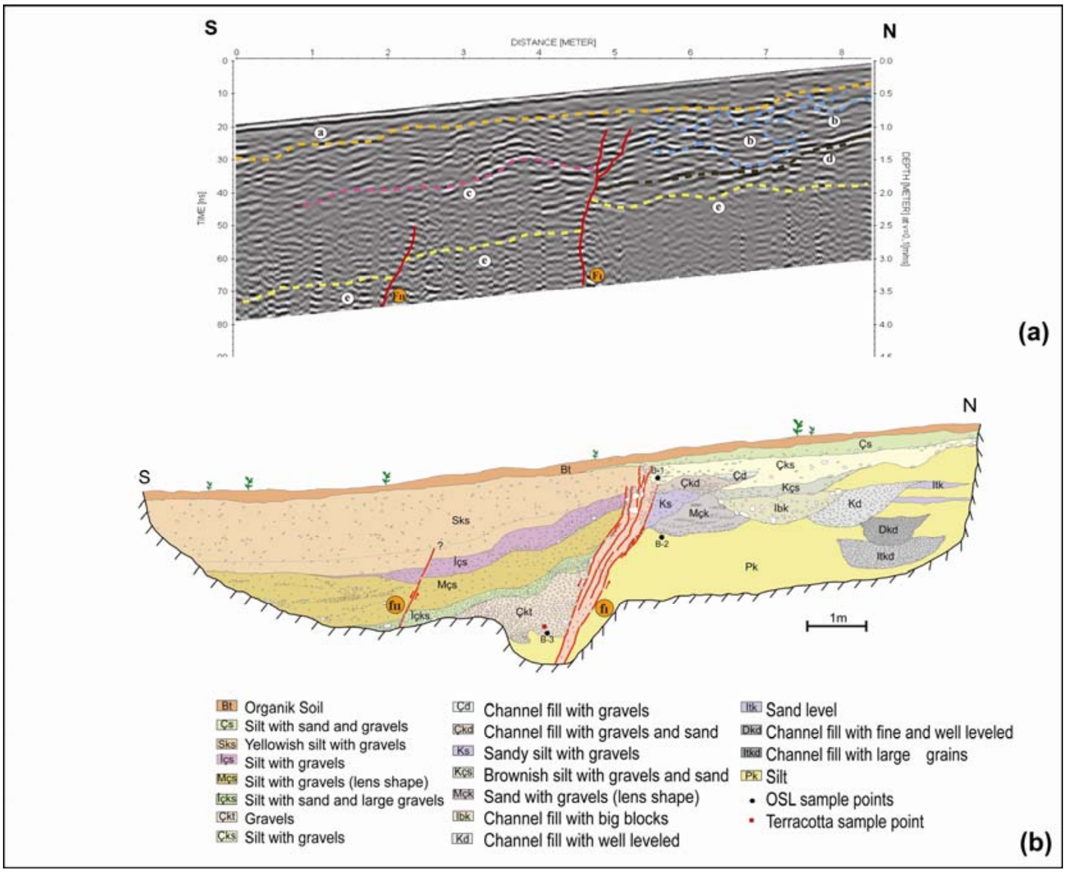

Figure 4.16: Comparison of the 500 MHz GPR profile (a) with the trench log (b). Both figures are in the same scale and no vertical exaggeration

The well exposed scarp between Quaternary deposits and Neogene units (Figures 3.9a and 4.10) represents the location of the active fault in this site. However, GPR and trench studies showed that the recent rupture does not follow the Quaternary – Neogene contact and it developed within the Quaternary deposits (Figure 3.9b). If GPR was not applied in this site, it would be impossible with existing surface evidence to see the fault propagation towards the basin.

4.2 GPR Applications to Offset Archaeological Features

Ground Penetrating Radar has long been used to investigate buried archaeological features (e.g. Conyers, 2006; Negri and Leucci, 2006; Leucci and Negri, 2006 and Limp, 2006). The main aim to use GPR in archaeology is to locate wall, road, void, grave etc. Application of GPR in archaeological studies is usually successful because of the sharp contrast between archaeological materials (marble blocks, voids, cooked clay etc.) and surrounding sediments is clear.

The GPR method has not been used on offset archaeological features in previous studies. Considering that offset archaeological features in the study area are made of stone blocks, it is most likely that GPR application to offset archaeological features provides important data for faulting. GPR studies conducted in three locations in this study: an Ottoman Bridge, Roman Road and next to a Roman Wall (Figure 4.1). Detail of the GPR studies are given in the next section.

4.2.1 Ottoman Bridge

Field observations:

The Ottoman Bridge is on the abandoned Menderes River near Sazlıköy (Figure 4.17). The bridge was built by an Ottoman General (called Ramazan Pasha) in 1595. Detail observations on the bridge showed that there is a bending near the eastern part of the bridge (Figure 4.18). Since the bridge is located within the fault zone (Figure 4.19), it is possible that the sudden bending on the bridge is related with the activity of the fault. Thus, this site is investigated in detail by GPR. GPR profiles were taken along the southern side of the bridge and on the bridge (Figure 4.20).

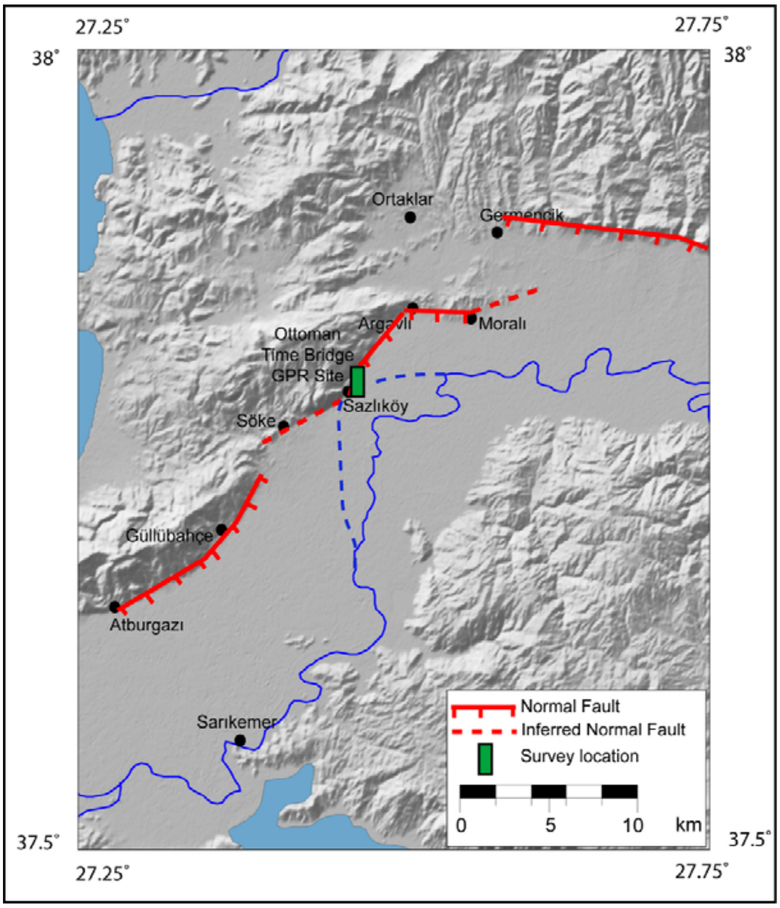

Figure 4.17: Shaded relief image shows active faults and Ottoman bridge study site in western part of the Büyük Menderes graben (dashed blue line represents the abandoned Menderes River bed).

Figure 4.18: Sudden bending on the Ottoman bridge (~50 cm) pointed with red arrows (looking towards northwest).

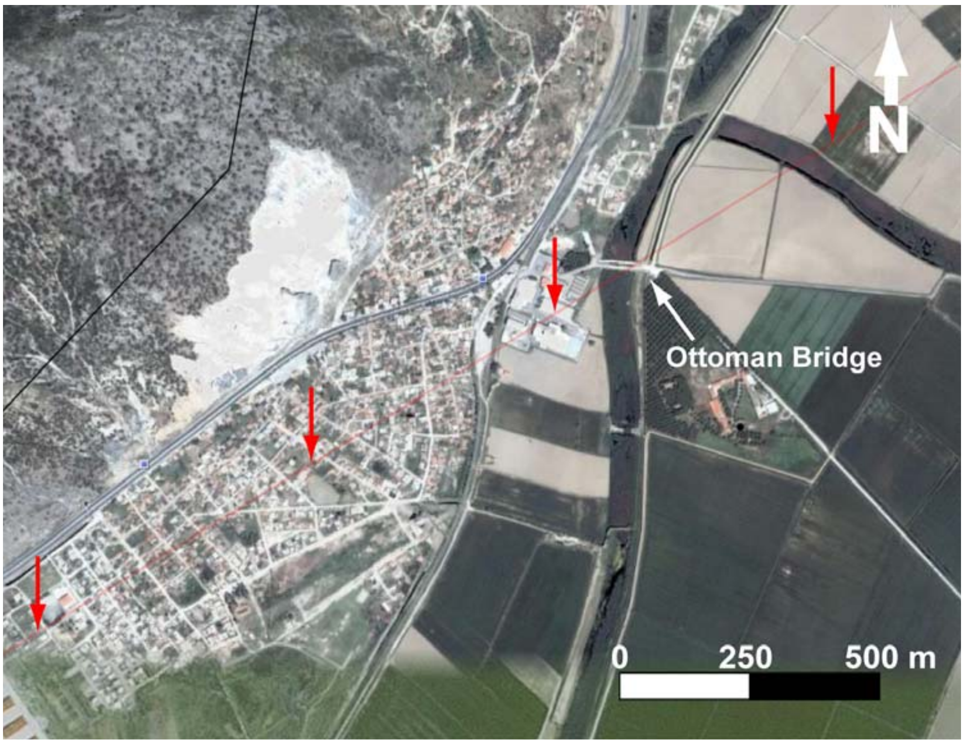

Figure 4.19: Google Earth photo of the investigation area near Sazlıköy (red arrows indicate possible fault zone).

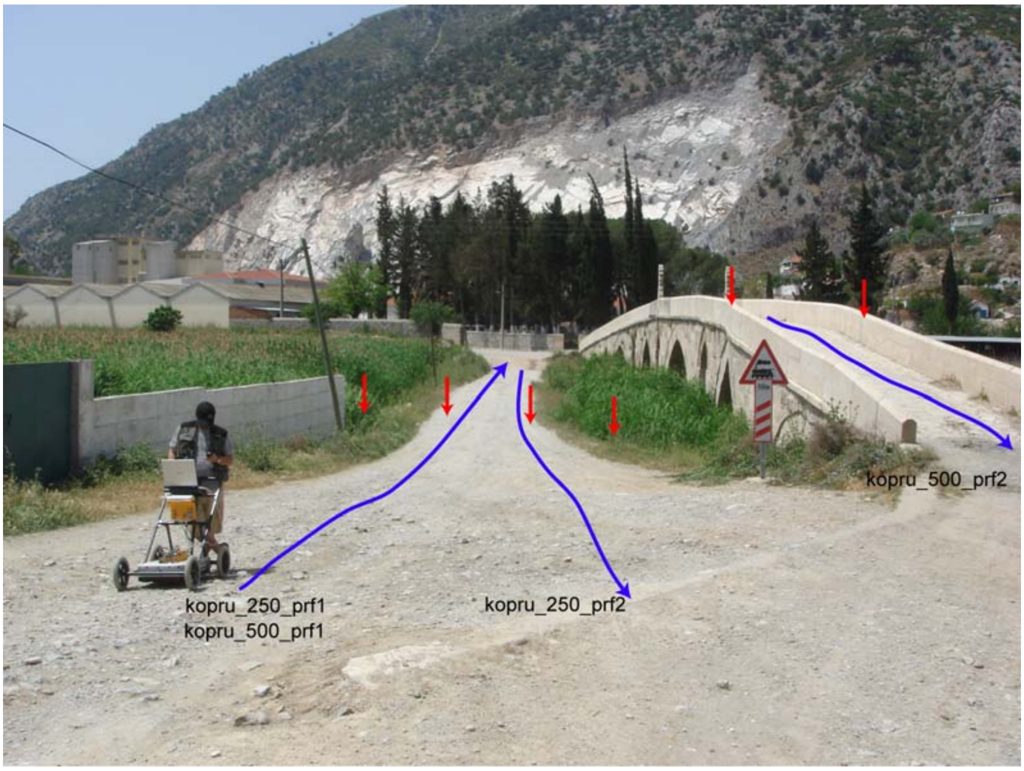

Figure 4.20: Location of GPR profiles (blue lines correspond to GPR profiles and red arrows indicate the possible fault zone).

Results of 250 MHz antenna:

Profile given in Figure 4.21 was taken from east to west, and profile given in Figure 4.22 from west to east with 3 m separations. Processed profiles show that reflectors and hyperbolas are similar in each profile. It is noticeable that there is about same amount of offset (~1 m) in the same location. It is also noticeable that there are small size of hyperbolas forming a group which is gently dipping to east. It is interpreted that the offset in the reflectors and the small hyperbolas reflect the location of the fault in agreement with the bending in the bridge.

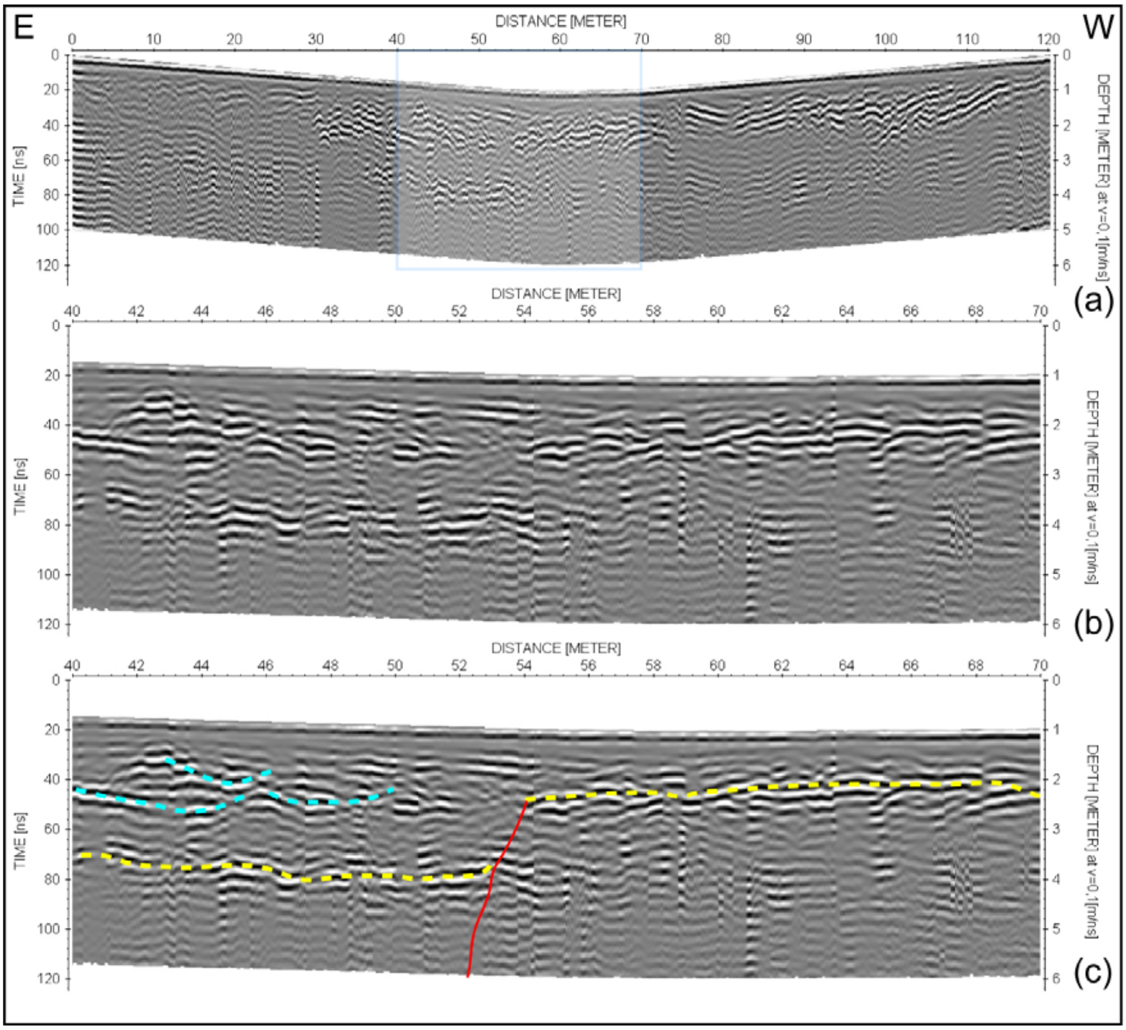

Figure 4.21: (a) Processed data of "kopru_250_prf1" GPR profile. (b) Zoomed on between 40 – 70 meter in highlighted square in "a". (c) Interpretation of "kopru_250_prf1" GPR profile. Yellow dashed line represents the layer, blue dashed lines represent channel fills and thin red line represents possible fault zone.

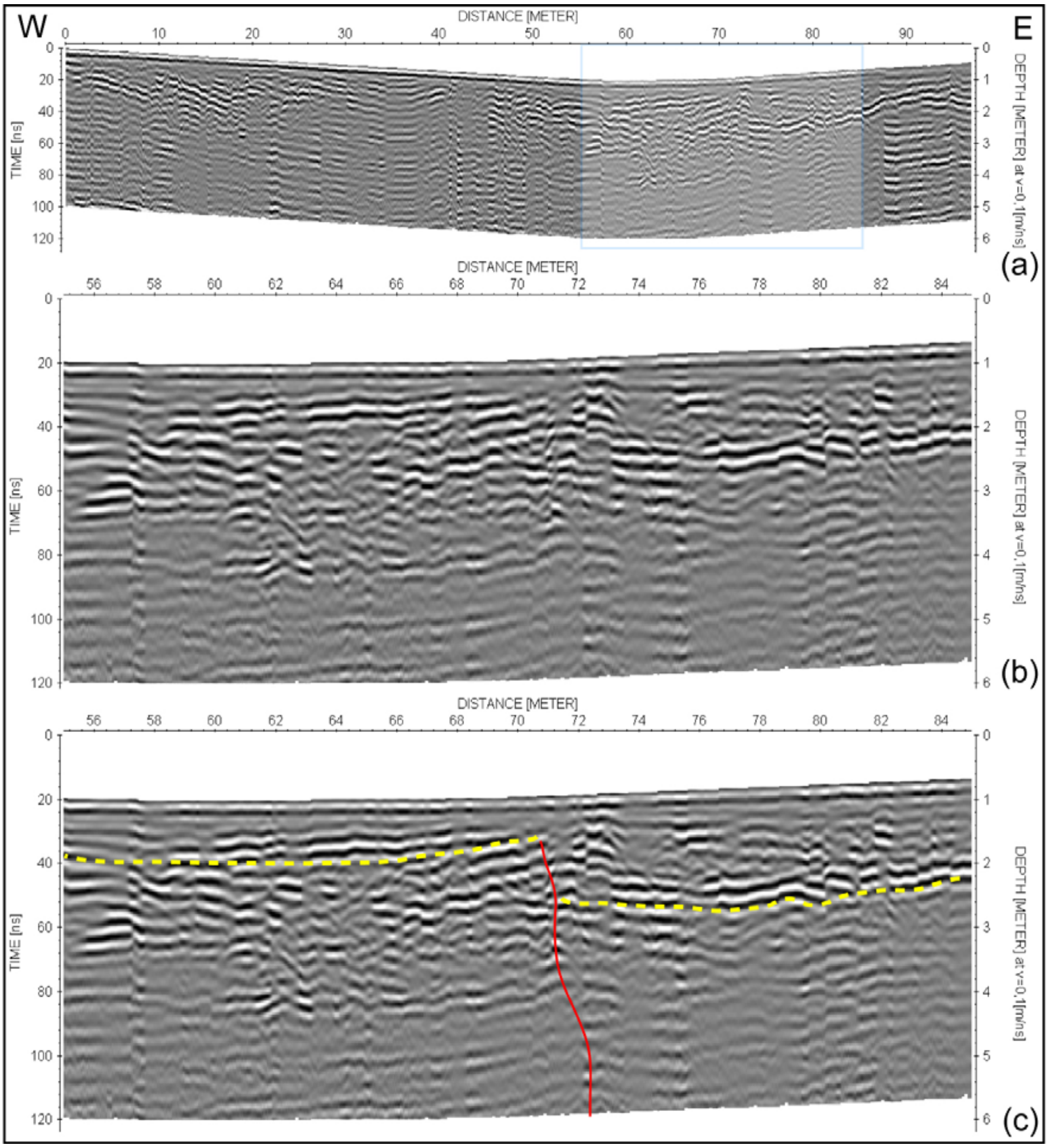

Figure 4.22: (a) Processed data of "kopru_250_prf2" GPR profile. (b) Zoomed on between 55 – 85 meter in highlighted square in "a". (c) Interpretation of "kopru_250_prf2" GPR profile. Dashed lines represent the layers, thin red line represents possible fault zone.

Results of 500 MHz antenna:

A profile was taken along the southern side of the bridge (Figure 4.20). Processing of profile shows offset reflectors (Figure 4.23) but it is not as clear as the profile of 250 MHz antenna. This is probably due to high conductivity near the surface which causes attenuation of the EM signal.

Another profile was taken on the bridge to investigate the difference between the bending part and undestroyed part of the bridge. Considering that there was a repair on the bridge, it would be possible to compare the repaired part with the original part using GPR because their reflectors would be different.

Figure 4.24 is the profile of the 500 MHz antenna along the bridge. About 7 m from the western entrance and about 10 m from eastern entrance reflect the same reflectors, which indicate the material. Various sizes of hyperbolas represent windows and arches on the bridge. It is clear that hyperbolas are symmetric. However, it is noticeable that there is no hyperbola between 84. and 86. m and GPR trace of this 2-m-wide zone is completely different than the rest of the bridge. Absence of hyperbola between 84. and 86. m suggests that the window is missing in this part of the bridge where there is the sudden bending on the bridge. Thus, it can be interpreted that this part of the bridge was repaired.

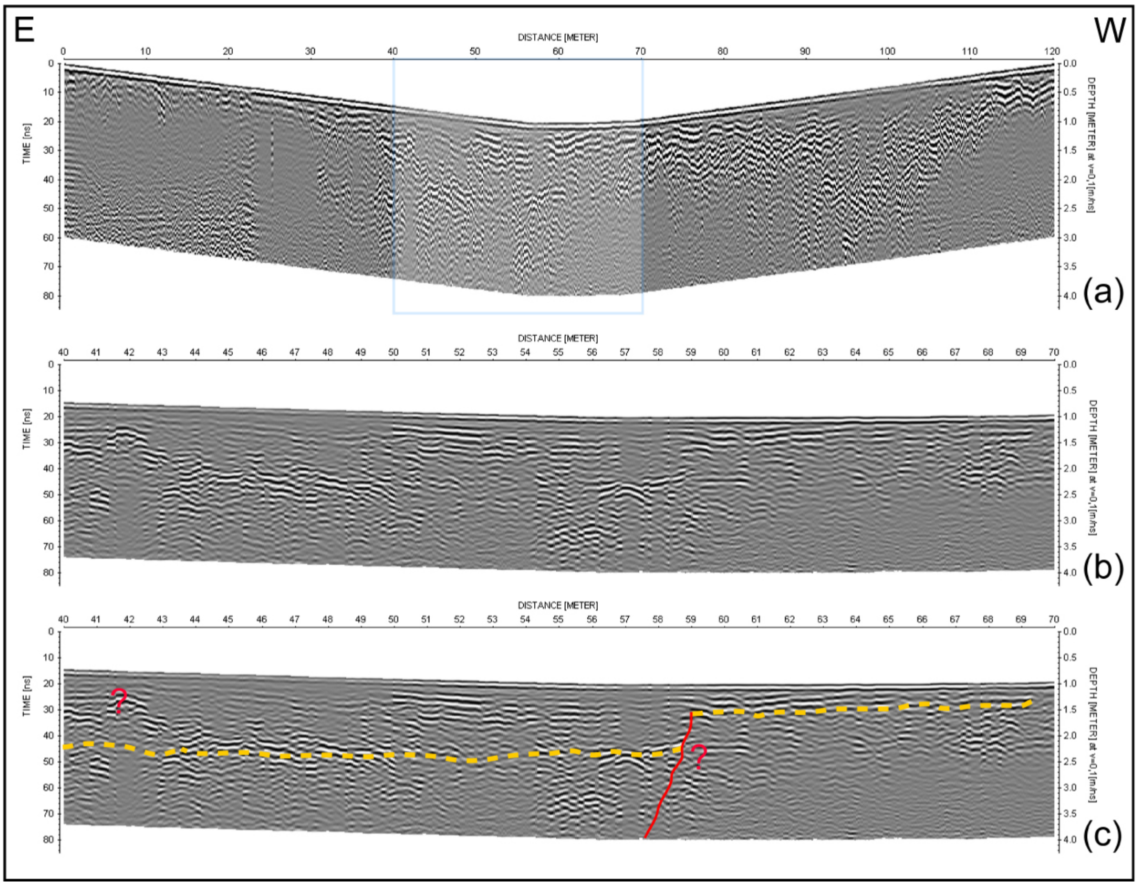

Figure 4.23: (a) Processed data of "kopru_500_prf1" GPR profile. (b) Zoomed on between 40 – 70 meter in highlighted square in "a". (c) Interpretation of "kopru_500_prf1" GPR profile. Dashed line represents the layers, thin red line represents possible fault zone.

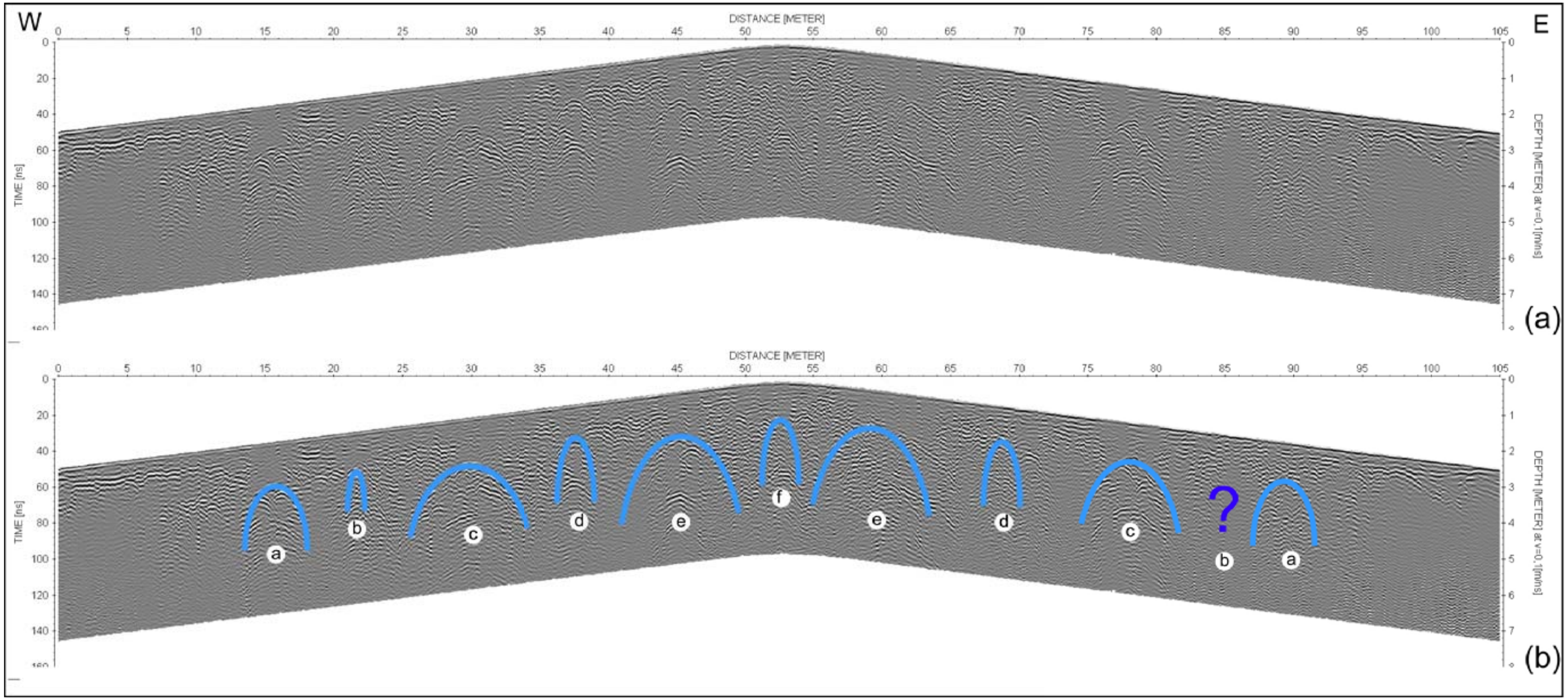

Figure 4.24: (a) Processed data of "kopru_500_prf2" GPR profile. (b) Interpretation of "kopru_500_prf" GPR profile. Hyperbolic blue lines represent the windows on the bridge.

4.2.2 Roman Wall

Field observations:

During mapping of active faults in the study area, a wall was observed along the western side of Dipcik stream. The wall is about 5 m high and it extends from the Roman Road Salavatlı (Figure 4.25). Considering the fault extent and position of the wall, it is noticed that this wall must cross the active fault (Figure 4.25). Detailed observations along the wall showed that some parts of the wall were repaired (Figure 4.26). LIDAR view of the repaired part indicates that the southern part is about 255 cm lower than the northern side (Figure 4.27). In order to investigate whether this downthrown on the wall is related with faulting or not, GPR studies were conducted in this location. The top of the wall did not allow to take GPR profile along the wall. Thus, GPR profiles were taken in the open field in the western side of the wall (Figure 4.28). GPR profiles were taken vertical to the extent of the fault (Figure 4.29). Only 250 MHz antenna was used in this location because the surface was not smooth enough to use the 500 MHz antenna.

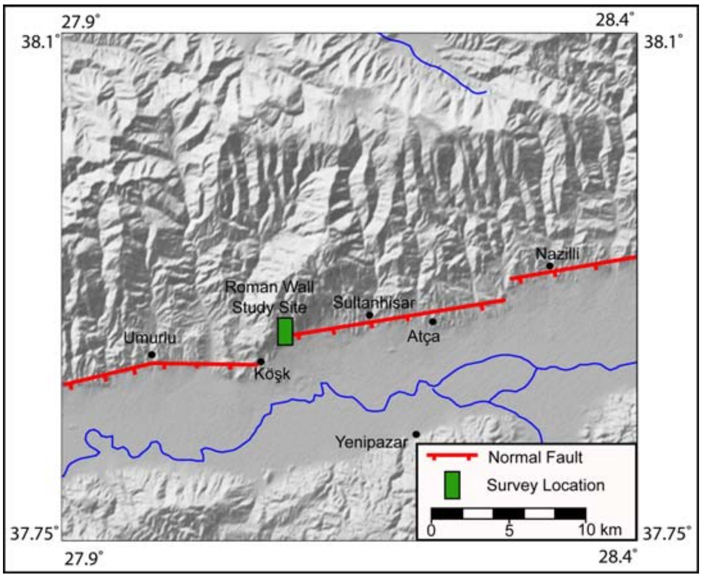

Figure 4.25: Shaded relief image shows active faults and Roman wall study site in northern part of the Büyük Menderes graben

Figure 4.26: The Roman wall and its disturbed part (Yellow signs show the same stone level and red arrows indicate disturbed part of the wall).

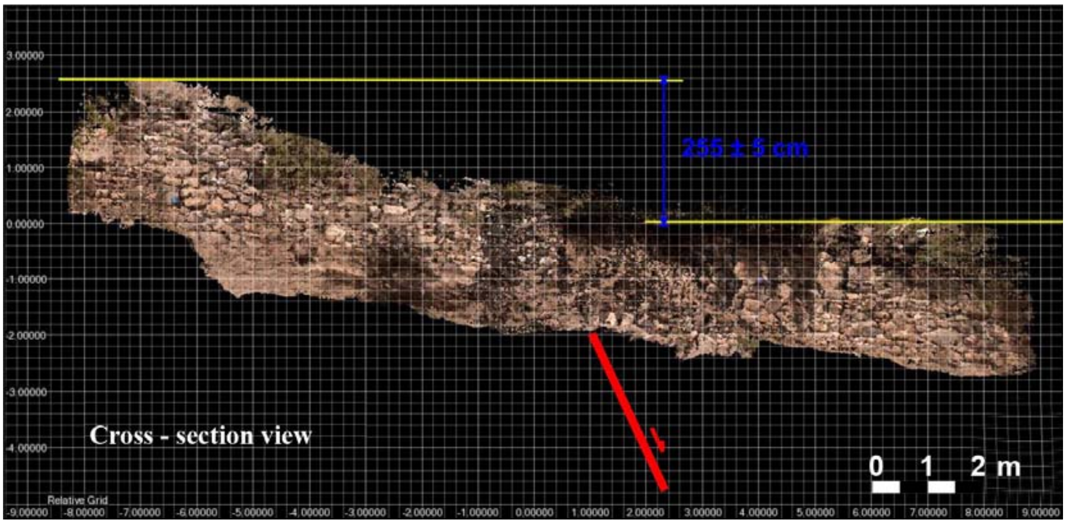

Figure 4.27: LIDAR illustration results for the wall. (a) Cross – section view (looking towards SW). (b) Plan view.

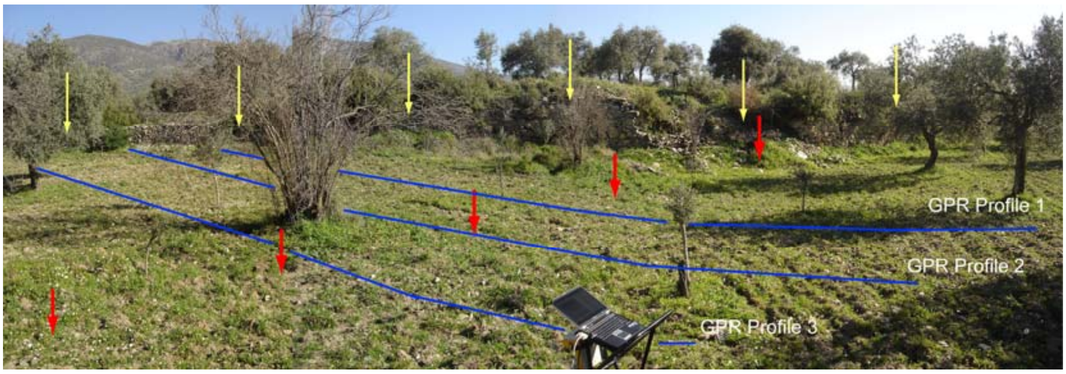

Figure 4.28: Picture shows the possition of the wall (yellow arrows), fault zone (red arrows) and GPR profiles (blue lines) (looking towards NE).

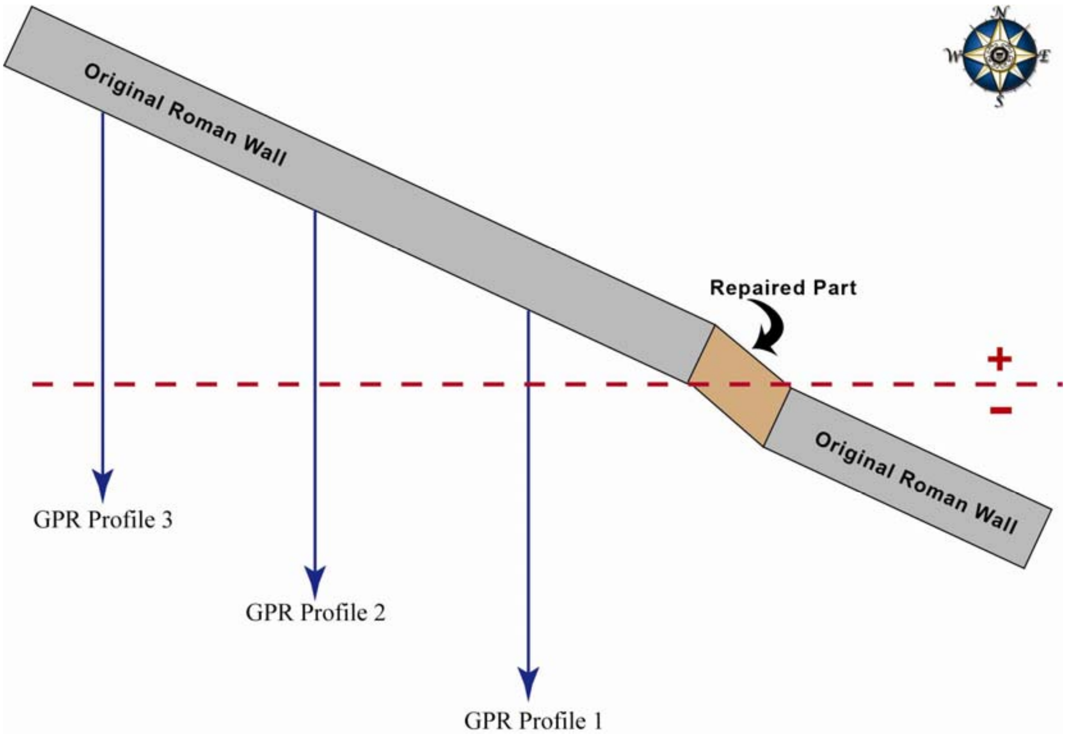

Figure 4.29: Schematic plan of the investigated area with the GPR profile.

Results of 250 MHz antenna:

The processed section of the first profile (GPR_profile_1 in Figure 4.28) shows that there is a continuous reflector near the surface which is not disturbed from one end to the other (Figure 4.30). However, other two reflectors at depth are offset by 80 – 90 cm. The processed section of the second and third profiles (GPR_profile_2 in Figure 4.28 and GPR_profile_3 in Figure 4.28) represent the similar undisturbed and offset reflectors near the surface and at depth, respectively (Figures 4.31 and 4.32).

The locations of offset reflectors were marked at the surface and a line was drawn through these three points (Figure 4.33). It is noticeable that the line meets with the wall where there is repair and downthrown on the wall.

The vertical downthrown on the wall is 255 cm, but 80 – 90 cm vertical offset was measured from GPR profiles. The wall is Roman in age (personal communication with Musa Kadıoğlu). The reliable penetration depth is about 3 meter in this site. Thus, it is possible that only recent faulting was observed in GPR profiles and previous offsets, which resulted the cumulative offset on the wall, are out of the GPR penetration range.

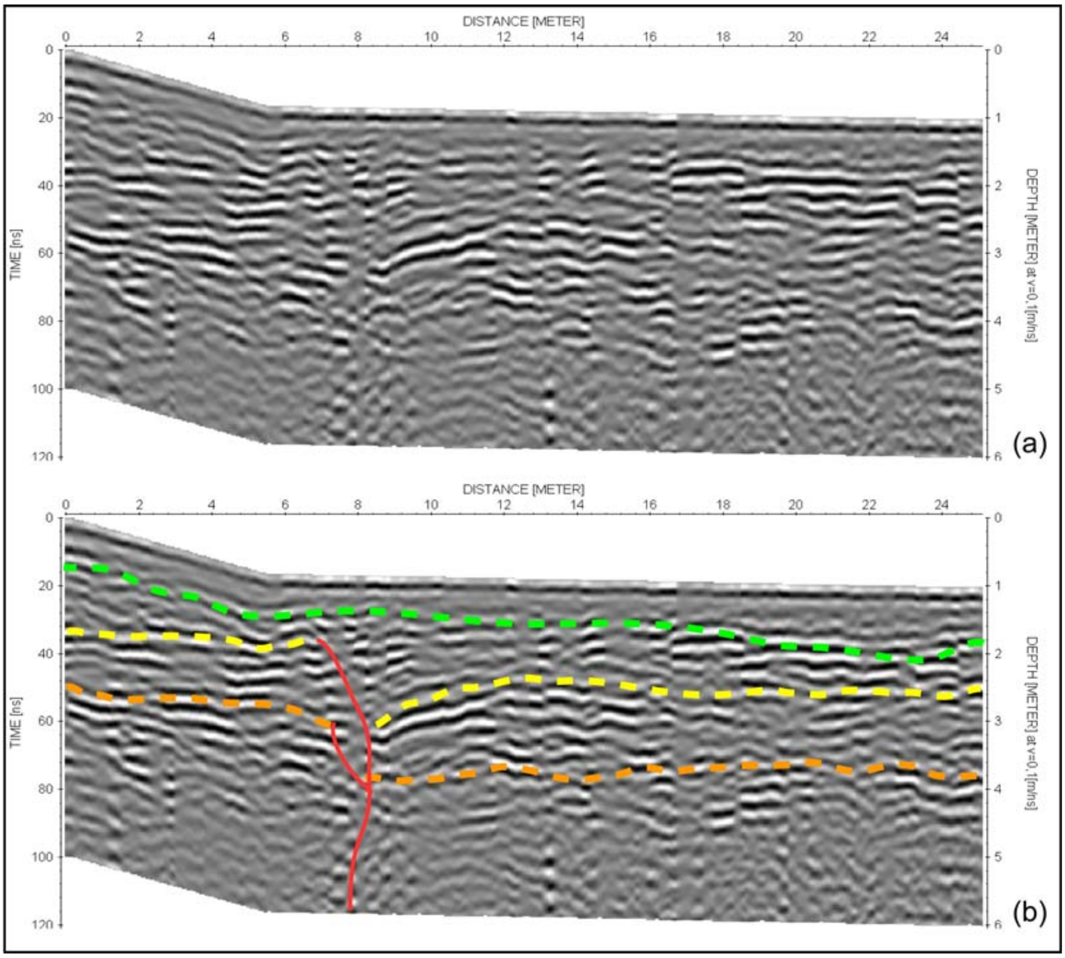

Figure 4.30: (a) Processed data of "GPR_profile_1" GPR profile. (b) Interpretation of "GPR_profile_1" GPR profile. Dashed lines represent the layers, thin red line represents possible fault zone.

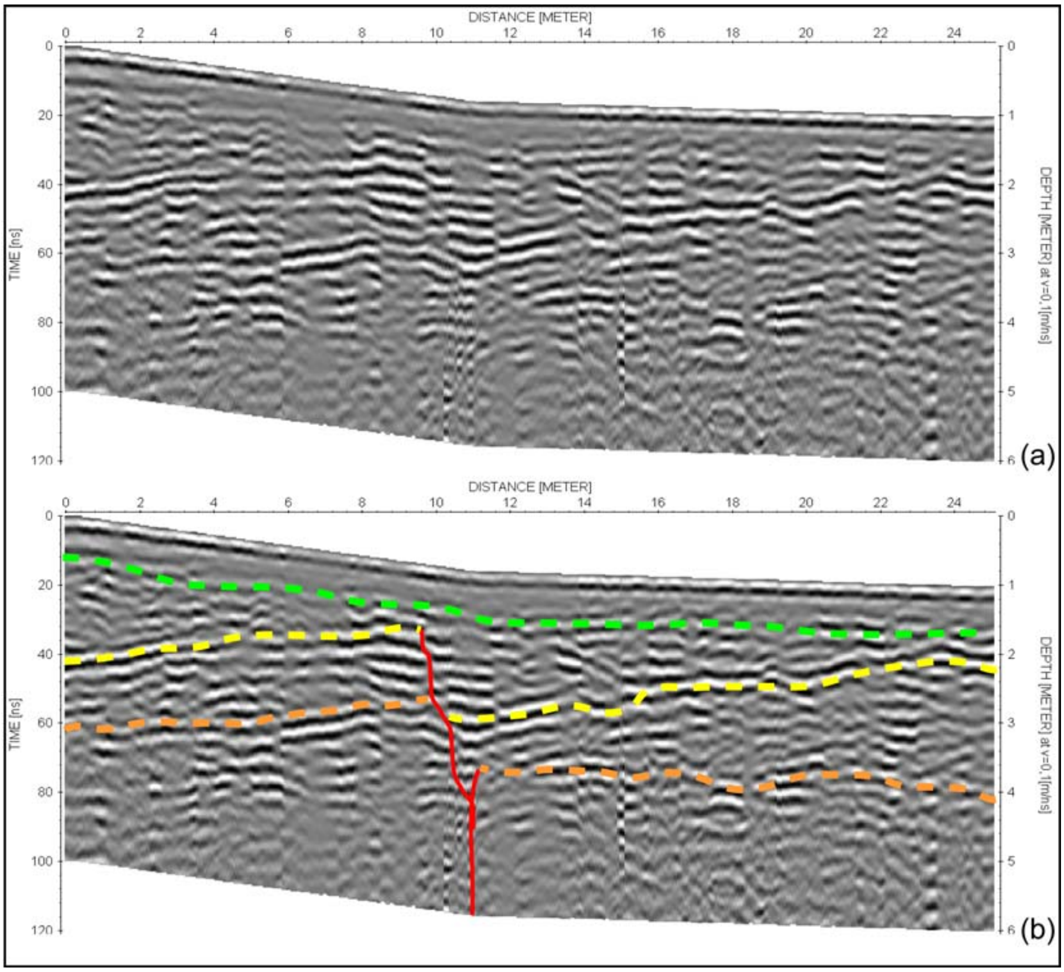

Figure 4.31: (a) Processed data of "GPR_profile_2" GPR profile. (b) Interpretation of "GPR_profile_2" GPR profile. Dashed lines represent the layers, thin red line represents possible fault zone.

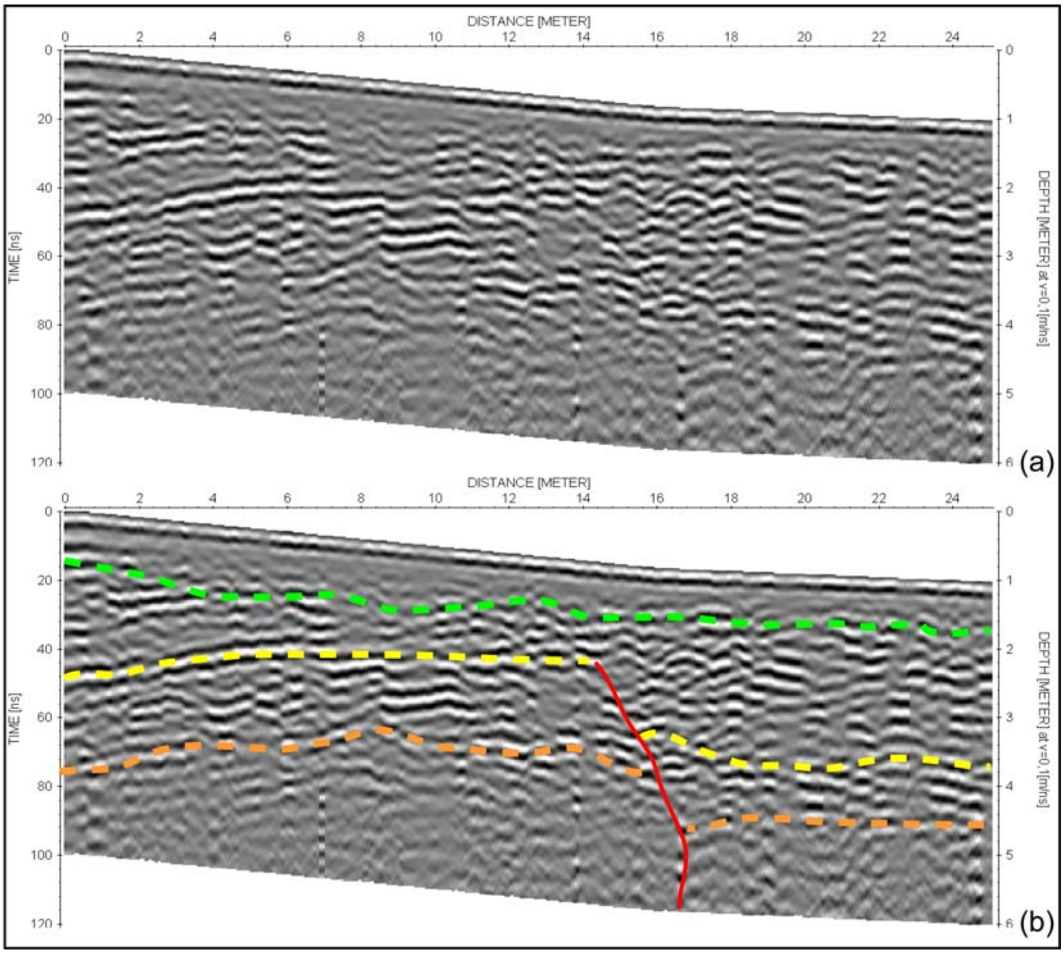

Figure 4.32: (a) Processed data of "GPR_profile_3" GPR profile. (b) Interpretation of "GPR_profile_3" GPR profile. Dashed lines represent the layers, thin red line represents possible fault zone.

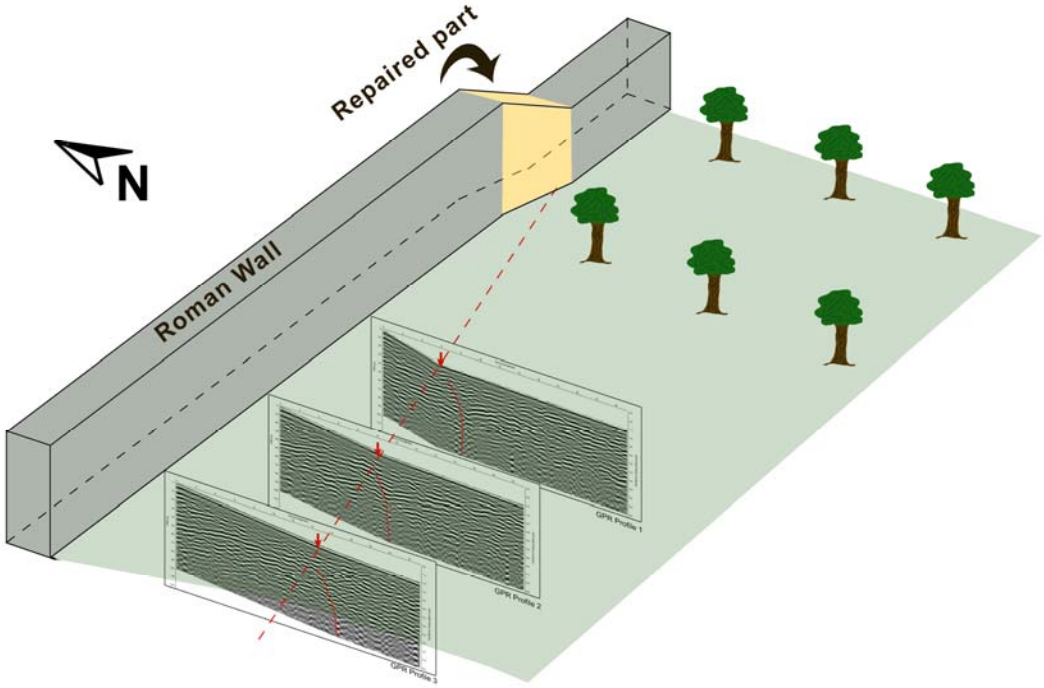

Figure 4.33: The schematic view of the wall with the GPR profiles and possible fault zone (red arrows indicate the disturbed zone in the GPR profiles, red dashed line represents the possible fault zone and yellowish part of the wall was repaired).

4.2.3 Roman Road

Field observations:

Mapping of both the Roman Road and active faults showed that they intersect about 2 km west of Sultanhisar (Figure 4.34). The Roman Road climbs up a 7 m-high morphological scarp in east of Çakırçek stream (Figure 4.35). This morphological scarp is interpreted as the location of active fault. The base of the Roman Road includes marble blocks (Figure 4.36). Thus, it would be possible to identify marble blocks on GPR sections. GPR studies applied in this site to see the effects of faulting on the road and to locate the fault precisely. Plan of using different GPR antennas is given in Figure 4.37.

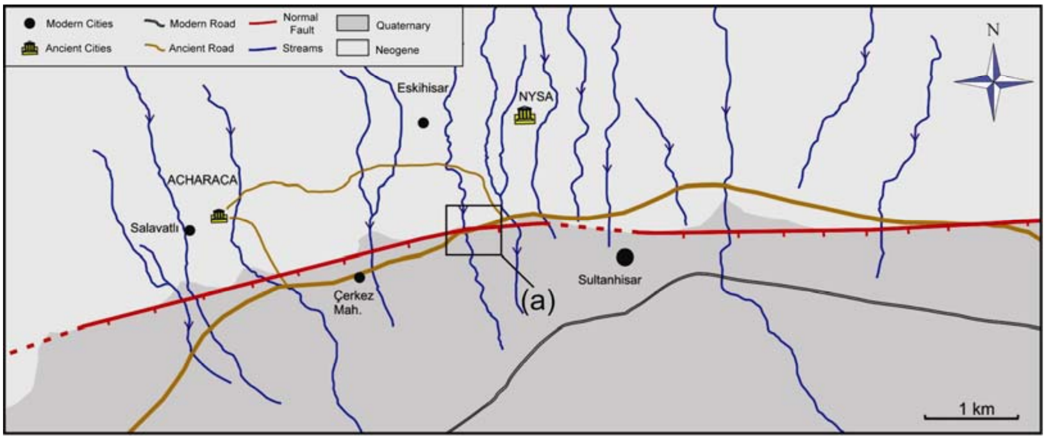

Figure 4.34: Position of the Roman road and the fault zone near Sultanhisar. Probably, fault zone and the ancient road intersect at two locations in the west of Sultanhisar. In the east he intersection point between fault zone and ancient road has not designated yet (black square "a" shows the intersection point in Figure 4.35a).

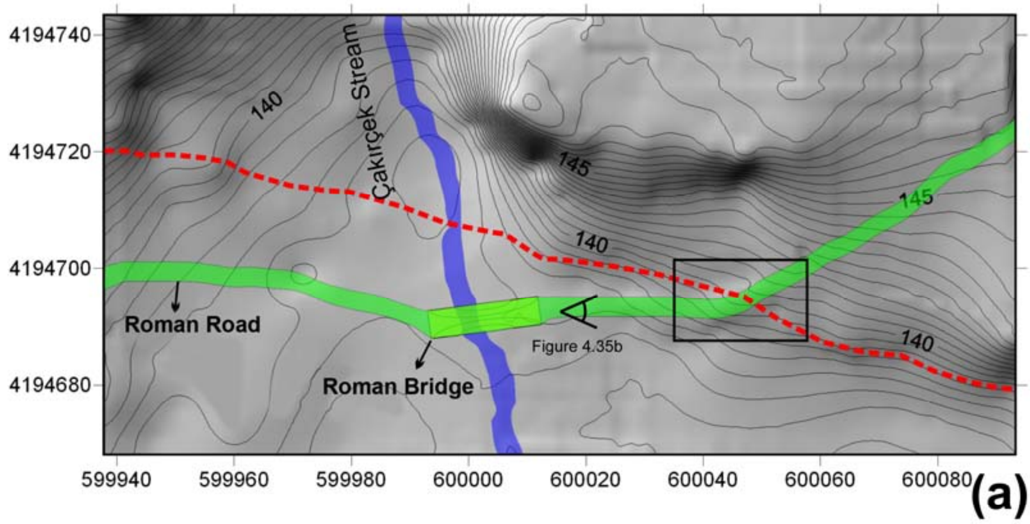

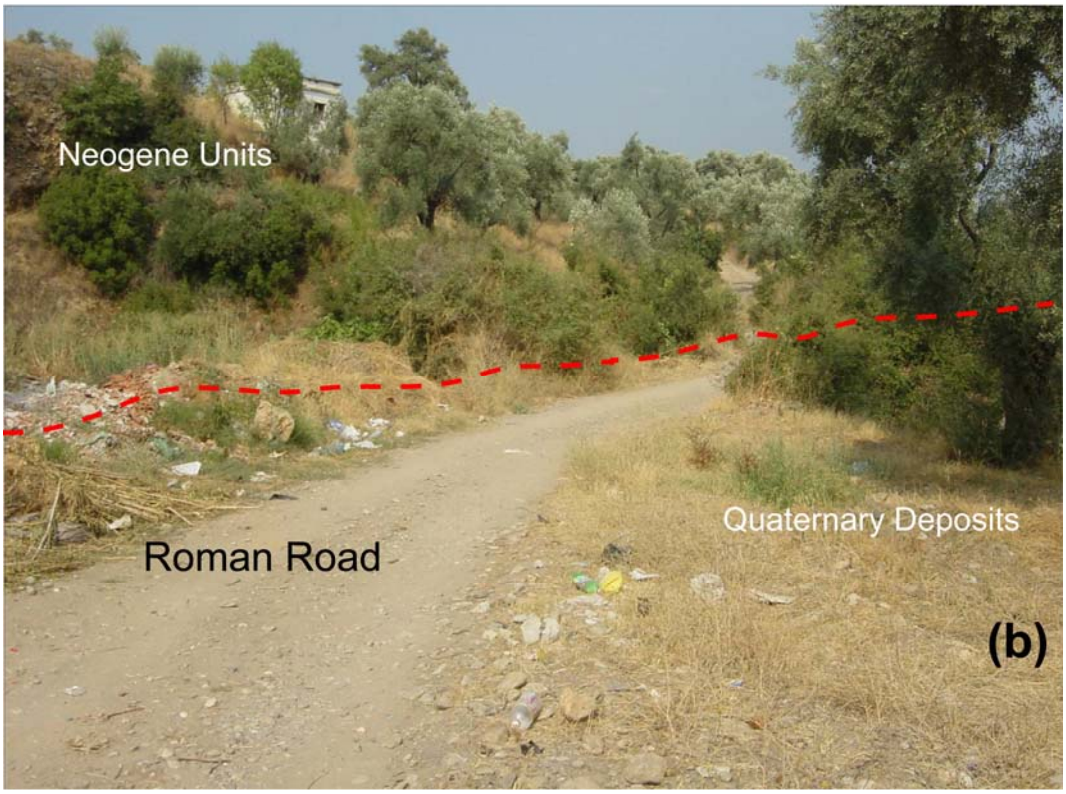

Figure 4.35: (a)The relief image map of the area "a" indicated in Figure 4.34 with square (the black square shows the GPR surveys area, the dashed red line corresponds with the fault zone and the green zone represents the ancient road). (b) The Roman road (looking towards east) (the dashed red line corresponds with the fault zone).

Figure 4.36: Stone blocks of the Roman Road near Sultanhisar (blue arrows indicate the stone blocks).

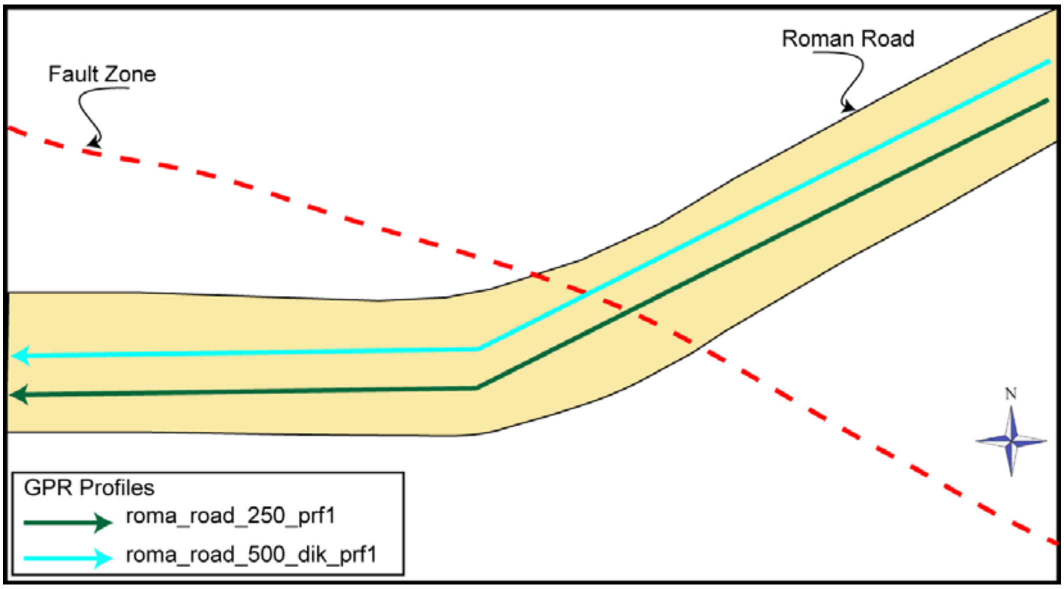

Figure 4.37: Unscale, schematic top view of the GPR profiles.

Results of 250 MHz antenna:

After data acquisition, we applied processing steps listed at the beginning of this chapter. From the processed 250 MHz profile (Figure 4.38a), we cropped the anomalous parts (Figure 4.38b) from the entire section (Figures 4.39a and 4.40a) for a better demonstration due to the profile length and for avoiding from vertical exaggerations in profile (roma_road_250_prf1 in Figure 4.37). The anomalous part of the profile is divided into two sub-sections (Figures 4.39 and 4.40). The processed and interpreted profiles of part 1 and part 2 are given in Figure 4.39 and Figure 4.40, respectively. The high contrast reflectors exist near the eastern and western sides of the profile but they disappear between 10 and 26 meters (Figure 4.38). Detail sections (part1 and part 2) show that there are several short high contrast reflectors at different depths between 10 and 26 meters. Detail sections (part1 and part2) also showed that there are normal reflectors below the high contrast reflectors but they are offset in three locations by about 40, 50 and 90 cm (Figures 4. 39 and 4.40).

The same road was also measured with the 500 MHz antenna with the same processing steps. However, processed profile is not satisfying to make any interpretation because noise effect of the rough surface is high (Figures 4.41, 4.42 and 4.43). Thus, interpretation of this location is based on only 250 MHz antenna.

The high contrast reflectors probably represent the base of the Roman Road. Existence of high contrast reflectors at various depths between 10 and 26 meters suggests that the road was damaged. Occurrence of offset reflectors in three locations may suggest that this is a 16-m-wide deformation zone. GPR traces between 10 and 26 meters are noticeably flat than other traces out of this zone. This difference probably suggests that the damaged part of the road was filled (or repaired) by different material.

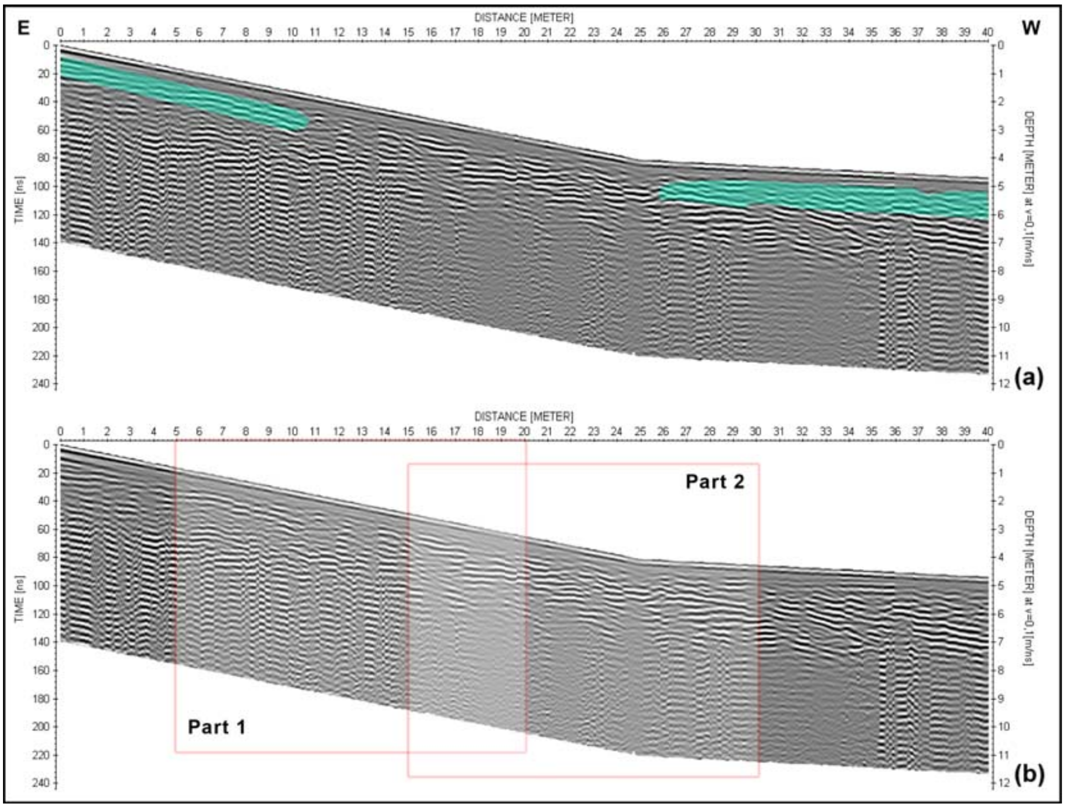

Figure 4.38: 250 MHz antenna profile of Roman Road. (a) Processed data of "roma_road_250_prf1" GPR profile (blue highlighted areas represent high contrast reflectors). (b) Two interpreted detailed area of the profile (Part 1and Part 2).

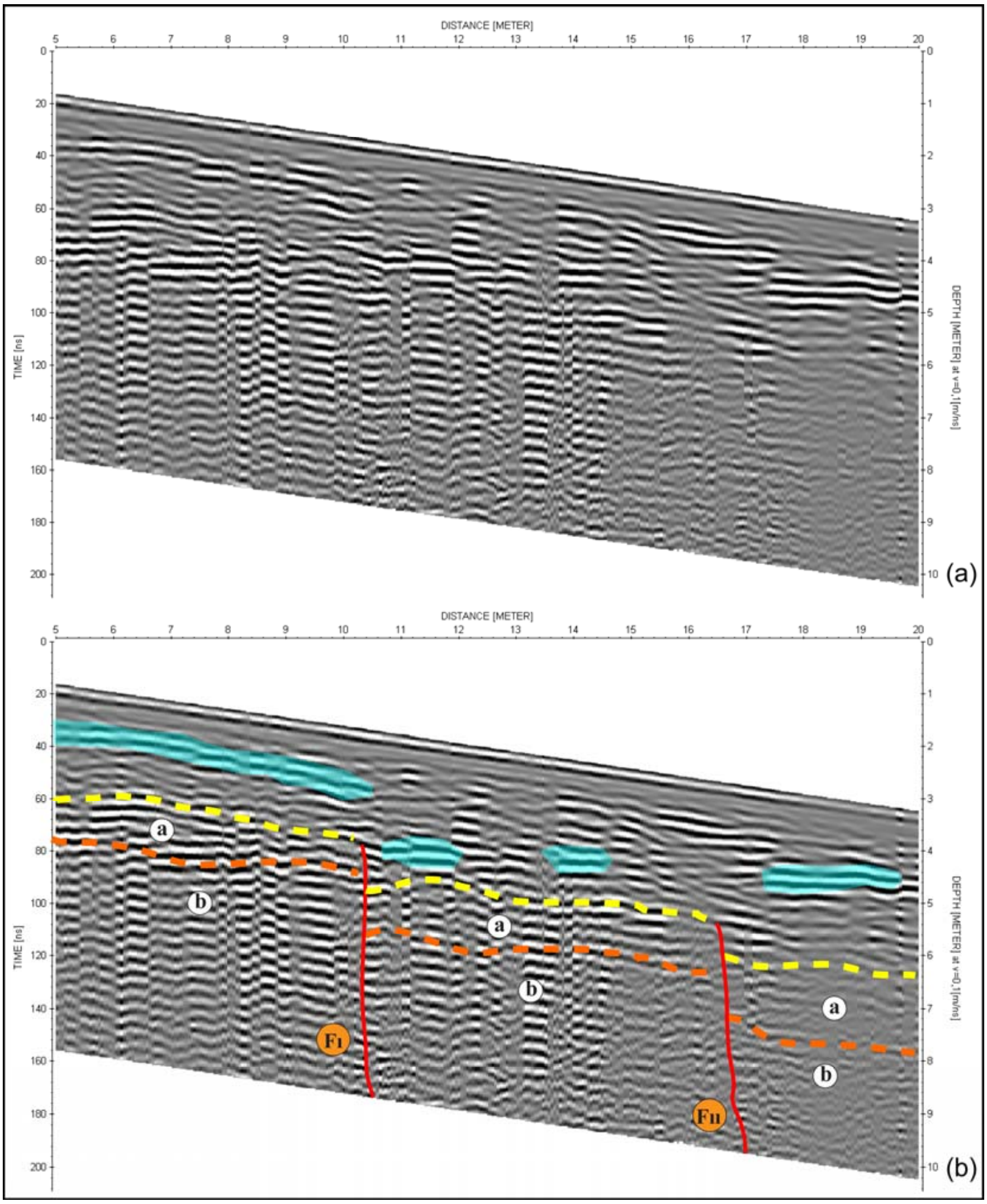

Figure 4.39: (a) Zoom view of the part 1 in Figure 4.38b. (b) Interpretation of the part 1. Blue highlighted areas represent high contrast reflectors, dashed lines and letters "a" and "b" represent the layers and thin red line with "FI" and "FII" represent possible fault zone.

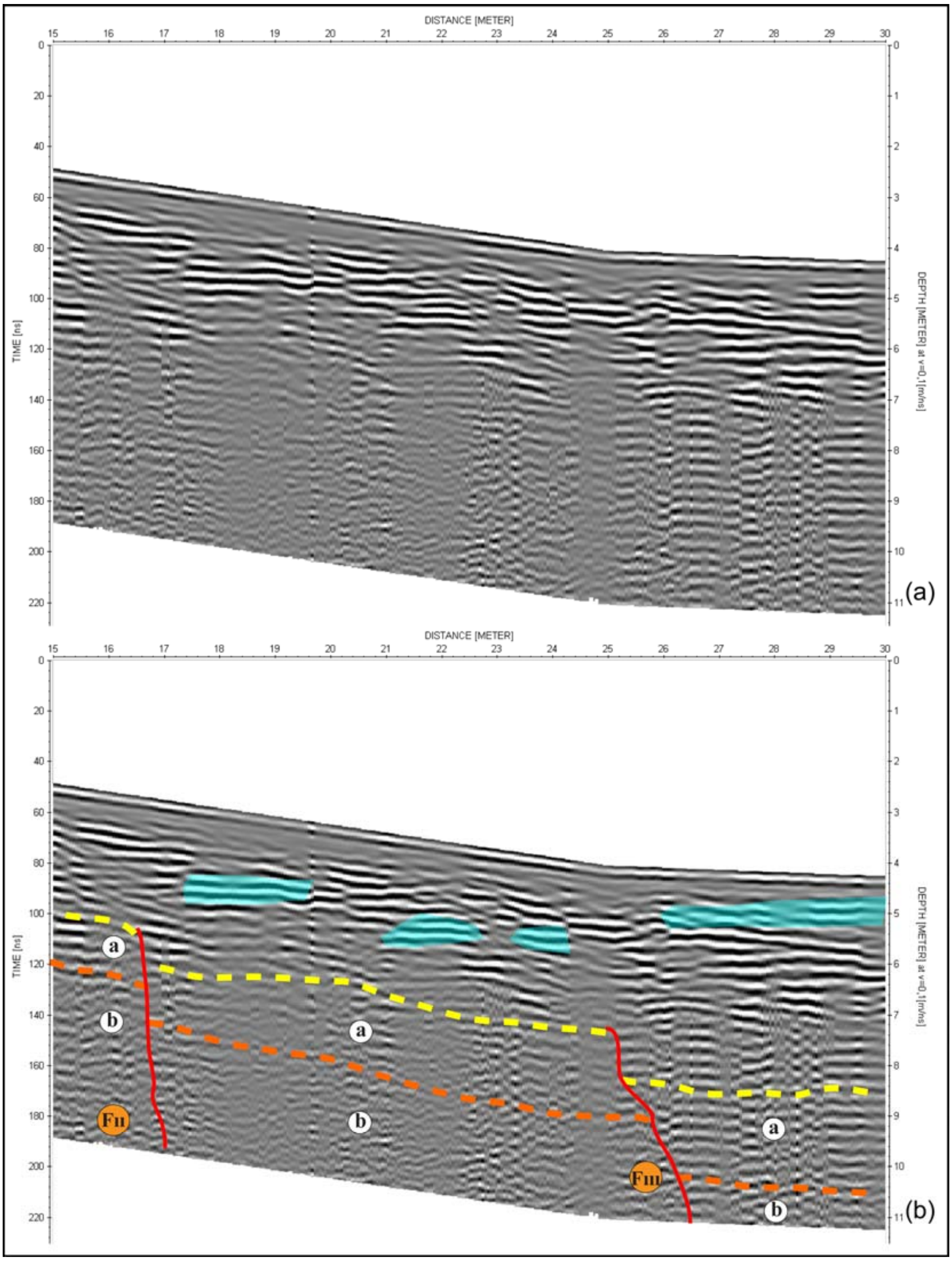

Figure 4.40: (a) Zoom view of the part 2 in Figure 4.38b. (b) Interpretation of the part 2. Blue highlighted areas represent high contrast reflectors, dashed lines and letters “a” and “b” represent the layers and thin red line with “FI” and “FII” represent possible fault zone.

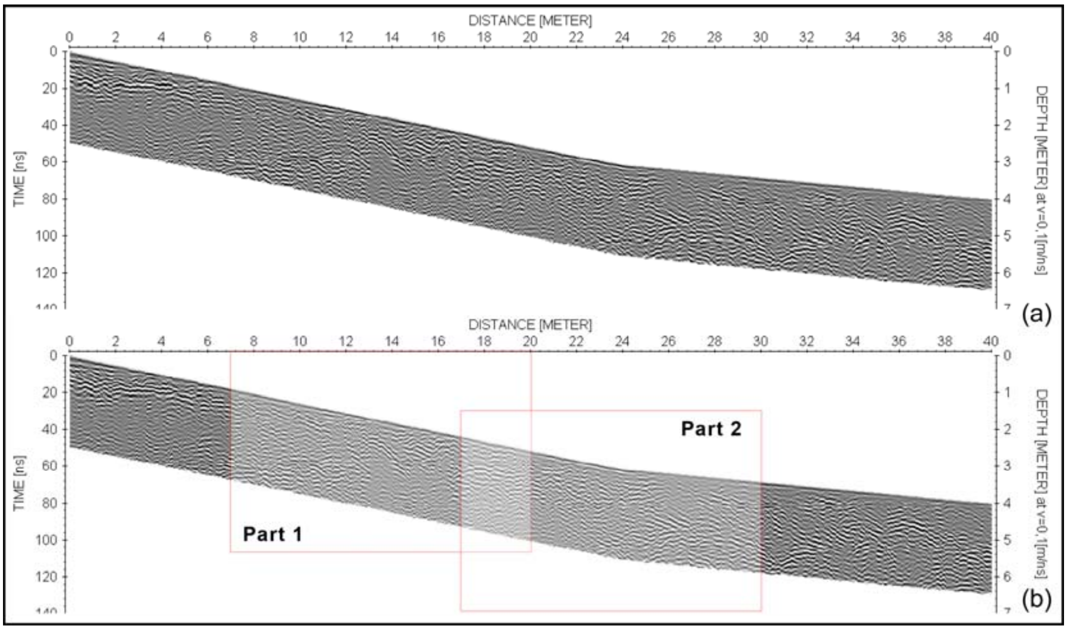

Figure 4.41: (a) Processed data of "roma_road_500_prf1" GPR profile. (b) Two interpreted detailed area of the profile (1. region and 2. region).

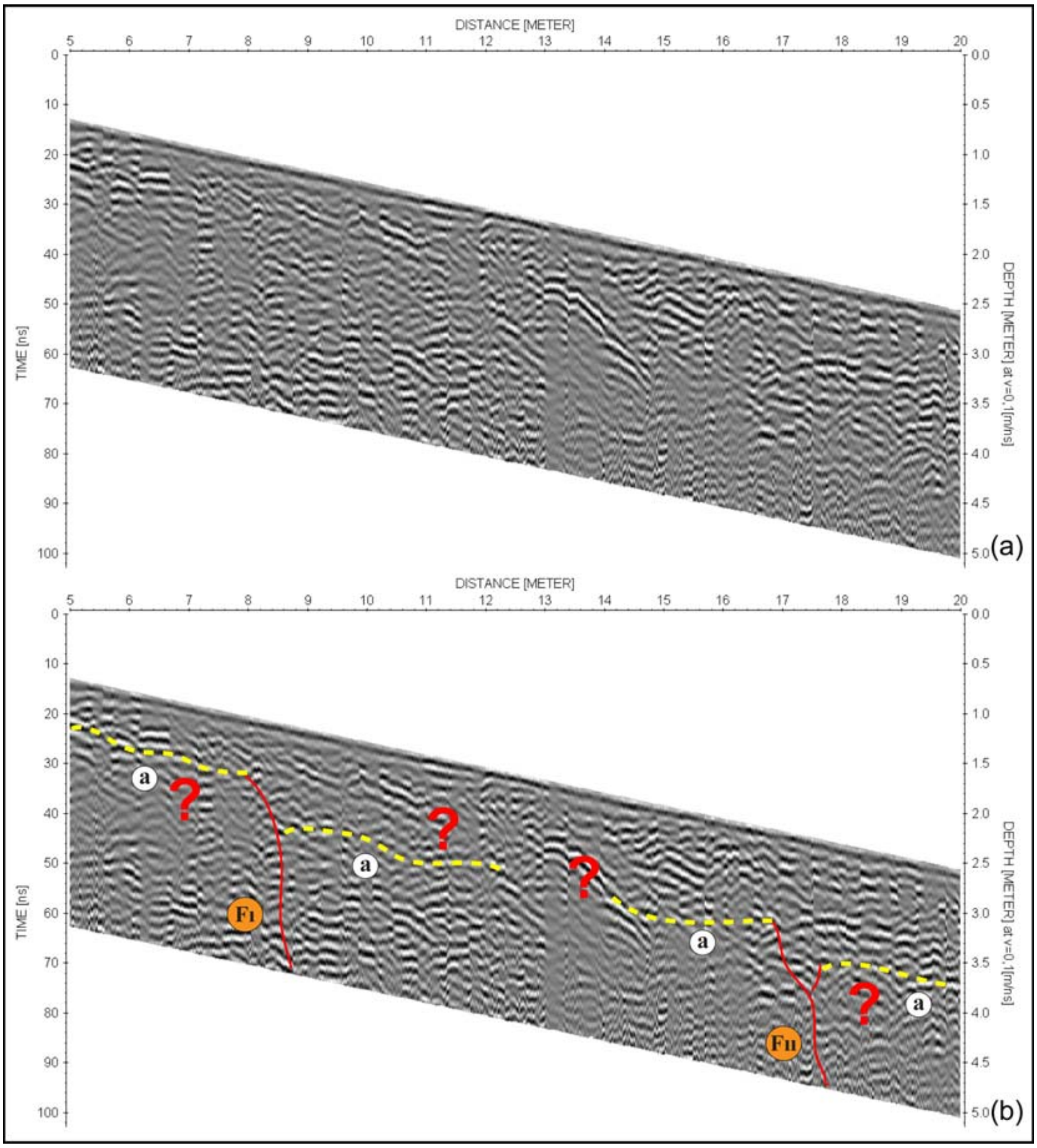

Figure 4.42: (a) Zoom view of the part 1 in Figure 4.41b. (b) Interpretation of the part 1. Dashed lines and letter "a" represent the layer and thin red line with "FI" and "FII" represent possible fault zone.

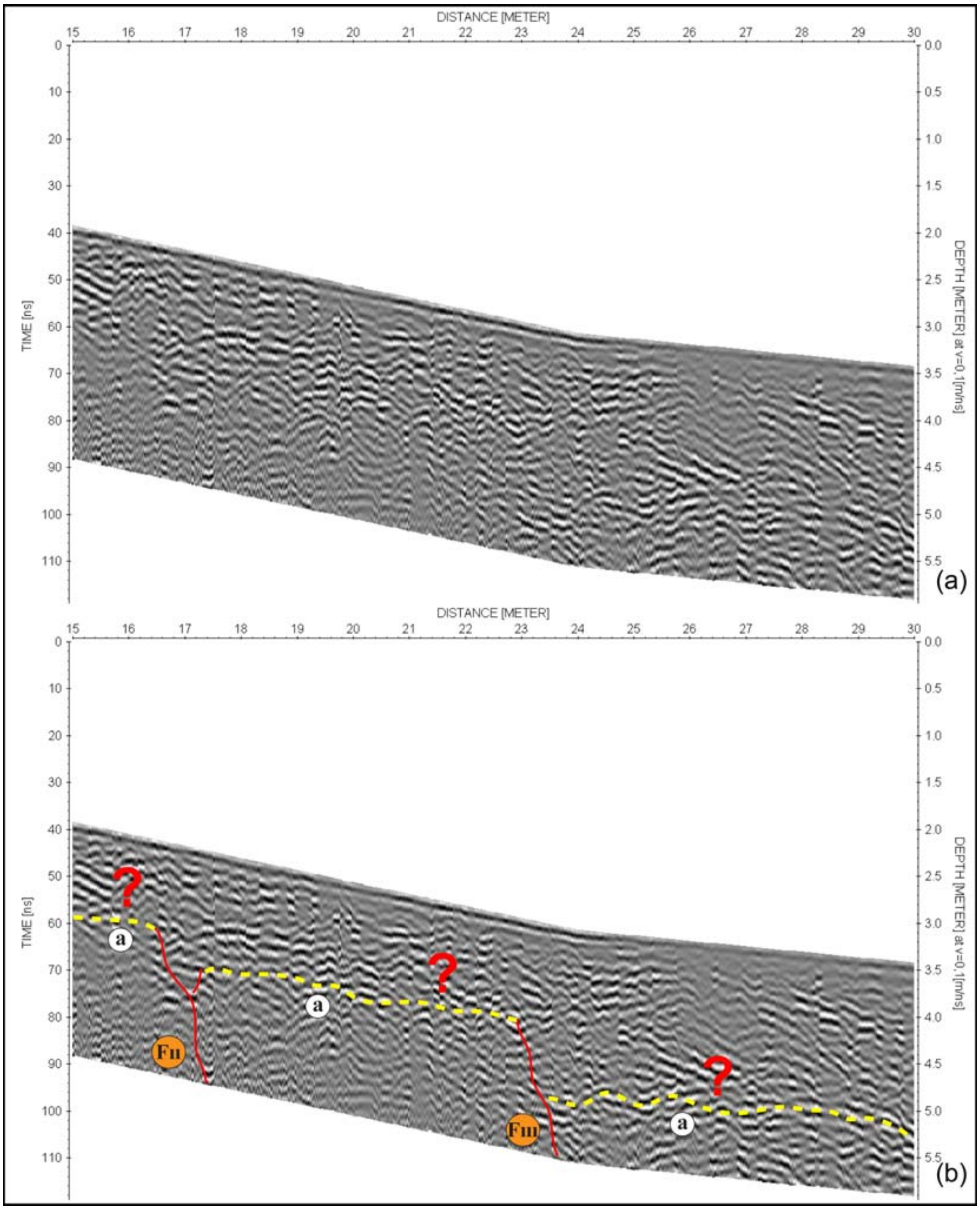

Figure 4.43: (a) Zoom view of the part 2 in Figure 4.41b. (b) Interpretation of the part 2. Dashed lines and letter “a” represent the layer and thin red line with “Fı” and “Fıı” represent possible fault zone.

4.3 GPR Applications to Buried Archaeological Features

NEW TEMPLE DISCOVERY AT THE ARCHAEOLOGICAL SITE OF NYSA (WESTERN TURKEY) USING GPR METHOD

Accepted Manuscript

Title: New temple discovery at the archaeological site of nysa (western turkey) using gpr method

Authors: C.Ç. Yalçıner, M. Bano, M. Kadioglu, V. Karabacak, M. Meghraoui, E. Altunel

PII: S0305-4403(08)00324-5

DOI: 10.1016/j.jas.2008.12.016

Reference: YJASC 2039

To appear in: *Journal of Archaeological Science*

Received Date: 13 May 2008

Revised Date: 8 December 2008

Accepted Date: 18 December 2008

New temple discovery at the archaeological site of Nysa (western Turkey) using GPR method

C.Ç. YALÇINER, M. BANO, M. KADIOGLU, V. KARABACAK, M. MEGHRAOUI and E. ALTUNEL

Journal of Archaeological Science, 2009, vol. 36, n° 8, pages 1680-1689

Pages 109-129 :

5 DISCUSSIONS AND CONCLUSIONS

The Büyük Menderes Graben (BMG) is a half-graben, located inside the wide extensional regime of the Aegean region and the main east-west trending part of it extends from Ortaklar in the west to Sarayköy in the east, a distance about 150 km, with a width of 8 - 12 km (Figure 1.1). It is bounded by active normal faults in the north and by secondary antithetic faults in the south. It is now widely accepted that the main active faults are located along the northern part of the graben (Cohen et al. 1995, Altunel 1999, Sözbilir 2000). There are clear and visible evidences of the historical activity in the region (Figure 3.15). Historical large earthquakes indications are also visible in man-made structures in the area, including shifted walls of ancient cities. The damage of these historical earthquakes is also examined in these structures in order to see the complete picture.

In the study of mapping of active faults in the north section of Büyük Menderes Graben, the observation of the surface ruptures was uneasy to perform and strictly limited in terms of visibility, mostly because of the erosion, land-slides, sedimentation and human activity. GPR is used in the area where the main segment is buried and no visual data of the fault's position is available. In this study, we have successfully located the buried faults in two regions.

Previous active fault mapping studies clearly show that the large historical earthquakes are generally leave characteristic signs on ancient structures. The ancient man-made structures which were built close to these fault systems (roads, walls, bridges, etc.) were usually affected by active tectonics. The signs of these activities give important information of faults' locations and their distinctiveness. In this work, using GPR method in three main locations, we have successfully pointed out the relationship between the fault characteristics and displacements in the man-made structures. During our GPR study, we have also discovered an ancient temple which was unknown before this work.

GPR studies we conducted in the Büyük Menderes graben gave excellent results especially in regions with suitable geological (dry and clay-free) and geomorphological (low inclination) conditions. Comparing the stratigraphy and geological structures seen in GPR profiles with those seen in trench and excavation walls confirms once again that the GPR method is an extremely useful and powerful tool to determine very precisely the fault traces, width of the shear zones and the amount of offset caused by faulting. Therefore, in regions where trench excavations are not possible, the GPR surveys may provide important information in characteristics of active faults.

5.1 Applications of GPR on Buried Active Faults

The main problem in mapping active faults and the external factors like erosion, sedimentation and/or human activity which make the observation very difficult. Sometimes it is impossible to trace the surface faulting. One of the most common solutions of this problem is shallow geophysics and preferably the high resolution GPR technique, since the method has been provided to be useful in exploring the buried structures with minimum geometrical and positional errors. The previous GPR studies on active faults generally focus on locating the discontinuity zones (e.g. Bano, et al., 2000; Meghraoui, et al., 2001; Audru, et al., 2001). In these studies the stratum are determined using Common Midpoint (CMP) techniques applied near these zones. In this work we were able to map the layers (and relevant faults and displacements) using different processing filters.

5.1.1 Argavlı

Büyük Menderes Graben alters its direction from E – W to NE – SW near town Germencik. Our study area near Argavlı is located close to the north of NE – SW elongation of BMG. The main fault segment in this area isolates the Quaternary deposits from Neogene units. During our mapping study it was seen that the morphological traces of the fault are destroyed by the agricultural activity in the area, thus the GPR method has been used to locate the precise location of buried fault. Both 250 MHz and 500 MHz antennas were used during these measurements.

Although the vertical resolution of the 250 MHz antenna is low (~20 cm), a total of 5 layers beneath the surface is mapped using the data from our first measurements. The most apparent attenuation zone is located between 5 – 11 m. Nevertheless, the results from 500 MHz antenna are more unclouded, since all the zones are more apparent and highly detailed with better resolution (~10 cm); four different displacements related to active tectonics has been clearly identified.

The trenching study which is performed after GPR measurements, focuses mainly on the east wall of the ~13 m long, ~1.5 m wide and ~2.5 m deep trench. The logs of this trench reveal a total of 6 main active faults on 12 different geological units spread over a ~7m wide zone.

The comparison of the results of GPR technique to trench study points a harmony between these two different methods. It must be noted that the 5 layer model of GPR justifies itself compared to the twelve layer of trench study since the trenching is a nose-to-the-stone method and it is also suitable for mapping small different layers "within" layers. The discontinuity zone is in the same width, both on GPR profile and trench logs. The main difference between them is the non-existent data on GPR profile where trench logged. Main comparison of found displacements from two methods is given in

Table 4.2; total amount (which is approximately 160 cm) is significant in two techniques.

5.1.2 Atça

Our study area is located on the north strand of Büyük Menderes Graben (where the fault is E – W) is 2 km east of town of Atça (Figure 4.9). The main fault segment in this area separates the Neogene units from Quaternary deposits (Figure 4.10). There are scarp formations between fairly traceable Neogene units and Quaternary deposits in the area, as well as a gentle scarp structure which is an uncommon feature of Quaternary sediments. In order to find the precise location and geometry of the buried fault and to reveal the reason of presence of this gentle scarp in the area, GPR technique is used. Main profile which is measured with 250 MHz antenna is surveyed from the south corner of the Neogene units and intersects the Quaternary sediments with gentle scarp. This long (approximately 50 m) profile reveals a large anomaly between 34 – 36 m on it. After it has been understood that these anomalies represent the gentle scarp in Quaternary deposits, more detailed short GPR surveys have been performed, using both 250 and 500 MHz antennas.

The detailed 250 MHz GPR profile reveals a total of 5 layers beneath the surface with two main faults which are clearly offset these layers. But since the leveling between the hanging-wall and the foot-wall is unclear, it is nearly impossible to comment about the amount of vertical displacement between these two blocks based on 250 MHz measurements. On the other hand, the other 500 MHz GPR survey performed in the same profile has clearly shown that there are two different stratigraphic packages present here, with a high ratio of contrast. Also 500 MHz GPR survey spots a total of 5 main layers, just like the previous 250 MHz measurement, but this time in much details. In addition to this, the 500 MHz GPR profile has shown some channel fillings in hanging-wall which are undetected previously and displacements along 2 different zones (~80 cm and ~50 cm).

The main trench excavated right after GPR surveying, is about 13 m long, ~1.5 m wide and ~3.5 m deep. The logs of this trench reveal a total of 2 main active faults and 6 channel fillings on 12 different geological units. The first fault (which carries an approximately 3.5 m of displacement) is exposed on the surface and is a shear zone. The second fault (which carries an approximately 0.5 m of displacement) is a single fault which terminates in 1.5 m below ground level.

The comparison of 500 MHz GPR surveying to trench logs reveals a good agreement, particularly where two faults are evident in both results (Figure 4.16). In GPR profile, the first fault lies as a single line on bedrock and while it develops to surface, it splits into two different segments. However, the same location has been identified as a 70 cm wide shear zone in trench logs. Although it is not possible to clearly separate the related slip planes from each other in GPR profile, a ~60 cm wide zone has been identified close to surface. The location and elongation of the second fault is successfully revealed in both methods with same specifications. Despite this, extra number of the channel fillings is brought to light with the trench logs, while GPR results show just 2 of them. The main reason of this deficiency is caused by the interference theory behind GPR technique; different grain sizes within "almost" homogenous geological units are mostly ignored by the electromagnetic waves collected.

Previous studies in the study area incorrectly interpreted the mentioned scarp (which is clearly traceable between Neogene units and Quaternary deposits) as the surface rupture of the main fault. However, our GPR surveying and trench study show that the current active fault is not following the Quaternary – Neogene contact, in fact, it is developed within Quaternary deposits. It is now known that if the combination of the GPR technique and trenching would not have been performed, the geological information gathered from the surface observations would mislead the researchers who are interested in region.

5.2 Applications of GPR on Offset Archaeological Features

GPR studies have been used widely in many archaeological studies (e.g. Hruska and Fuchs, 1999; Dabas et al., 2000; Piro et al., 2001; Lualdi and Zanzi, 2002; Chianese et al., 2004; Persson and Olofsson, 2004; Leucci and Negri, 2006). The main aim of usage of the GPR technique in archaeological research is to explore the buried structures like roads, walls, cavities, burial places and graves, etc. These archaeological structures, which made from materials different from the surrounding resources, are usually easy to spot by GPR since their characteristics form sharp contrasts beneath the surface.

Despite the often usage of GPR method in archaeological research, this method has not been applied sufficiently for investigation of active faults which generally left signs of historical activity on archaeological remains. It is now known that the GPR method provides information about these earthquakes on damaged archaeological subjects and furthermore, in most cases, a slip amount is also measurable. The comparison of the GPR results and surface observations may help researchers to increase their knowledge on historically active faults, time intervals of large earthquakes and most importantly, the location of buried and/or unknown fault systems. In this study, we have worked in three different places where surface ruptures intersect with archaeological remains: Ottoman Bridge, Roman Road and Roman Wall.

5.2.1 Ottoman Bridge

Ottoman bridge is near the town of Sazlıköy and it located on the old riverbed of Menderes River (Figure 4.16). The bridge was built by Ramazan Pasha in 1595 and there is a significant displacement on the east edge of it (Figure 4.17). It has been thought that since the bridge has been built on the fault zone this displacement may be a result of active tectonics in the area. Thus, GPR surveys have been performed on the bridge and in the south section.

In order to find any discontinuity zones related to the damage on the bridge, two 250 MHz GPR profiles are mapped along the south edge but in opposite directions and 3 m apart from each other. Both profiles show the same reflectors and hyperbolas which are corresponding to same levels beneath the surface. Again, both profiles frame an approximately 1 m of vertical displacement, very close the section where the bridge is damaged. The second GPR survey is performed along the same line – in opposite direction- and this time with a 500 MHz antenna; but since the ground has high conductivity and this causes some noticeable noise in data, 250 MHz results are more precise than the second survey.

Another 500 MHz GRP survey is carried out along the bridge for the purpose of determining the effects of the damage caused by a possible fault. It is also possible to compare the remaining original construction to the restored section using GPR. When investigated, this profile reveals similar reflectors on both ends: the first 7 m of the west-side and the first 10 m of the east). The remaining central part between these sections represents the constructional parts of the bridge like arches and windows which reveal themselves as symmetric hyperboles. One of the conspicuous matters in this GPR profile can be pointed out between 84 – 86 m where there is no hyperbole and traces are in different characteristics from the rest of the profile data. It is thought that this significant matter might indicate a reparation of the bridge in this section, probably an attempt to erase the damage of an earthquake since this renovation is in same place where the displacement occurs.

5.2.2 Roman Wall

During the fault mapping stage of the study, it was realized that a wall with a 5m height stands on the top of an active fault in the area (Figure 3.12). This Roman wall is located near Salavatlı and has an approximate N – S trend. Although a direct visual comparison of this wall to the fault direction does not show a clear result, a detailed study revealed that some parts of the wall has been restored, particularly the parts where the wall intersects with the fault. Also LIDAR images have shown approximately 255 cm of vertical displacement in this section of the wall (Figure 4.26). A total of three west-side profiles measured perpendicular to the proposed fault direction to investigate the displacement on this Roman wall. Unfortunately, no GPR surveying was available on the wall itself since the condition on the surface of the wall is not well-matched the requirements of GPR profiling. In addition to this, the 500 MHz antenna was not able to perform in this section, because of the angles which made the surface unsuitable for GPR profiling.

The first GPR profile reveals a reflector which has not been displaced and goes from the beginning to the end of the profile continuously close to the surface; but beneath this, two different reflectors have been detected with an average slip of 80 – 90 cm. These reflectors are also traceable in the other two GPR profiles surveyed later. When the surface traces of the displacements are joined together with a flat line, the direction of the formed linearity coincides with the restored section of the wall (Figure 4.32).

The vertical offset measured by observations on the surface of the wall is approximately 255 cm; on the other hand, GPR measures an offset of 80 – 90 cm in the same place. It is thought that since the wall has been built during Roman times, the offset which revealed by the first 3m of the GPR profile represents the latest activity. However, in this case, the penetration depth of GPR is not in acceptable limits to explore all the tectonic activities beneath the surface.

5.2.3 Roman Road

Fault maps show an intersection between the Roman road and the main fault which is located ~2 km west of the town of Sultanhisar (Figure 4.33). 7m high slope with offsets on is noticeable in this intersection and it is thought that this slope is resulted from the main displacement. It is also thought that since the floor of the Roman road is made from marble blocks, GPR method can map the absolute location of the fault. 250 MHz and 500 MHz GPR measurements are performed according to this idea.

Based on the interpretation of the 250 MHz GPR profile, collected data are divided into several sub-sections in order to make a detailed investigation of vertical / horizontal offsets. The sections which carry the main anomalies are considered as two different windows to reveal the real-life dimensions of the measured parts (part 1 and part 2). The high contrast reflectors fade out between 10 – 26 m while they are significant on the other sections of the GPR profile. The parts where a detailed investigation has been made (part 1 and part 2) includes multiple sized and shaped high contrast reflectors in various depths. Detail sections (part1 and part2) also showed that there are normal reflectors below the high contrast reflectors, but they are offset in three locations by about 40, 50 and 90 cm (Figures 4. 39 and 4.40). The same line is also measured with 500 MHz GPR and processed in same manner. However, processed profile is not in satisfactory limits in order to make any solid interpretation since the noise effect of the rough surface is high (Figures 4.41, 4.42 and 4.43). Thus, interpretation of this location is based on only 250 MHz antenna.

It is thought that the high contrast reflectors would represent the base of the Roman Road. Existence of high contrast reflectors at various depths (between 10 and 26 meters) may suggest that the road was damaged during the historical activity. Occurrence of offset reflectors in three different locations may suggest that this is a 16m wide deformation zone. GPR traces between 10 and 26 meters are noticeably flat than other traces out of this zone. This difference probably suggests that the damaged part of the road was filled (or repaired) by different material.

5.3 Applications of GPR on Archaeology

A wide range of shallow geophysical methodologies is now available for obtaining high-resolution images that may enhance the archaeological field investigations. There is extensive literature concerning the applications of GPR in the archaeological field. In general the survey targets include the identification and mapping of buried artefacts or construction features, the localization of tombs, burial mounds, shallow graves and the reconstruction of archaeological layers (e.g. roads, walls, channels) (Vaughan, 1986; Goodman, 1994; Goodman et al., 1995; McCann, 1995; Hruska and Fuchs, 1999; Dabas et al., 2000; Piro et al., 2001; Lualdi and Zanzi, 2002; Chianese et al., 2004; Persson and Olofsson, 2004; Leucci and Negri, 2006). The GPR investigation depth depends on the EM wave attenuation (which grows as the conductivity of the subsoil materials increases) and on the frequencies level. The lower the frequency, the greater the penetration depth that varies from a few meters in conductive materials to 50 m for low conductivity (less than 1 ms/m) media (Davis and Annan, 1989; Smith and Jol, 1995). The vertical resolution depends on the frequency used and the EM velocity of the subsurface, it varies from 0.15 to 0.76 m for frequencies of 100-250 MHz (Jol, 1995), which makes this technique suitable for high-resolution shallow studies in archaeological applications.

5.3.1 Nysa

We carried out a GPR study at specific sites around the Nysa (west Turkey) city to assess the potential of detection method and imaging of buried archaeological features. As a major educational and cultural Aegean city during the Hellenistic and Roman s, Nysa has been the focus of archaeological investigations for the last 100 yrs. Past and ongoing excavations have revealed major ancient buildings such as theatres, amphitheatres, a library and shops. However, it is suspected that the original city may have extended further and reached a larger size. We collected 22 profiles using a GPR system equipped with two shielded antennas of 250 and 500 MHz central frequencies. After processing steps, GPR results revealed the existence of buried walls located at ~50 m west of the library. They systematically display a characteristic signature (hyperbolic anomalies) in GPR profiles and may be described in terms of location, geometry, and dimension and to a certain extent of construction style.

The archaeological remnants are buried 2-3 m thick colluvial sediments consisting of coarse sand with large gravels overlain by organic soil (0 – 0.8 m). The absence of thick clay deposits with in the unconsolidated colluvial sediments and the deep water table allowed us to image the archaeological remnants at a high resolution. Unlike most archaeological sites, the flat topography of the survey site and the nonexistence of archaeological structures at the surface allow us to acquire good quality GPR profiles. Testing two different frequency of GPR antenna showed that the roots of olive trees hide the buried archaeological remnants if a 500 MHz central frequency antenna is used. This difficulty was overcome by using the 250 MHz GPR antenna. Therefore, this suggests that relatively lower frequency antennas should be used in areas covered by trees.

In order to map the 3D distribution of the archaeological remnants and determine their size we have carried out our surveys in a grid manner. This allowed us to reveal the architecture of the temple in fine detail, which, in turn, allowed the archaeologists to expedite their archaeological excavation.

The findings in all excavations were not sufficient enough to precisely determine the age of temple. The lime daub stone walls and the library in the same Insula (island) with temple could help for dating the temple. The date of library construction that is early 2nd century AD can be applied to date of construction for this temple. Unfortunately no evidence of dedication was found for temple construction. However, if we accept the temple date as early 2nd century AD, it was probably dedicated to the Roman Emperor Trajan (98-117 AD) or Hadrian (117-138 AD). It is most likely that the In-antis plan building is a Heroon (monument buildings for heroes).

5.4 Suggestions

Although the GPR method has been used for long to image the underground by various researchers, the results of this method are not comprehensible by scientists dealing with the other branches. Unless interpreted, even the processed GPR profile tells nothing to those who are not familiar with these profiles. It is obvious that the hardware and software under development shall be very useful to make the GPR profiles more clear and understandable.

The choice of the frequency of the antenna depends on the depth of the target to be studied; the larger the depth of the target, the lower the frequency of the antenna that should be used. This is the case for GPR investigations in geological studies. On the other hand, the shallower the depth of the target of interest, the higher the frequency of the antenna to be chosen. This is the case for GPR investigatins in archaeological studies. For this kind of situations, a multi-channel GPR system can be used.

In addition to GPR surveys, other shallow geophysical methods like magnetic, electromagnetic, seismic, electrical resistivity and IP can be performed to investigate the buried faults and archaeological remnants where the GPR surveys are difficult to conduct or provide poor GPR results due to, for example, rough surfaces, heavy vegetation, clayey lithology and steep slops.

REFERENCES

Akurgal, E., 1995. Anadolu Uygarlıkları. Net yayınları, İstanbul

Allen, C.R., 1975. Geologic criteria for evaluating seismicity, Geological Society of America Bulletin 86 (1975), pp. 1041–1056.

Altunel, E., 1999. Geological and geomorphological observations in relation to the 20 September 1899 Menderes earthquake, Western Turkey Journal of the Geological Society, London, vol. 156, pp.241 – 246.

Altunel, E., Akyüz, H. S., Meghraoui, M., Kiyak, N. G., Karabacak, V., Yalçıner, C. Ç., 2009, Archeoseismology and Paleoseismology of Büyük Menderes fault zone, TÜBİTAK Project (Project no: 105y348), 205 pp.

Ambraseys, N.N. 1988. Engineering Seismology. Earthquake Engineering, Structure and Dynamics, 17, 1-105.

Ambraseys, N.N. and Finkel C.F. 1995. Türkiye'de ve komşu bölgelerde sismik etkinlikler; Bir Tarihsel İnceleme 1500-1800. TÜBİTAK Yayınları Akademik Dizi-4.

Ambraseys and Jackson, 1998 N.N. Ambraseys and J.A. Jackson, Faulting associated with historical and recent earthquakes in the Eastern Mediterranean region, Geophysical Journal International 133 (1998), pp. 390–406.

Anderson, K.B., Spotila, A. and Hole J.A. 2003. Application of geomorphic analysis and ground-penetrating radar to characterization of paleoseismic sites in dynamic alluvial environments: an example from southern California. Tectonophysics, 368, 25 – 32.

Angelier, J., Recent quaternary tectonics in the hellenic arc: Examples of geological observations on land. Tectonophysics, 52, 1-4.

Annan, A.P., Waller, W.M., Strangway, D.W., Rossiter, J.R., Redman, J.D., and Watts, R.D., 1975, The electromagnetic response of a low-loss, 2-layer, dielectric earth for horizontal electric dipole excitation. Geophysics, Vol. 40, No. 2, 285-298

Annan A.P. & Cosway SW. 1992. Simplified GPR beam model for survey design. Extended Abstracts of 62nd Annual International Meeting of the Society of Exploration Geophysicist, New Orleans, 25–29 October. Reprinted by Sensors and Software Inc. PEMP

Ateş, R.C. and Bayülke N., 1982. The 19 August 1976 Denizli, Turkey, earthquake: Evalution of the strong motion accelerograph record. Bull. Of the Seis. Soc. Am., 72, 5, 1635-1649.

Audru J.-C., Bano M., Begg J., Berryman K., Henrys S. and Niviere B., 2001. GPR investigations on active faults in urban areas: the Georisc-NZ project in Wellington, New Zealand. Earth and Planetary Science, Volume 333, Number 8, 31 October 2001 , pp. 447-454(8).

Bano, M., Marquis, G., Nivière, B., Maurin J.-C., and Cushing M., 2000. Investigating alluvial and tectonic features with ground-penetrating radar and analysing diffraction patterns. J. Appl. Geophys. 43, pp. 33–41.

Bean, G. 1989, Turkey Beyond the Maeveer (revised version of 1971), Ernest Benn, London (Revised and edited by J. Bean (1980) and published by John Murray, London.

Bozkurt, E., and Park R.G., 1994. Southern Menderes massif: an incipient metamorphic core complex in western Anatolia, Turkey. Journal of the Geological Society, London, 151,213-216.

Bozkurt, E., 2000. Timing of extension on the Büyük Menderes graben, Western Turkey, and its tectonic implications.

Calligeros, E., Hehir, D., and Jacobs, R., 1997. Invention of Radar.

Carrozzo, M.T., Leucci, G., Negri, S., Nuzzo L., 2003b. GPR Survey to Understand The Stratigraphy of The Roman Ships Archaeological Site (Pisa, Italy), Archaeological Prospection, 10, 57-72.

Chianese, D., D'Emilio, M., Di Salvia, S., Lapenna, V., Ragosta, M., Rizzo, E., 2004. Magnetic mapping, ground penetrating radar surveys and magnetic susceptibility measurements for the study of the archaeological site of Serra di Vaglio (southern Italy). Journal of Archaeological Science 31, 633-643.

Cohen, H.A., Dart C.J, Akyüz H.S., and Barka A. 1995. Syn-rift sedimantation and structural development of the Gediz and Büyük Menderes graben, Western Turkey. Journal of the Earth Society, London, Vol.152, pp. 629-638.

Conyers, L. B., 2004. Ground-penetrating Radar for Archaeology. Altamira Press, Walnut Creek, California.

Conyers, L. B., 2006. Ground-penetrating radar techniques to discover and map historic graves. Historical Archaeology, v 40, n. 3, pp. 64-73.

Cook, John C. (1960). "Proposed monocycle-pulse, VHF radar for airborne ice and snow measurements." AIEE Trans. Commun. And Electron., 79(2), 588-594.

Dabas, M., Camerlynck, C., Freixas, I., Camps, P., 2000. Simultaneous use of electrostatic quadrupole and GPR in urban context: investigation of the basement of the Cathedral of Girona (Catalunya, Spain). Geophysics 65 (2), 526-532.

Daniels, D. J., 2004. Ground Penetrating Radar 2nd Edition, published by the Iee Radar, Sonar, Navigation and Avionics Series, London, United Kingdom.

Davis, J.L., Annan, A.P., 1989. Ground penetrating radar for high resolution mapping of soil and rock stratigraphy: Geophysical Prospecting, 37: 531-551.

Dewey, J.F. and Şengör, A.M.C., 1979. Aegean and surrounding regions: complex multiplate and continuum tectonics in a convergent zone. Geological Society of America Bul/etin 90, 84-92.

Dikmen, G., 1952. Nazilli Tarih ve Cografyasi. M.E.B. Aydin City Library.

Emre, T. ve Sözbilir, H., 1995, Field evidence for metamorp-hic core complex detachment faulting and accommo-dation faults in the Gediz and Büyük Menderes gra-bens (West Turkey): International Earth SciencesColloquium on Aegean Regions, Izmir, Program andabstracts, 15.

Ergin, K., Güçlü U. and Uz Z., 1967. A catalog of earthquake for Turkey and surrounding area (11 A.D. to 1964 A.D.) İTÜ Faculty of Mining Enginering, İstanbul, Turkey.

Ferry, M., Meghraoui, M., Girard, J.-F., Rockwell, T.K., Kozaci, Ö., Akyuz, S. and Barka, A., 2004. Ground-penetrating radar investigations along the North Anatolian fault near Izmit. Geology, Volume 32/1, pp. 85-88.

Gencoğlu, S., İnan E. and Güler H., 1990. Türkiye'nin deprem tehlikesi, Türkiye Jeofizik Mühendisleri Odası, Ankara.

Girard, J.-F., 2000. Imagerie géoradar et modélisation des diffractions multiples, PhD thesis, Universite Louis Pasteur, Strasbourg.

Goidobani, E., Comastri, A. and Traina, G., 1994, Catalogue of ancient earthquakes in the Mediterranean area up to the 10 th century. Inst. Nazionale di Geofisica. 504 s.

Goodman, D., 1994. Ground penetrating radar simulation in engineering and archaeology. Geophysics 59 (2), 224-232.

Goodman, D., Nishimura, Y., Rogers, J.D., 1995. GPR time slices in archaeological prospection. Archaeological Prospection 2, 85-89.

Görür et al., 1995 N. Görür, M. Sakınç, A. Barka, A. Akkök and Ş. Ersoy, Miocene to Pliocene paleogeographic evolution of Turkey and its surroundings, Journal of Human Evolution 28. pp. 309–324.

Green, A., Gross, R., Holliger, K., Horstmeyer, H., Baldwin, J.,2003. Results of 3-D georadar surveying and trenching the San Andreas fault near its northern landward limit Tectonophysics 368 7 –23.

Gross, R., Green, A., Holliger, K., Horstmeyer, H., Baldwin, J.,2002. Shallow geometry and displacements on the San Andreas fault near Point Arena based on trenching and 3D georadar surveying. Geophys. Res. Lett. 29, 34-1– 34-4.

Hakyemez, Y.H., Erkal, T. and Göktaş F., 1999. Late Quaternary evolution of the Gediz and Büyük Menderes grabens, Western Anatolia, Turkey. Quaternary Science Rewievs, 18, 549-554.

Hruska, J., Fuchs, G., 1999. GPR prospection in ancient Ephesos. Journal of Applied Geophysics 41, 293-312.

İlhan, E., 1971. Earthquakes in Turkey. In: Geology and History of Turkey (edited by Campbell, A.S.) Petroleum Exploration Society of Libya, 431-442.

Jol, H., M., 1995. Ground penetrating radar antennae frequencies and transmitter powers compared for penetration depth, resolution and reflection continuity, Geophysical Prospecting, 43, 693-709.

Jackson, J., McKenzie, D.P., 1988. The relationship between plate motions and seismicmoment tensors, and the rates of active deformation in the Mediterranean and Middle East. Geophysical Journal of Royal Astronomical Society 93, 45–73.

Kadioglu, M., 2006. Die Scaenae frons des Theaters von Nysa am Mäander. Forschungen in Nysa am Mäander I. Ankara University, Ankara.

Le Pıchon, X. and Angelier, J. 1979. The Hellenic arc and trench system: a key to the neotectonic evolution of the Eastern Mediterranean area. Tecronophysics, 60, 1-42.

Leckebusch, J., 2003. Ground-penetrating radar: A modern three-dimensional prospection method. Archaeological prospection 10, 213-240.

Leckebusch, J., 2005. Use of antenna arrays for GPR surveying in archaeology. Near Surface Geophysics Vol. 3-2, 111-115.

Leckebusch, J., and Rychener J., 2007. Verification and topographic correction of GPR data in three dimensions. Near Surface Geophysics Vol. 5-6, 395-403.

Leckebusch, J., Weibel A. and Bühler F., 2008. Semi-automatic feature extraction from GPR data. Near Surface Geophysics Vol. 6-2, 75-84.

Leucci, G., Negri, S., 2006. Use of ground penetrating radar to map subsurface archaeological features in an urban area. Journal of Archaeological Science 33, 502-512.

Limp, F., 2006. Review of Ground Penetrating Radar for Archaeology (Conyers). Journal of Field Archaeology. Vol.31, 105 – 107.

Lualdi, M., Zanzi, L., 2002. GPR investigations to reconstruct the geometry of the wooden structures in historical buildings. In: Proceedings of the 9th Int. Conf. On Ground Penetrating Radar (GPR 2002), April 29-pMay 2, Santa Barbara, CA, pp. 63-67.

McCann, W.A., 1995. GPR and archaeology in central London. Archaeological Prospection 2, 155-166.

Martinez, A. and Byrnes, A. P., 2001. Modeling Dielectric-constant Values of Geologic Materials: An Aid to Ground-penetrating Radar Data Collection and Interpretation. Kansas Geological Survey, Current Research in Earth Sciences, Bulletin 247, part 1.

McCalpin, J.P., 1996. Paleoseismology, Academic Press, 588p.

McKenzie, D.P., 1972. Active tectonics of the Mediterranean Region.Geophysical Journal of Royal Astronomical Society 30, 109– 185.

McClusky, S., Reilinger R., Mahmoud S., Ben Sari D. and Tealeb A., 2003. GPS constraints on Africa (Nubia) and Arabia plate emotions. Geophys. Journal int. 155, 126-138.

Meghraoui, M., Camelbeeck, T., Vanneste, K., Brondeel, M. and Jongmans D., 2001. Active faulting and paleoseismology along the Bree fault, lower Rhine graben, Belgium. J. Geophys. Res., 105(B6), 13,809–13,841.

Moffatt, D. L., and Puskar, R. J., 1976. A subsurface electromagnetic pulse radar. Geophysics, 41(3), 506-518.

Negri, S., Leucci, G., 2006. Geophysical investigation of the Temple of Apollo(Hierapolis, Turkey) Journal of Archaeological Science 33, 1505-1513

Ocakoğlu, F., Dirik, K., Demirtaş R., Özsayın, E. and Açıkalın, S. 2007. Karacasu and Bozdoğan çapraz Grabenlerinin (batı Anadolu) Stratigrafik, Sedimantolojik and Tektonik Evrimi. Eskişehir Osmangazi Üni. Bilimsel Araştırmalar Komisyonu Raporu.

Olhoeft, G. R., 2000. “Maximizing the information return from ground penetrating radar.” J. of Applied Geophysics, 43(2-4), 175-187.

Paton, S., 1992 Active normal faulting, drainage patterns and sedimentation in southwestern Turkey. J. geol. Soc. Lond., 149, 1031-1044.

Pekman, A., 1991. Strabon Geography: Anatolia (Books:XII, XIII, XIV) Turkish translation by, Arkeoloji ve Sanat Yayinlari, Istanbul.

Persson, K., Olofsson, B., 2004. Inside a mound: applied geophysics in archaeological prospecting at the Kings' mounds, Gamla Uppsala, Sweden. Journal of Archaeological Science 31, 551-562.

Piro, S., Goodman, D., Nishimura, Y., 2001. High resolution ground penetrating radar survey at Forum Novum, in ''Forum Novum e Vescovio: studying urbanism in the Tiber Valley''. Journal of Roman Archaeology 14, 59-79.

Rizzo, E., Chianese, D., Lapenna, V., 2005. Magnetic, GPR and geoelectrical measurements for studying the archaeological site of 'Masseria Nigro' (Viggiano, southern Italy). Near-Surface Geophysics 3(1), 13-19.

Roberts, R.L. & Daniels, J.D., 1996. Analysis of GPR polarization phenomena, Journal of Environmental and Engineering Geophysics, Vol. 1, No. 2,.

Sandmeier, K. J., 2003. Reflexw 4.2 Manuel Book. Sandmeier Software, Zipser Strabe 1, D-76227 Karlsruhe, Germany.

Schukin, A., Kaploun I., Yarovoy A. and Ligthart L., 2000. Evolution of GPR antennas, pulse generators and sample recorders. Conference Proceedings on CD-ROM, Millennium Conference on Antennas & Propagation, Davos, Switzerland, 9-14 April, 2000, 4p.

Seyitoglu, G. and Scott, B.C., 1992. The age of Buyukmenderes graben (western Turkey) and its tectonic implication. Geological Magazine,129, 239-242.

Seyitoglu, G., Cemen, I. & Tekeli, O. 2000. Extensional folding in the Alasehir (Gediz) graben, western Turkey. Journal of the Geological Society, London, 157, 1097 -1100.

Seyitoglu, G., Isik, V., Cemen, I. 2004. Complete Tertiary exhumation history of the Menderes massif, western Turkey: an alternative working hypothesis. Terra Nova, 16, 358-364.

Sipahioğlu, S., 1979. Büyük Menderes açılımı ile Menderes Masifi yükseliminin sınırını oluşturan kuşağa uygulanan bir deprem öncesi çalışma, Deprem Araştırma Enstitüsü Bülteni, 25, 5-27.

Smith, D., G. & Jol, H. M., 1995. Ground penetrating radar: antenna frequencies and maximum probable depth soft penetration in Quaternary sediments. The Journal of Applied Geophysics. 33, 93-100.

Soysal, H. Sipahioğlu, S. Kolçak, D. and Altınok, Y., 1981, Türkiye tarihsel deprem kataloğu, TÜBİTAK Proje No: TBAG 341, ss 86.

Sözbilir, H., 2000. Batı Anadolu'dan örneklerle aktif faylar ve potansiyel aktif faylar. Batı Anadolu'nun Depremselliği Sempozyumu.

Şengör, A.M.C., 1979, The North Anatolian Transform Fault: its age, offset and tectonic significance. Jour. Geol. Soc. London, 136, 269-282.

Şengör, A.M.C., Görür, N. and Şaroğlu, F., 1985. Strike-slip deformation basin formation and sedimentation: strike-slip fauHing and related basin formation in zones of tectonic escape: Turkey as a case study. Society of Economic Paleontologists and Mineralogists, Special Publication 37, 227-64.

Şengör, A.M.C. 1987. Cross-fauHs and differential stretching of hanging walls in regions of low angle normal fauHing: Examples from western Turkey. In Continental Extensional Tectonics (eds M. P. Coward, J. F. Dewey and P. L. Rancoek), pp. 575-89. Geological Society Special Publication no. 28.

Tan, O., Tapırdamaz, C. and Yörük A., 2008. The Earthquake Catalogues for Turkey. Turkish Journal of Earth Sciences (Turkish J. Earth Sci.), Vol. 17, 2008, pp. 405–418.

Taymaz, T., Jackson, J and McKenzie, D., 1991Active tectonics of the north and central Aegean Sea. Geophysical Journal International. Vol: 106 No: 2 pp: 433-490.

Travassos, J. M., Menezes, P. T. L.; 2004: GPR exploration for groundwater in a crystalline rockterrain; Journal of Applied Geophysics; ; 55; 239; 248

Ulriksen, P. F., 1982. Application of impulse radar to civil engineering: Ph.D. Thesis. Lund University of Technology, Sweden. 179 pp.

Vaughan, C.J., 1986. Ground penetrating radar surveys used in archaeological investigations. Geophysics 51, 595-604.

Weymouth, J. W., 1986. Geophysical methods of archaeological site surveying, in Michael B. Schiffer (ed.), Advances in archaeological method and theory. Vol. 9:311-395. New York: Academic Press.

Wyatt, D. E., Waddell, M. G., and Sexton, G. B., 1996. Geophysics and shallow faults in unconsolidated sediments. Ground Water, 34(2), 326-334.

Yılmaz, Y., Genç, Ş. C., Gürer, F., Bozcu, M., Yılmaz, K., Karacık, Z., Altunkaynak, Ş. and Elmas, A., 2000, When did the Anatolian grabens begin to develop, Geological Society, London, 173, 353-384.

CURRICULUM VITAE

Cahit Çağlar YALÇINER

Born: January 23rd, 1976 in Zonguldak, Turkey.

Expected degree: PhD in Sciences, 2009.

Master degree (2004)

Title: *UsingVLF-EM Method on Active Fault Studies: A Case Study on the Eskişehir Fault Zone.*

Geological Engineering Department Eskişehir Osmangazi University

Supervisor: Prof. Dr. Erhan ALTUNEL

Graduation report (1999)

Title: *Investigation of Bademagacı Tell with Geophisical Methods.*

Geophisical Engineering Department İstanbul Tecnical University

Supervisor: Associated Prof. Dr. Gülçin Karlık